Advanced Control for Smart Microgrids in Vietnam

Hung Dung PHAM

B.E. (Electrical Engineering)

School of Electrical, Mechanical and Mechatronic Systems

University of Technology Sydney, Australia

Submitted to the Graduate School of the
University of Technology Sydney for the Degree of
DOCTOR OF PHILOSOPHY

August 2016

STATEMENT OF ORIGINAL AUTHORSHIP

This thesis is the result of a research candidature conducted jointly with another University as part of a collaborative Doctoral degree. I certify that the work in this thesis has not previously been submitted for a degree nor has it been submitted as part of requirements for a degree except as part of the collaborative doctoral degree and/or fully acknowledged within the text.

I also certify that the thesis has been written by me. Any help that I have received in my research work and the preparation of the thesis itself has been acknowledged. In addition, I certify that all information sources and literature used are indicated in the thesis.

Signature of Student:

Date: September 2017

ACKNOWLEDGEMENTS

First and foremost I would like to express my sincere gratitude to my supervisor, Professor Jianguo Zhu, who has supported and guided me throughout my thesis with his patience and knowledge. Without his priceless guidance, enthusiastic help, and consistent encouragement this thesis would not have been completed. I have learnt a lot from him through my PhD studies. I could not have wished for a better supervisor.

I would like to thank Dr. Li Li and Dr. Gregory Hunter, for agreeing to be my co-supervisors and supporting me for the past few years. Their knowledge and assistance did help me a lot to finish this thesis.

I would like to express my thanks to past colleagues, Dr.Jiefeng Hu and Dr. Mohammad Rabiul Islam, and all the current members from Centre of Electrical Machines and Power Electronics for the technical and much needed non-technical discussions. I also would like to thank my colleagues in Hanoi University of Science and Technology for all the valuable advises during my study.

Finally, I appreciate the encouragement of my friends and families, especially my parents and my wife, who have always been supporting me all the time.

SUMMARY OF THE THESIS

In recent years, researchers all over the world have been focusing on renewable energy more than ever. Vietnam is a tropical country, where there is not only a high potential of renewable energy but also a challenging electrical demand in years to come. This thesis will offer a solution to help the Vietnamese power scheme with a new smart micro grid concept. This new smart microgrid also brings some control challenges to researchers such as power quality and reliability control, power sharing control, system stability, and power flow management, etc. Among the power flow management control, model predictive control has also drawn strong attention among recent control strategies. This thesis will describe the control of grid-connected inverter with model predictive control to obtain the desired real and reactive powers that transfer between the microgrid and utility grid. Numerical simulation and experimental test results will be presented in this thesis also.

The literature review in Chapter Two draws the whole background of the picture. It presents the current state of the power scheme in Vietnam, the smart grid and its characteristics along with the control techniques used in a smart microgrid. To understand the smart microgrid, a detailed microgrid is described with distributed generations (DGs), loads, and power converters. The term “smart” used in “smart microgrid” is defined in this chapter also. The state of art of the microgrid control technique is revealed afterwards. Moreover, several control methods and strategies for microgrids are presented in the last part of this chapter.

With all the demand in the upcoming years from Vietnamese power scenario and its renewable energy potential, the Vietnamese Government is trying to develop the national electrical system in both stability and capacity to ensure the supply throughout the country. Chapter Three offers a whole new structure of the smart micro grid with a major part of the energy coming from renewable sources. This chapter also presents several study cases about different scenario of various power scales in Vietnam. This not only helps to solve the problem of being blackouts that both individual and industrial customers will have to face with years to come but also can take advantage of the great amount of renewable energy sources that are plentiful in Vietnam.

To specify the structure of the microgrid, Chapter Four designs a detail smart microgrid which consists of a hybrid AC-DC bus, with its renewable energy sources as photovoltaics and wind turbines, energy storage, and AC and DC loads. The whole smart micro grid system that fits into the rural areas of Vietnam in the next 10 to 15 years not only benefits the end-user customer but also helps the main grid in case the Vietnamese Government have a change in the energy policy in the near future to encourage people extract more and more green energy. This chapter also describes the several operation options of either cost or energy efficiency of the smart microgrid.

To connect the smart microgrid with the main grid, a grid-interfaced inverter is used in this thesis to control the power flow between the microgrid and utility grid. In Chapter Five, several control methods and strategies to control real and reactive power have been applied. Firstly, the system is transformed into the *d-q* rotating frame; therefore the active and reactive power can be controlled separately by controlling the d and q axis current components, id and iq. The first method uses the traditional PI control with feedforward to improve the control performance.

In Chapter Six, the other control method known as model predictive control is also used to control the active and reactive power flows based on the *d-q* rotating frame. Recently, the direct power control and model predictive control of real and reactive power flows has also been applied widely in the power electronic converter control. These new control techniques appear very attractive with several advantages in comparison with classical modulation methods, especially its excellent dynamic response, simple concept and easy implementation. In the model predictive control, a model is used to predict the future behaviour of the controlled variables. This information is then used in a cost function as the criterion to select the optimal switching state for the system. The control objectives can vary with different cost functions.

In this thesis, a new smart micro grid is designed with its special features along with the model predictive control technique for the grid-connected inverter control. The results have been numerically simulated by both MATLAB Simulink and PSIM software. A protocol has been tested for the grid-connected inverter control. Important conclusions based on the research findings through the thesis project are drawn, and possible future work for further development of the technology are suggested in the last chapter.

TABLE OF CONTENTS

LIST OF FIRGURES

LIST OF TABLES

LIST OF SYMBOLS

C	Filter Capacitance [µf]
L	Line Inductance [Mh]
R	Line Resistance [Ω]
S_i	Switching State of Phase *i (i= a, b, c)* Leg of the IGBT Bridges [0,1]
V_d, V_q	*d*-Axis and *q*-Axis Output Voltages of Grid-Connected Inverter in Rotating *d-q* Reference Frame [V]
$V_d^*/V_{d,Ref}$, $V_q^*/V_{q,Ref}$	Reference Value Of V_d, V_q [V]
i_d, i_q	*d*-Axis and *q*-Axis Currents in Rotating *d-q* Reference Frame [A]
$i_d^*/i_{d,ref}$, $i_q^*/i_{q,ref}$	Reference Value of i_d, i_q [A]
$V_{out,a}$, $V_{out,b}$, $V_{out,c}$	Output Voltages Of Grid-Connected Inverter Leg [V]
i_a, i_b, i_c	Inverter-Side Inductor Currents of Phase *a, b, c* [A]
V_α, V_β	Voltage in *α-β* Reference Frame [V]
i_α, i_β	Current in *α-β* Reference Frame [A]
f	Source Voltage Frequency [Hz]
I_{pv}	Photovoltaic Current [A]
N	Coincidence Point
N_s	Number of Cells
p	Number of Pole Pairs
R_s, R_p	Equivalent Series and Parallel Resistance of PV [Ω]

P, Q	Active and Reactive Power Transfer/Receive from the Grid [W]
T_s	Sampling Period [ms]
δ	Power Angle [rad]
ψ_a, ψ_b, ψ_c	Flux Linkage of Phase a,b,c [Wb]
ψ_d, ψ_q	d-axis and q-axis flux Linkage [Wb]
ψ_{pm}	Permanent Magnet Flux Linkage [Wb]

LIST OF ABBREVIATIONS

AMI	Advanced Metering Infrastructure
CHP	Combined Heat and Power Stations
CDMA	Code-Division Multiple-Access
DFIG	Doubly-Fed Induction Generator
DG	Distributed Generation
DPC	Direct Power Control
DSP	Digital Signal Processor
DTC	Direct Torque Control
DSL	Digital Subscriber Lines
ESS	Energy Storage System
EVN	Vietnam Electrical
GPS	Global Positioning System
HAN	Home Area Network
IGBT	Insulated Gate Bipolar Transistor
IEEE	Institute of Electrical and Electronics Engineers
ISM	Industrial Scientific and Medical
MPC	Model Predictive Control
MPP	Maximum Power Point
MPPT	Maximum Power Tracking Point
MS	Master-Slave
NIST	National Institute Of Standard And Technology
OQPSK	Offset Quadrature Phase-Shift Keying
PC	Personal Computer

PI	Proportional-Integral
PLC	Powerline Communication
PMSG	Permanent Magnet Synchronous Generator
PV	Photovoltaic
PWM	Pulse Width Modulation
Sine-PWM	Sine-Coded Pulse Width Modulation
SCADA	Supervisory Control and Data Acquisition
SCIG	Squirrel Gage Induction Generator
SEP	Smart Energy Profile
SOC	State Of Charge
STATCOM	Static Synchronous Compensator
SVM	Space Vector Modulation
THD	Total Harmonic Distortion
TOE	Tons of Oil Equivalent
TSR	Tip Speed Ratio
UMTS	Universal Mobile Telecommunications System
UPS	Uninterruptible Power Supply
VOC	Voltage-Oriented Control
VSC	Voltage Source Converter
VSI	Voltage Source Inverter
WCDMA	Wideband Code-Division Multiple-Access
WLANs	Wireless Local Area Networks
WiMAX	Worldwide Interoperability for Microwave Access

CHAPTER 1. INTRODUCTION

1.1. SIGNIFICANT AND BACKGROUND

To begin with Vietnam, a tropical developing country where the electrical demand has been increasing by an average of 14.5% annually over the last 15 years, one of the most important tasks that the Government has been struggling to solve recently is the electricity. Although the total amount of energy used per person is still relatively small in comparison to that of other Asian countries as well as all over the world, the rapid growth in electricity demand will continue to be a big pressure on Vietnam in the future. Given the favorable hydrological conditions, many newly completed power generation and network projects were added to the national power system, enabling Vietnam Electrical (EVN) to ensure sufficient power supply for socioeconomic development. However, the total electricity production still cannot meet the demand of the country. Currently in Vietnam, 80% of people are living in the rural areas, which do not have a reliable utility grid. A majority of them are still doing agricultural works for living. In years to come, with the integration of advance technology as well as mechanized equipment, rural people will have to face the rising problem of power supply sooner or later. The electrical grid in the rural area is very unreliable and unstable, which causes a lot of troubles to Vietnamese rural people. One of the foreseeable solutions is the wide use of distributed power generations.

This is also the direction for the developed countries like USA, EU and Japan from 2000 to date to deal with the crisis on oil prices, environmental pollution and global warming caused by emissions of greenhouse gases, such as CO_2, CH_4 and N_2O. Also, due to the environmental issues and the international agreement on the trade of emission quota, the calculated price of oil is forecast to increase to USD 190 per barrel in 2020. This forces the government to promote the diversification of energy sources, especially to encourage the use of renewable energy sources (RESs). An interesting example of attempts to solve this problem is that the Australian Government helps its citizens by a refund of money when they set up solar panels at home, so as to encourage people to utilize more and more RESs. The most exploited RESs are hydroelectric, photovoltaic (PV), and wind. Over the years, RESs have experienced one of the largest growths in percentage, being comparable with the growth of coal and lignite energy but still below that of natural gas. Between 2004 and 2009, grid connected PV capacity increased at an annual average rate of 60% and over this five-year-period, annual growth rates for cumulative wind power capacity averaged 27%. On the other hand, the global wind power installed capacity has increased from about 40,000 MW in 2003 to 59,091 MW in 2006. That number is expected to grow to well over 1,260,000 MW in 2020, which will be sufficient for 12% of the world's electricity consumption.

In order to help the Vietnamese rural people keep the development pace with other countries all over the world, this thesis aims to exploit the local RESs in Vietnam. According to the Vietnam Electricity Annual Report in 2016, the potential of wind energy in Vietnam is relatively high, and the energy density is evaluated at about 800 to 1,400 kWh per square meter per year on islands, 500 to 1,000 kWh in coastal regions and highlands, and under 500 kWh in other areas. For solar energy,

located in the tropic area, Vietnam has the average sunshine hours of approximately about 2,000 to 2,500 hours per year with a total solar radiation of about 1,700 kWh per square meter per year, giving a theoretical potential of about 43.90 billion tons of oil equivalent (TOE, each TOE equals 11,630 kWh) per year. Vietnam also has potential of biogas energy about 43-46 million TOE per year including timber, firewood, straw, garbage, but only about 10% has been exploited so far. For this reason, this thesis will focus on helping the Vietnamese people especially in rural areas maximize the power that can be extracted from the renewable resources.

On the other hand, as the distributed generations' number increases, the distribution networks are becoming active distributed systems where the generation and load nodes are mixed. This trend leads to many technical issues in power flows, voltage change, increase in network fault levels, and power quality, thus, leading to the introduction of microgrid concept, which is composed of renewable power generators, loads, energy storage devices and distribution control units. The microgrid term was proposed in early 2000s and developed throughout the world in the last two decades as an effective means to integrate intermittent renewable power sources in the power grids. More recently, the smart microgrid was also introduced and has attracted many research attentions all over the world. The newly developed smart microgrid will have several state of the art features such as smart infrastructure, smart communication system, and smart power flow control, etc. This thesis will present a new smart microgrid structure that can be applied to various Vietnamese scenarios including a design for a rural farm in detail.

The operations of the smart microgrid will not only help the rural people in Vietnam to have a high-quality power supply but also can help the main grid improve in many aspects. One of the most important features is the active and reactive power

flow control of the smart microgrid. It can be explained that the sub-grid can inject the exact amount of active and reactive power to the main grid when needed. In order to function as described, the proposed smart microgrid uses a grid-connected inverter to control the power flow between it and the main grid. This thesis will also focus on studying the control strategy of this interfacing-inverter. Moreover, the model predictive control, which is a very popular control method recently, is also applied to improve the performance of the system. The power flow control of this grid-connected inverter is the numerical simulation by both Software for Power Electronics Simulation (PSIM) and MATLAB Simulink software packages and experimental verification by tests in the laboratory. This powerful model predictive control method along with different constrains in the cost function will also optimize the smart microgrid performance by reducing its operational cost. Numerous case studies for smart microgrids are also presented in the thesis.

1.2. AIM AND SCOPE OF THE THESIS

In order to exploit the potential of RESs in Vietnam with the optimized operation in the smart microgrid, this thesis focuses on the technical issues related to the structure, modelling, control and management of power flow control of smart microgrids. The main objectives of this thesis will be:

- To develop a new structure for smart microgrids that helps to improve the Vietnamese power scheme with different scenarios,
- To achieve smart microgrids operation to reduce the operating cost for customers and help the main grid as well, and

- To achieve power flow control management with feedback plus feedforward control and the new model predictive control technique applied.

.

1.3. OUTLINE OF THE THESIS

This thesis is divided into seven chapters where the first chapter is the general introduction of the thesis and remaining chapters of the thesis are presented as follows.

- Chapter 2 with the literature review draws the whole background of the thesis. It presents the current state of the power scheme in Vietnam, the smart grid and its characteristics along with the control techniques used in a smart microgrid. To understand the smart microgrid, a detailed structure is designed with DGs, loads, power converters. The term “smart” used in “smart microgrid” is also defined in this chapter. The state of art of the smart microgrid control technique is revealed afterwards. Moreover, several control methods and strategies for smart microgrid are presented in the last part of this chapter.

- Chapter 3 proposes a new structure of the smart micro grid with a major part of the energy coming from RESs. This chapter also presents several case studies about different scenarios of various power scales in Vietnam. It not only helps to solve the problem of being blackouts that both individual and industrial customers will have to face with years to come but also can take advantage of the great amount of RESs that are plentiful in Vietnam.

- Chapter 4 designs a detailed smart microgrid which consists of a hybrid AC-DC bus, the RESs such as PVs and WTs, energy storage, AC and DC loads as well. The smart micro grid system that fits into the rural areas of Vietnam in the next 10 to

15 years not only benefits the end-user customers but also helps the main grid in case the Vietnamese Government has a change in the energy policy in the near future to encourage people to extract more and more green energy. This chapter also describes several operating options of either cost or energy efficiency of the smart microgrid.

- Chapter 5 and 6 propose several control methods and strategies to control the active and reactive power that flow between the utility grid and microgrid. The first method uses the traditional PI control with feedforward to improve the control performance. The other control method called MPC is also used to control the active and reactive power by controlling the currents in the *d-q* rotating frame. Recently, DPC as well as MPC of active and reactive power has also been applied widely in the power electronics control. The results have been obtained from simulations in both MATLAB Simulink and PSIM software. The experiment has been tested for the grid-connected inverter control.

- Chapter 7 concludes the thesis achievements and proposes future work for smart microgrid control.

CHAPTER 2. LITERATURE REVIEW

2.1. INTRODUCTION

This chapter presents a literature review on the current state of the power scheme in Vietnam, the smart grid and its characteristics along with the control techniques used in smart microgrids. To understand the smart microgrid concept, a detailed microgrid with distributed generations (DGs), loads, power converters, etc. as an example is described. A novel smart microgrid to apply for a specific area in Vietnam will also be presented. The gap that needs to be bridged through the thesis project in the microgrid control technique is revealed afterwards and a new strategy for microgrid control is proposed in the last part of this chapter.

2.2. POWER SCHEME IN VIETNAM

Vietnam is a developing country where the electricity demand has been increasing by an average of 14.5% annually over the last 15 years. Although the total amount of energy used per person is still relatively small (approximately 900 kWh per person per year) in comparison to other Asian countries as well as all over the world (e.g. 2,680 kWh and 15,370 kWh in Thailand and USA, respectively), the rapid growth in electricity demand will continue to be a big pressure on Vietnam in the

future. Table 2-I illustrates a prediction of the future energy needs according to the general energy planning scheme of the government.

TABLE 2- I. FORECAST OF ELECTRICAL DEMAND AND POWER SUPPLY OF VIETNAM UNTIL 2025

Year	2009	2013	2017	2021	2025
Annual energy used, in GWh	85,596	130,069	188,736	263,438	349,523
Peak power, in MW	14,929	22,248	31,671	43,584	57,826

In Vietnam, the main traditional energy resources are coal, oil, gas and hydropower. Currently a large number of hydro-electric power systems have been installed with the 10 major rivers in the country fully exploited. Crude oil extraction has actually decreased in recent years (17.4 million tons in 2006, 15.9 million tons in 2007 and 15.0 million tons in 2008). The amount that can be exploited is not as much as predicted. The fluctuation of oil and coal prices placed Vietnam in an extremely difficult position to meet the energy demand in the near future. For that reason, the government has planned a project to increase the amount of DG and renewable energy systems. The potential of wind energy in Vietnam is relatively high, and the energy density is evaluated at about 800 to 1,400 kWh per square meter per year on islands, 500 to 1,000 kWh in coastal region and highlands, and under 500 kWh in other areas. For solar energy, located in the tropic area, Vietnam has the average sunshine hours of approximate about 2,000 to 2,500 hours per year with a total solar radiation of about 1,700 kWh per square meter per year, giving a theoretical potential of about 43.90 billion ton of oil equivalent (TOE, each TOE equals 11,630 kWh) per year. Vietnam also has potential of biogas energy about 43-46 million TOE per year including timber, firewood, straw, garbage, but only about 10% has been exploited so far.

2.3. SMART MICROGRIDS

2.3.1. An outline

Access to modern trends in the management, utilization and power consumption by applying new technology is the best way to ensure energy needs for the foreseeable future. This is the direction by the developed countries like USA, EU and Japan from 2000 to date to deal with the crisis on oil prices, environmental pollution, global warming caused by emissions of CO_2, CH_4 and N_2O. Also, due to the environmental issues and the international agreement on the sale of emission quota, the calculated price of oil is forecast to increase to 190 USD per barrel in 2020. This forces the government to promote the diversification of energy sources, especially to encourage the use of RESs. An interesting example of an attempt to solve this problem is that the Australian Government helps its citizens by a refund of money when they set up solar panels at home, so as to encourage people to utilize more and more RESs. The most exploited RESs are hydroelectric, PV, and wind. Over the years, renewable energies have experienced one of the largest growths in percentage, being comparable with the growth of coal and lignite energy but still below that of natural gas.

Various DGs have been connected to electrical distribution networks in recent years, such as fuel cells, wind turbines (WTs), small hydro power plants, and combined heat and power plants (CHP). As the number of DGs increases, distribution networks are becoming active distributed systems where generation and load nodes are mixed. This trend leads to many technical issues in power flows, voltage change, increase in network fault levels, and power quality. Therefore, this literature review will concentrate on possible solutions to these technical issues such as DGs and the smart microgrid concept with grid-connected and stand-alone modes.

2.3.2. Distributed generations

From the inception of electricity as an industry, it has competed against gas for customers. Indeed, electric arc lighting, a mid-19th century stand-alone system located on the customer's premises, attempted to replace the less expensive but volatile gas lamps supplied with "town gas", a mixture of hydrogen and carbon monoxide. In that time, the light was poor, tremendous waste heat made rooms smoky and hot, and the noxious elements of town gas mentioned earlier left room for a cleaner, better alternative in the marketplace, and that was electricity. Thomas Edison created the first electric utility system, mimicking the gas lighting industry but supplying energy through virtual "mains" to light filaments instead of via gas burners. The same reduction in capital cost per unit of power generated applied to electricity as it did to gas. From that moment, the inexorable trend toward centralized power generation, distribution, and system management began. Initially, the systems were isolated, without connection to other utilities. By the end of the 1920s, however, utility grids adjoined one another, and the interconnection brought obvious benefits such as back-up power and sharing peak load coverage. Years later, fuel cells were first developed for space flight, and aero derivative gas turbines that powered jet aircraft found a market in stationary power. The pursuit of soft path, environmentally sustainable economies produced solar engineering and PV systems. Those were among many types of DGs that operated in many different industries all over the world.

DG is any small-scale electrical power generation technology that provides electric power at or near the load site; it is interconnected to the distribution system, directly to the customer's facilities, or both. The advantages of DG applications can be listed as follows:

- High reliability of power supply, especially when interruption of service is unacceptable,
- More flexible to exploit the RESs,
- High power quality, and
- Ideal power supply for remote areas where utility grid is unavailable for customers.

Research indicates that the distributed power has the potential to capture up to 20% of all new generating capacity, or 35 GW, over the next two decades. DG technologies include small and micro combustion turbine generators, internal combustion reciprocating engines and generators, PV panels, and fuel cells. Other technologies including solar thermal conversion, Stirling engines, and biomass conversion can also be considered as DGs.

Despite the benefits provided by DGs mentioned above, there are technical limits in reality on the degree to which DGs can be connected. The main concerns of connecting DGs can be summarized as the following:

- Possible power quality problems, such as voltage sag and current surge, and harmonics,
- The effects of connecting or disconnecting DGs on the power quality and stability of the utility grid,
- The efficiency of DGs when connected to the grid,
- The fluctuation of DG output power due to the intermittent nature of RESs, which could cause negative impacts on electric appliances, and
- Impact on power system dynamics performance.

2.3.3. Microgrids and smart microgrid

The concept of microgrid, which is composed of DGs, renewable power generations, such as solar PVs, WTs and fuel cells, together with customer loads, energy storage devices and power converters, was introduced in the early 2000s [2.1] and developed throughout the world in the last decade as an effective means to integrate intermittent renewable power sources in power grids [2.2-2.7].

A smart microgrid can be operated in two different modes: grid-connected mode or stand-alone mode (islanded mode) in order to provide power to the emergency load during system outages. The stand-alone power system is used primarily in remote areas where utility lines are uneconomical to install due to the terrain, right-of-way difficulties, and environmental concerns. Building new transmission lines is expensive even without these constraints. A 230 kV line costs more than USD 1 million per mile. A stand-alone wind system would be more economical for some potential consumers (especially households), who

- Are wanting connections to an electrical network, but are located at a long distance from the network (high interconnection costs, potential place for installation of autonomous renewable energy systems, for example wind generator and battery);
- Plan to increase their power demand, but could not be satisfied (without substantial distribution investments) due to bottlenecks in the network;
- Would like to be independent from the centralized power supply and prefer to have their own base-load generator; such consumers remain connected to the central power supply to exchange a surplus (top-up) and deficit (back up, usually to cover its peak load demand) of power;

- Distribution system operators, who may be interested in enhancement of power quality (especially voltage problems); and
- Isolated consumers / energy systems, such as oil derricks, and islands.

To satisfy all these needs, a novel power flow control method for autonomous operation of micro-grids in the island mode was presented in [2.8]. By using a controller, the power flow from an inverter and synchronous generator to the load can be controlled. In this particular case, the proposed power flow controller makes use of a new adaptive estimation unit, which can estimate the amplitude, phase angle, and frequency of the fundamental component of potentially non-stationary power signal, as well as the associated active and reactive power. This method is very useful for power systems containing many different DGs to operate in the standalone mode. However, controlling parallel-connected inverters in a standalone AC supply system is a very important target to achieve. For that reason, a scheme was designed, which is suitable for controlling inverters in distributed source environments, such as isolated AC systems, large and distributed uninterruptible power supply (UPS) systems, PV systems connected to AC grids, and low voltage DC power transmission meshes [2.9]. A key feature of the control scheme is that it uses the feedback of only those variables that can be measured locally at the inverter and does not need communication of control signals among the inverters. However, the system dynamic performance can be substantially improved if an observer structure is used to determine the frequency. The position of the AC system voltage vector can be determined very accurately at any time.

However, when a large number of RESs are connected to the grid, a power system with DGs should be designed. Both the wind and PV systems interface with the grid at the output terminals of a synchronizing breaker after the inverter. The

power flows in either direction depending on the site voltage at the breaker terminals. The fundamental requirements on the site voltage for interfacing with the grid are as follows:

- The voltage magnitude and phase angle must equal that required for the desired magnitude and direction of the power flow. The voltage is controlled by the transformer turns ratio or the power electronic converter firing-angle in a closed-loop control system.
- The frequency must be exactly equal to that of the grid or else the system will not work. To meet the exact frequency requirement, the only effective means is to use the utility frequency as the inverter switching frequency reference.
- In the wind system, the base-load synchronous generators in the grid provide the magnetizing current for the induction generator.

A distributed power system that was controlled by an autonomous state estimation method was reported in [2.10]. The infrastructure is a combination of distributed hardware and software tools that modernize the distribution grid. A noticeable advance of this method is the communication between devices through the global positioning system (GPS). For that reason, it is considered as a real-time supervisory control and data acquisition (SCADA) system with distributed reliable and high-speed communication devices. This paper also offers a load levelization method. Further work was proposed on security problems of the GPS system and bringing more convenience to users when levelising the load.

As suggested in [2.11], the control method using multi-agent systems, such as distributed energy resource agent, database agent, control agent, user agent are more and more widely employed nowadays. These SCADA systems provide

communication architecture capable of controlling and maintaining power system hardware using certain signalling protocols, and the control agent contains software to perform generator synchronization, maintain operating frequency and voltage, sustain suitable real and reactive power, and loading and unloading. One disadvantage of this method is that each agent requires a lot of specifically developed software and hardware.

The load conditions and voltage sags can also be factors used to regulates the terminal voltage of sensitive loads in the island mode and power flow in the grid-connected mode [2.11]. In [2.12], a closed-loop controller for the filter capacitor voltage and a feed-forward loop for the load current are presented. An outer control loop was designed for sharing the real and reactive power in the grid-connected mode which determined variation of the magnitude and phase angle of the three-phase capacitor voltage space vector. In [2.13], the transition between grid-connected mode and island mode is mentioned to provide a useful method to change from one mode to another if needed.

However, there are several issues which needed to be addressed are power quality and reliability, system stability and protection. Unstable output power from DGs, unbalanced and nonlinear loads, and disturbance of the grid could be a challenge for stabilization of the frequency and voltage, which can be evaluated in terms of voltage (magnitude and frequency) variation, flicker, and harmonics, etc. In [2.14] and [2.15], compensators were designed for a microgrid with unbalanced and nonlinear loads with the purpose of improving power quality. On the other hand, much attention has been paid to enhance the microgrid power quality under grid voltage disturbance [2.16-2.18].

In addition, the system stability during load sharing, the transient stability of the power system with high penetration level of power electronics interfaced DG, the low frequency stability problem with change in power demand and the robust stability of the control system are also concerned .The influence of control parameters on system stability should be taken into account in terms of sensitivity analysis, using qualitative analysis and small-signal techniques [2.19-2.21].

Therefore, the definition of smart microgrid can be introduced as following: A smart microgrid is a microgrid with smart infrastructures including metering and communication system along with smart control techniques applied. A novel structure of the microgrid, smart control strategies and control algorithms will be studied and presented in this thesis. For the smart operation of a microgrid system, all the DG units should be able to participate in the optimized control mechanism. The basic requirements for a microgrid to achieve smart operation can be described as:

- Provide high quality power for the loads, i.e., establish a stable output voltage regardless of intermittent power generation and the fluctuating power demand; and
- Provide utility grid support such as voltage boost and frequency stabilization during grid faults, by exploiting the static synchronous compensator (STATCOM) capability of the power electronics within the microgird.

2.3.4. Communication System For Smart Microgrids

The smart microgrid concept can enable new network management strategies to provide effective grid integration of DGs for demand side management and energy storage for DG load balancing, etc. [2.22],[2.23]. While the RESs are widely studied by many researchers [2.24], the effective integration of RESs, to reduce the system

loss and increase the reliability, efficiency and security of electricity supply to customers are some of the advantages that the smart grid system can provide [2.25]. In contrast to the existing power grid which has limited communication capabilities, a smart power grid infrastructure is full of enhanced sensing and advanced communication and computing abilities. Different components of the system are linked together with communication paths and sensor nodes to provide interoperability among them, such as distribution, transmission and substations, as well as residential, commercial, and industrial sites.

The communications technologies available for smart microgrids are introduced as follows.

2.3.4.1. ZigBee

ZigBee is a wireless communication technology that is relatively low in power usage, data rate, complexity, and cost of deployment. It is an ideal technology for smart lightning, energy monitoring, home automation, and automatic meter reading, ZigBee and ZigBee Smart Energy Profile (SEP) have been realized as the most suitable communication standards for a smart grid residential network domain by the U.S. National Institute for Standards and Technology (NIST) [2.26]. The communication between smart meters, as well as among intelligent home appliances and in home displays, is very important. Many Advanced Metering Infrastructure (AMI) vendors, such as Itron, Elster, and Landis Gyr, prefer smart meters, that the ZigBee protocol can be integrated into [2.27]. ZigBee integrated smart meters can communicate with the ZigBee integrated devices and control them. ZigBee SEP provides utilities to send messages to the home owners, and home owners can reach the information of their real-time energy consumption.

The following is a brief outline of the advantages and disadvantages of ZigBee:

- Advantages:
  - ZigBee has 16 channels in the 2.4 GHz band, each with 5 MHz of bandwidth. 0 dBm (1 mW) is the maximum output power of the radios with a transmission range between 1 and 100 m with a 250 Kb/s data rate and OQPSK modulation[2.26].
  - ZigBee is considered as a good option for metering and energy management and ideal for smart grid implementations along with its simplicity, mobility, robustness, low bandwidth requirements, low cost of deployment, its operation within an unlicensed spectrum, easy network implementation, being a standardized protocol based on the IEEE 802.15.4 standard [2.28].
  - ZigBee SEP also has some advantages for gas, water and electricity utilities, such as load control and reduction, demand response, real-time pricing programs, real-time system monitoring, and advanced metering support [2.26],[2.29].
- Disadvantages:
  - There are some constraints on ZigBee for practical implementations, such as low processing capabilities, small memory size, small delay requirements and being subject to interference with other appliances, which share the same transmission medium, license-free industrial, scientific and medical (ISM) frequency band ranging from IEEE 802.11

wireless local area networks (WLANs), Wi-Fi, Bluetooth and Microwave [2.26].

- The robustness of ZigBee under noise conditions increases the possibility of corrupting the entire communications channel due to the interference of 802.11/b/g in the vicinity of ZigBee [2.30].
- Interference detection schemes, interference avoidance schemes and energy-efficient routing protocols, should be implemented to extend the network life time and provide a reliable and energy-efficient network performance.

2.3.4.2. Wireless Mesh

A mesh network is a flexible network consisting of a group of nodes, where new nodes can join the group and each node can act as an independent router. The self-healing characteristic of the network enables the communication signals to find another route via the active nodes, if any node should drop out of the network. Each meter acts as a signal repeater until the collected data reaches the electric network access point. Then, collected data is transferred to the utility via a communication network. A private company, Sky Pilot Networks uses mesh networking for smart grid applications due to the redundancy and high availability features of mesh technology [2.27].

The following is a brief outline of the pros and cons of wireless mesh:

- Advantages:
  - Mesh networking is a cost effective solution with dynamic self-organization, self-healing, self-configuration, high scalability services, which provides many advantages, such as improving

the network performance, balancing the load on the network, extending the network coverage range [2.31].

- Good coverage can be provided in urban and suburban areas with the ability of multichip routing.
- Acting as signal repeaters and adding more repeaters to the network can extend the coverage and capacity of the network.
- AMI and home energy management are some of the applications it can be used for.

- Disadvantages:
  - Network capacity, fading and interference can be counted as the major challenges of networking systems.
  - In urban areas, mesh networks have been faced with a coverage challenge since the meter density cannot provide complete coverage of the communications network.
  - Providing the balance between reliable and flexible routing, a sufficient number of smart nodes, taking into account node cost, are very critical for mesh networks.
  - A third party company is required to manage the network, and since the metering information passes through every access point, some encryption techniques are applied to the data for security purposes.
  - Data packets travel around many neighbours, there can be loop problems causing additional overheads in the communications channel that would result in a reduction of the available bandwidth [2.9].

2.3.4.3. Cellular Network Communication

The existing cellular networks can be a good option for communicating between smart meters and the utility and between far nodes. The existing communications infrastructure avoids utilities from spending operational costs and additional time for building a dedicated communications infrastructure. Cellular network solutions also enable smart metering deployments spreading to a wide area environment. 2G, 2.5G, 3G, WiMAX, and LTE are the cellular communication technologies available to utilities for smart metering deployments. When a data transfer interval between the meter and the utility of typical 15 min is used, a huge amount of data will be generated and a high data rate connection would be required to transfer the data to the utility. Code-division multiple-access (CDMA), wideband code-division multiple-access (WCDMA), and Universal Mobile Telecommunications System (UMTS) wireless technologies are also used in smart grid projects. A CDMA smart grid solution for the residential utility market has been introduced by Verizon, and Verizon's 3G CDMA network will be used as the backbone of the smart grid communications with the Smart Synch smart grid solutions [2.27]. UMTS is IP-based and a packet oriented service that is suitable for metering applications [2.27] Telenor with Cinclus technology is offering UMTS technology for smart grid communications [2.27]. An Australian energy delivery company, SP AusNet, is building a dedicated communications network for smart grid applications and chose WiMAX technology for the communications need of the smart meters. WiMAX chip sets are embedded into the smart meters and wireless communication is dedicated between smart meters and the central system in SP AusNet's system. Some major companies, such as Cisco, Silver Springs Network, and Verizon, also implement WiMAX smart grid applications. The world's largest

WiMAX vendor, Alvarion, has announced its partnership with a U.S. utility company, National Grid, for a WiMAX-based smart grid project. Lower deployment and operating costs, proper security protocols, smooth communications, high data speeds (up to 75 Mb/s), an appropriate amount of bandwidth and scalability are the advantages of today's WiMAX technology.

The advantages and disadvantages of cellular network communication can be summarized as the following:

- Advantages:
    - Cellular networks already exist so utilities do not have to incur extra cost for building the communications infrastructure required for a smart grid.
    - Due to data gathering at smaller intervals, a huge amount of data will be generated and the cellular networks will provide sufficient bandwidth for such applications.
    - Secure data transmissions with strong security controls.
    - Having a wide area deployment capability of smart grid since the cellular networks coverage has reached almost 100%. In addition, GSM technology performs up to 14.4 Kb/s, GPRS performs up to 170 Kb/s and they both support AMI and Demand Response applications.
    - Lower cost, better coverage, lower maintenance costs, and fast installation features highlight why cellular networks can be the best candidate as a smart grid communications technology for the applications, such as demand response management, AMI, HAN, outage management.

- Disadvantages:
    - Some power grid mission-critical applications need continuous availability of communications.
    - The services of cellular networks are shared by the customer market and this may result in network congestion or decrease in network performance in emergency situations.
    - In abnormal situations, such as a wind storm, cellular network providers may not provide guaranteed service. Compared to public networks, private networks may handle these kinds of situations better due by the usage of a variety of technologies and spectrum bands.

2.3.4.4. Powerline Communication

Powerline communication (PLC) is a technique that uses the existing powerlines to transmit high-speed (2–3 Mb/s) data signals from one device to the other. PLC has been the first choice for communication with the electricity meter due to the direct connection with the meter [2.30] and successful implementations of AMI in urban areas where other solutions struggle to meet the needs of utilities. PLC systems based on the LV distribution network have been one of the research topics for smart grid applications in China [2.32]. In a typical PLC network, smart meters are connected to the data concentrator through powerlines and data is transferred to the data centre via cellular network technologies. PLC technology is chosen for data communication between the smart meters and the data concentrator, while GPRS technology is used for transferring the data from the data concentrator to the utility's data centre [2.27].

The following is a summary of the advantages and disadvantages of power line communication technology:

- Advantages:
  - Existing infrastructure decreases the installation cost of the communications infrastructure. The standardization efforts on PLC networks, the cost-effective, ubiquitous nature, and widely available infrastructure of PLC, can be the reasons for its strength and popularity [2.33].
  - Data transmissions are broadcast in nature for PLC, so the security aspects are critical. Confidentiality, authentication, integrity, and user intervention are some of the critical issues in smart grid communications.
- Disadvantages:
  - The powerline transmission medium is a harsh and noisy environment that makes the channel difficult to be modelled. The low-bandwidth characteristic (20 kb/s for neighbourhood area networks) restricts the PLC technology for applications that need higher bandwidth [2.27].
  - The network topology, the number and type of the devices connected to the powerlines, wiring distance between transmitter and receiver, all, adversely affect the quality of signal that is transmitted over the powerlines [2.27].
  - The sensitivity of PLC to disturbances and dependency on the quality of signal are the disadvantages that make PLC technology not suited for data transmission.

2.3.4.5. Digital Subscriber Lines

Digital Subscriber Lines (DSLs) is a high-speed digital data transmission technology that uses the wires of the voice telephone network. It is common to see frequencies greater than 1 MHz through an ADSL enabled telephone line [2.34]. The already existing infrastructure of DSL lines reduces installation cost. Hence, many companies chose DSL technology for their smart grid projects.

The pros and cons of digital subscriber lines can be summarized as the following:

- Advantages:
  - Widespread availability, low-cost
  - High bandwidth data transmissions
- Disadvantages:
  - The reliability and potential down time of DSL technology may not be acceptable for mission critical applications.
  - Distance dependence and lack of standardization may cause additional problems.
  - The wired DSL-based communications systems require communications cables to be installed and regularly maintained, and thus, cannot be implemented in rural areas due to the high cost of installing fixed infrastructure for low-density areas.
  - Wired technologies, such as DSL, PLC, optical fibre, are costly for wide area deployments but they have the ability to increase the communications capacity, reliability and security. On the

other hand, wireless technologies can reduce the installation costs, but provide constrained bandwidth and security options.

To conclude, each of these communication systems is applicable to smart microgrids. However, for certain scenario, one might be better than the others due to its advantages and disadvantages. For example, when considering smart system for a small building, a wireless mesh is the perfect solution for its coverage, management and advanced infrastructure.

2.4. CONTROL OF MICROGRIDS

2.4.1. Control Of Power Electronic Converters In Microgrids

The following are the common definitions in the field of power electronics:

- **Power electronic components** are those semiconductor devices, such as diodes, thyristor, transistors, that are used in the power circuit of a converter. In power electronics, they are used in the non-linear switching mode (on/off mode) and not as linear amplifiers.
- **A power electronic converter** or "converter" for short is an assembly of power electronic components that converts one or more of the characteristics of an electric power system. For example, a converter can be used to change
    - AC to DC
    - DC to AC
    - Frequency
    - Voltage level
    - Current level, and

- Number of phases

There are also some different types of converters depending on the purpose of converters such as:

- *A rectifier* is a converter that converts AC to DC
- *An inverter* is a converter that converts DC to AC
- *An AC to AC converter* is a converter that converts AC of one voltage and frequency to AC of another voltage and frequency, which are often variable
- *An AC frequency converter* is a special type of AC converter
- *A DC to DC converter* is a converter that converts DC of one voltage to DC of another voltage
- *An electronic switch* is a device that electronically connects or disconnects an AC or DC circuit and can usually be switched ON and/or OFF.

In this case, we will investigate further about some types of power converter.

2.4.1.1. AC/DC converters

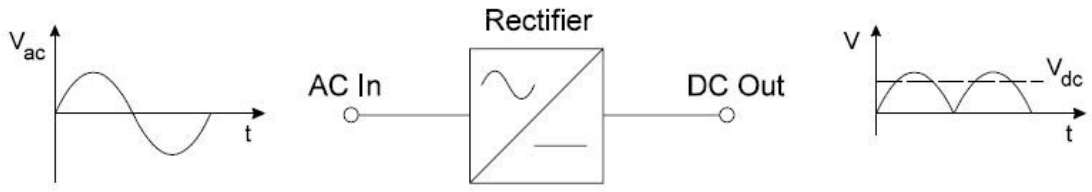

Fig.2.1. Basic concept of rectifier

The first stage of an AC frequency converter is the conversion of a 3 phase AC power supply to a smooth DC voltage and current. Simple bi-stable devices, such as the diode and thyristor, can effectively be used for this purpose. In a diode rectifier

circuit, a diode turns ON and starts to conduct current when there is a forward voltage across it, i.e. the forward voltage across it becomes positive. This process usually results in the forward voltage across another diode becoming negative, which then turns off and stops the conducting current. In a thyristor rectifier circuit, the switches additionally need a gate signal to turn them on or off.

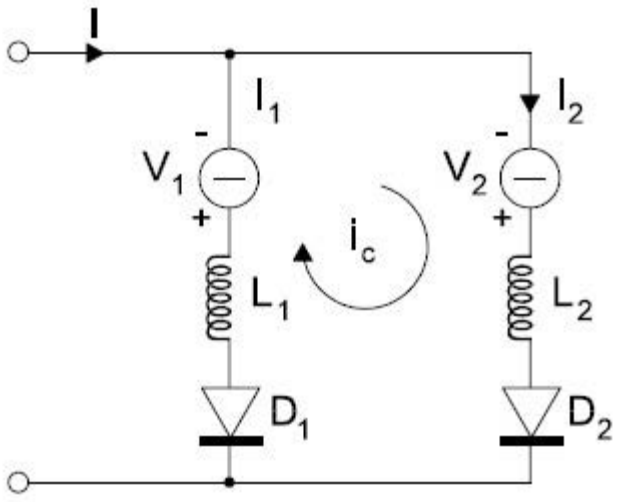

Fig.2.2. A simple circuit showing commutation from diode D1 to D2

The factors affecting commutation may be illustrated in the idealized diode circuit in Figure 2.2, which shows two circuit branches, each with its own variable DC voltage source and circuit inductance. Assume, initially, that a current I is flowing through the circuit and that the magnitude of the voltage V_1 is larger than V_2. Since $V_1 > V_2$, diode D_1 has a positive forward voltage across it and it conducts a current I_1 through its circuit inductance L_1. Diode D_2 has a negative forward voltage across it and is blocking and carries no current.

Practical power electronic converter circuits follow the same basic sequence above. The figure below shows a typical 6-pulse rectifier bridge circuit to convert 3-phase AC currents I_A, I_B and I_C, to a DC current I_D.

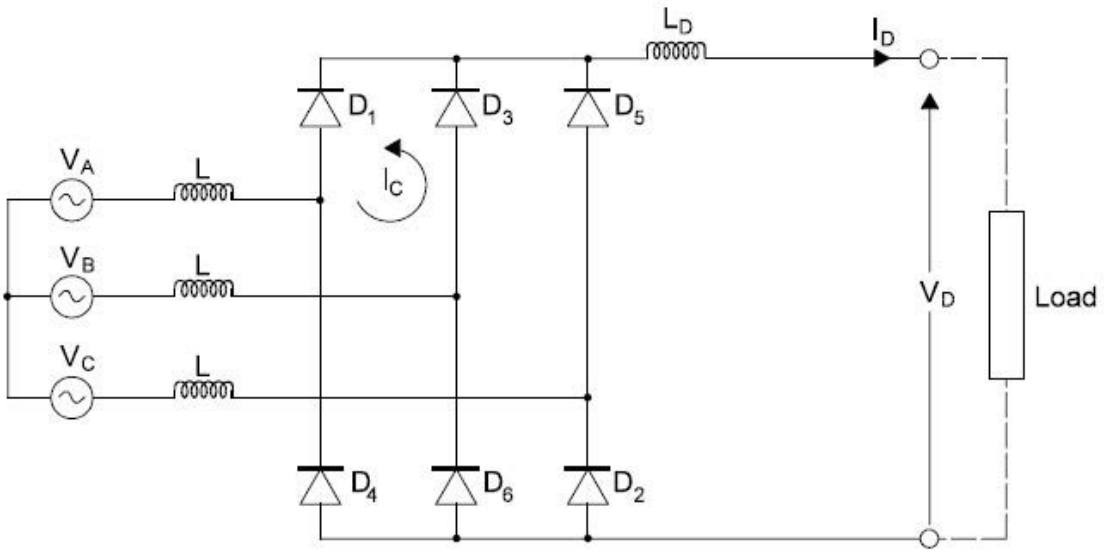

Fig.2.3. Phase commutation with a 6-pulse diode bridge

This type of circuit is relatively simple to analyse because only 2 of the 6 diodes conduct current at any one time. The idealized commutation circuit can easily be identified. In this example, commutation is assumed to be taking place from diode D_1 to D_3 in the positive group, while D_2 conducts in the negative group.

The output DC voltage and operating sequence of the diode rectifier above is dependent on the continuous changes in the supply line voltages and is not dependent on any control circuit. This type of converter is called an *uncontrolled diode rectifier bridge* because the DC voltage output is not controlled and is fixed at $1.35 \times V_{RMS}$. If the diodes are replaced with thyristors, it then becomes possible to control the point at which the thyristors are triggered and therefore the magnitude of the DC output voltage can be controlled. This type of converter is called a *controlled thyristor rectifier bridge* and requires an additional control circuit to trigger the thyristor at the right instant. A typical 6-pulse thyristor converter is shown in Figure 2.5.

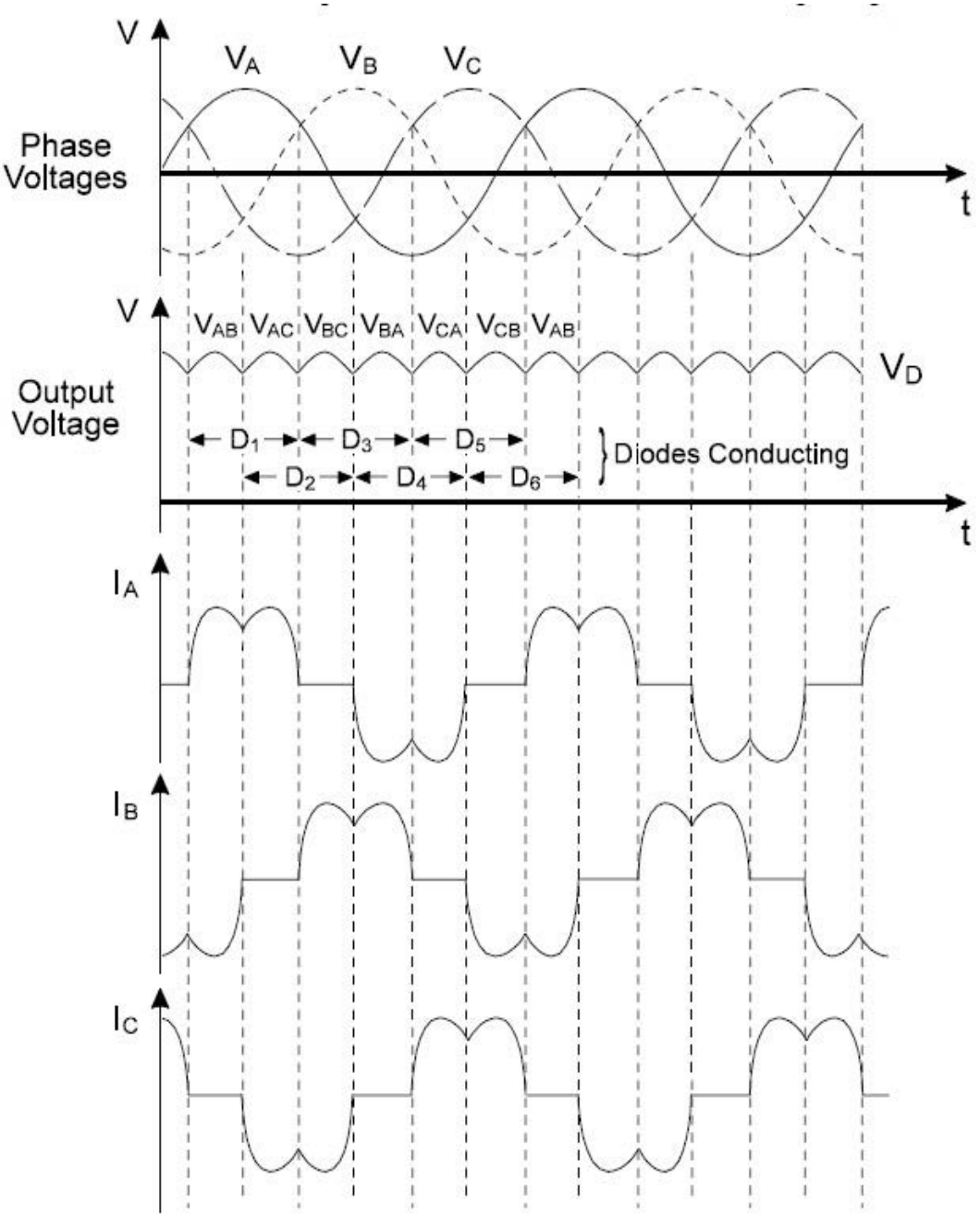

Fig.2.4. Voltage and current waveforms during commutation

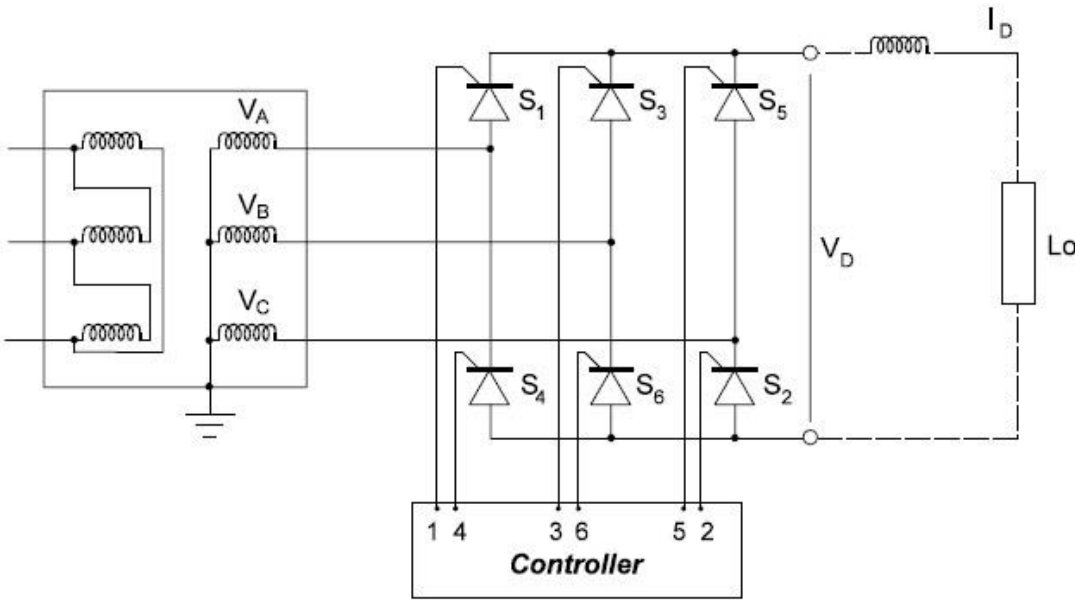

Fig.2.5. Pulse controlled thyristor Rectifier Bridge

The output of the rectifier bridge can be controlled by delaying the instant at which the thyristor receives a triggering pulse. This delay is usually measured in degrees from the point at which the switch can turn on, due to the forward voltage becoming positive. The angle of delay is called the *delay angle*, or sometimes the *firing angle*, and is designated by the symbol α. The reference point, for the angle of delay, is the point where a phase voltage wave crosses the voltage of the previous phase and becomes positive relative to it. A diode rectifier can be thought of as a converter with a *delay angle of* α= 0°.

At a delay angle α, the DC voltage is given by:

$$V_D = 1.35 \times V_{RMS} \times Cos\alpha$$

Fig.2.6 shows the voltage waveforms of a controlled rectifier.

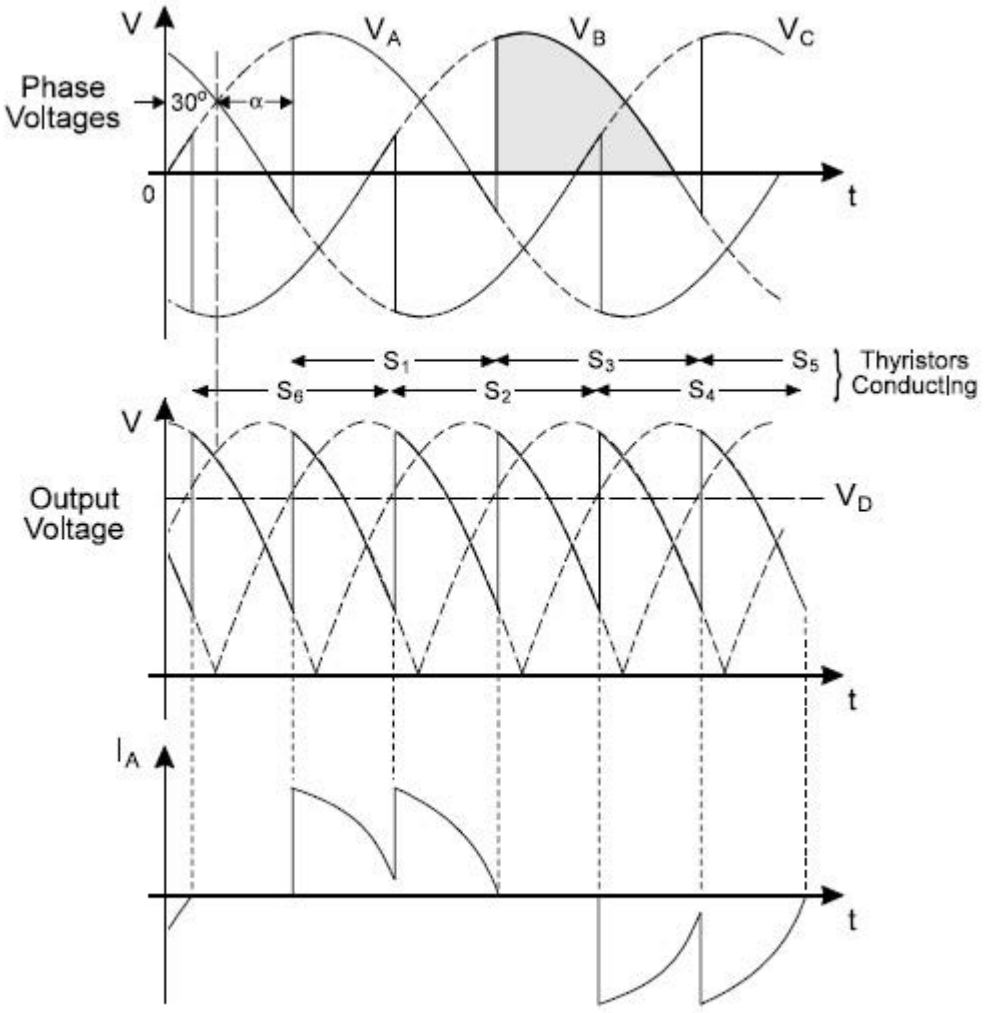

Fig.2.6. Voltage waveforms of a controlled rectifier

Most of AC/DC converters nowadays are controllable and are based on the fundamental description above. Some people all over the world have developed the AC/DC converter for better performance such as for step-up voltage conversions [2.35-2.37], step-down-only voltage conversions [2.38, 2.39], and also for step-up/down voltage conversions [2.40, 2.41]. Lung-Sheng Yang and Tsorng-Juu Liang have designed a novel three-phase buck-boost converter that operated in discontinuous conduction mode by using the PWM technique [2.42]. This converter can simply achieve purely sinusoidal input current, high power factor, low total

harmonic distortion (THD) of the input current, and step-up/down output voltage. Moreover, Dylan Dah-Chuan Lu proposed a single-stage AC/DC converter with high power factor, regulated bus voltage, and output voltage [2.43]. This power converter is formed by integrating a boost power factor correction converter, which is based on the concept in [2.44, 2.45], with a two-switch clamped flyback converter into a single power stage circuit.

Recently, Zhao et al [2.46] designed a new AC/DC/DC isolated converter with bidirectional power flow capability. This novel converter consists of a three-phase current source converter and a special DC/DC isolated converter. In this DC/DC converter, the primary side is a current source converter and the secondary side is a voltage source converter (VSC). Using a single switch to provide a bypass for the inductor current, the voltage spikes are reduced and the safety of current flow is realised. In addition, the direction of the current flow in the inductor remains the same in both the power and load modes.

2.4.1.2. DC/AC converters

To establish the principles of inverter circuits, Figure 2.7 below shows four semiconductor power switches feeding an inductive load from a single-phase supply.

This circuit can be considered to be an electronic reversing switch, which allows the input DC voltage V_D to be connected to the inductive load in any one of the following ways:

(1) S_1 = on, S_4 = on, giving $+V_D$ at the load

(2) S_2 = on, S_3 = on, giving $-V_D$ at the load

(3) S_1 = on, S_2 = on, giving zero volts at the load

S_3 = on, S_4 = on, giving zero volts at the load

(4) S_1 = on, S_3 = on, giving a short circuit fault

S_2 = on, S_4 = on, giving a short circuit fault

However, these four switches can be controlled to give a square waveform across the inductive load as shown in Figure 2.7.

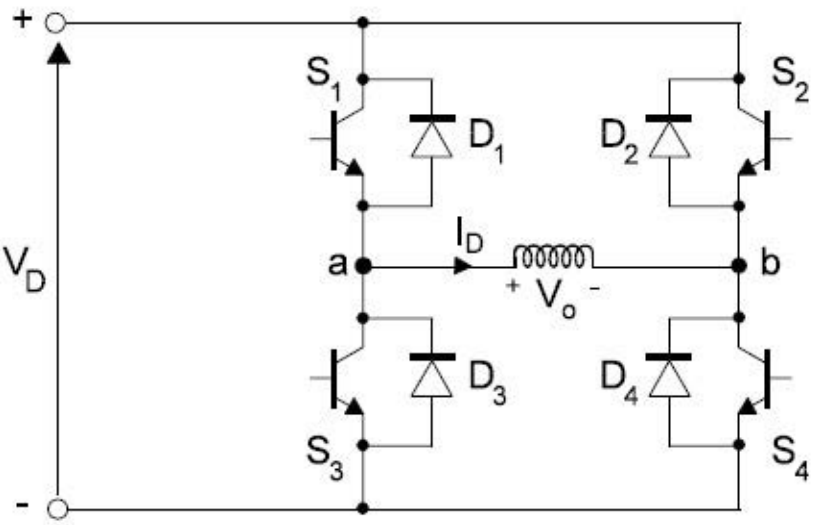

Fig.2.7. Single-phase DC to AC inverter

This makes use of switch configuration (1) and (2), but not switches configuration (3) or (4). Clearly, for continued safe operation, option (4) should always be avoided. In the case of a purely inductive load, the current waveform is a triangular waveform as shown in the Figure 2.8.

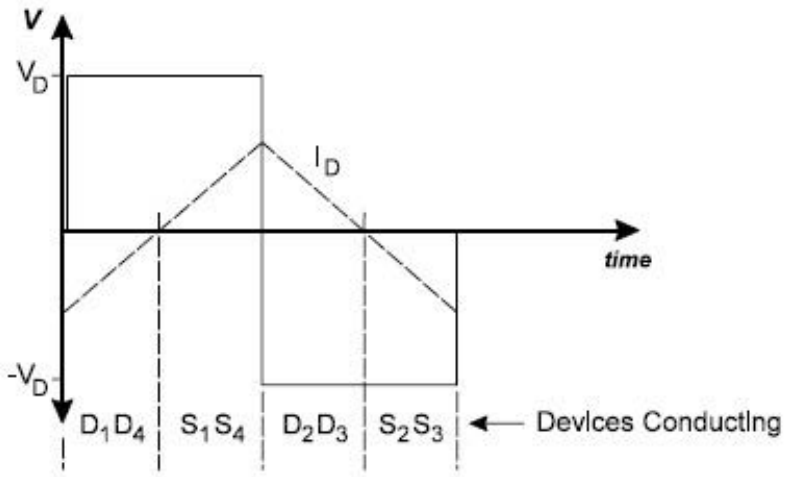

Fig.2.8. Square wave modulation waveforms

In the first part of the cycle, the current is negative although only switches S_1 and S_4 are on. Since most power-electronic devices cannot conduct negatively, to avoid damage to the switches, this negative current would have to be diverted around them. Consequently, diodes are usually provided in anti-parallel with the switches to allow the current flow to continue. These diodes are sometimes called *reactive* or *free-wheeling diodes* and conduct whenever the voltage and current polarities are opposite. This occurs whenever there is a reverse power flow back to the DC supply.

The frequency of the periodic square wave output is called the fundamental frequency. Using the Fourier analysis, any repetitive waveform can be resolved into a number of sinusoidal waveforms, comprising one sinusoid at fundamental frequency plus a number of sinusoidal harmonics at higher frequencies, which are multiples of the fundamental frequency. The harmonic spectrum for a single-phase square wave output is shown in the figure below. The amplitude of the higher order harmonics voltages falls off rapidly with increasing frequency.

This illustrates that the square wave output voltage has a lot of unwanted components of reasonably large magnitude at frequencies close to the fundamental. The current flowing in the load because of the output voltage is distorted, as demonstrated by the non-sinusoidal current wave-shape. In this example, the current has a triangular shape. If the square-wave voltage were presented to a single-phase induction motor, the motor would run at the frequency of the square-wave but, being a linear device (inductive/ resistive load), it would draw non-sinusoidal currents and would suffer additional heating due to the harmonic currents. These currents may also produce pulsating torques. If it is required to also control the magnitude of the output voltage, the average inverter output voltage can be reduced by inserting periods of zero voltage, using switch configuration (3) as shown in Figure 2.9.

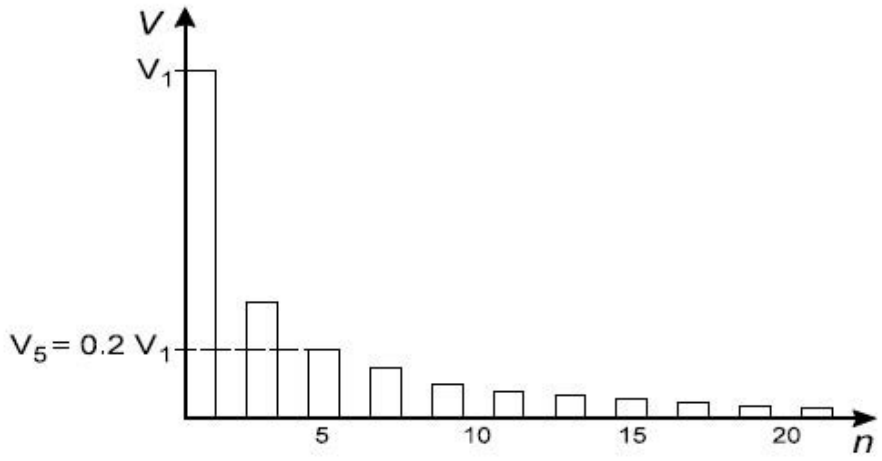

Fig.2.9. Square-wave harmonic spectrum

Each half cycle then consists of a square pulse that is only a portion of a half period as shown in the Figure 2.10 below.

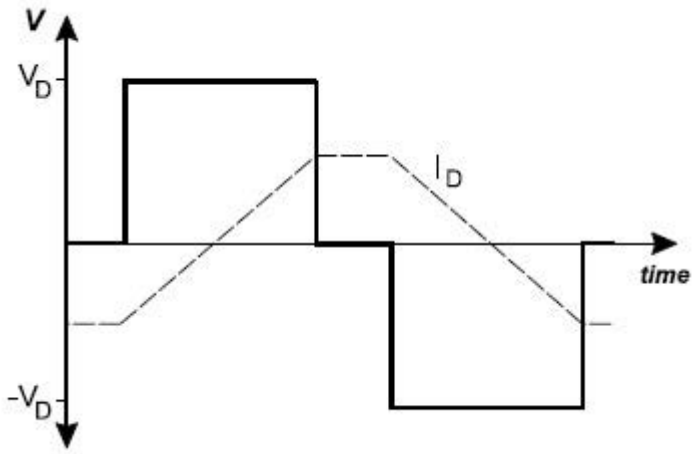

Fig.2.10. Square wave modulation with reduced voltage pulse width

The process of changing the width of the pulse to reduce the average RMS value of a waveform is called pulse width modulation (PWM). On the other hand, the ideal inverter output is one that results in a current waveform of low harmonic distortion. Since an AC induction motor is predominantly inductive, with a reactance

that depends on the frequency ($X_L = j2\pi fL$), it is beneficial if the voltage harmonic distortion can be pushed into the high frequencies, where the motor impedance is high and not much distorted current will flow. One technique for achieving this is *sine-coded pulse width modulation (sine-PWM)*. This requires the power devices to be switched at frequencies much greater than that of the fundamental frequency producing a number of pulses for each period of the desired output period. The frequency of the pulses is called the *modulation frequency*. The width of the pulses is varied throughout the cycle in a sinusoidal manner giving a voltage waveform as shown in Figure 2.11. This figure also shows the current waveform for an inductive load showing the improvement in the waveform.

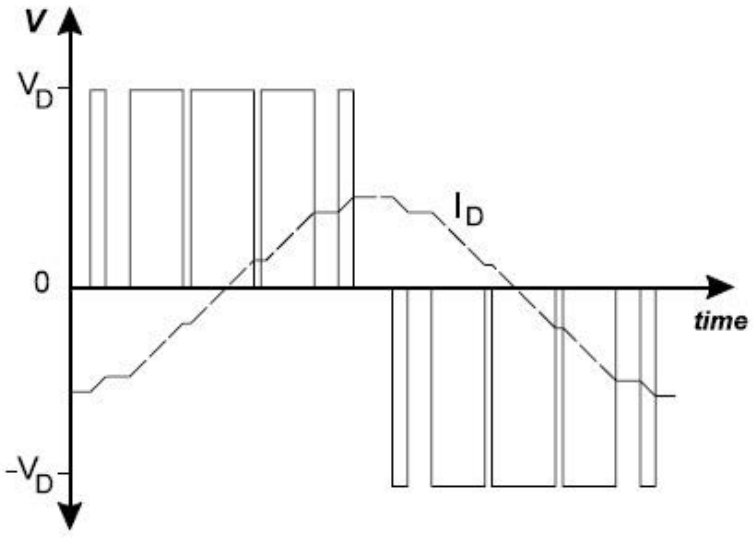

Fig.2.11. Sine-wave pulse width modulated voltage and current

Increasing the *modulation frequency* will improve the current waveform, but at the expense of increased losses in the switching devices of the inverter. Therefore, at low modulation frequencies, the losses in the inverter are low. At high modulation frequencies, the losses in the inverter increase.

One of the most common techniques for achieving sine-wave PWM in practical inverters is the sine-triangle intersection method shown in Figure 2.12. A triangular *saw-tooth* waveform is produced in the control circuit at the desired inverter switching frequency. This is compared in a comparator with a sinusoidal reference signal, which is equal in frequency and proportional in magnitude to that of the desired sinusoidal output voltage. The voltage V_{AN} (Figure 2.12(b)) is switched high whenever the reference waveform is greater than the triangle waveform. The voltage V_{BN} (Figure 2.12(c)) is controlled by the same triangle waveform but with a reference waveform shifted by 180°.

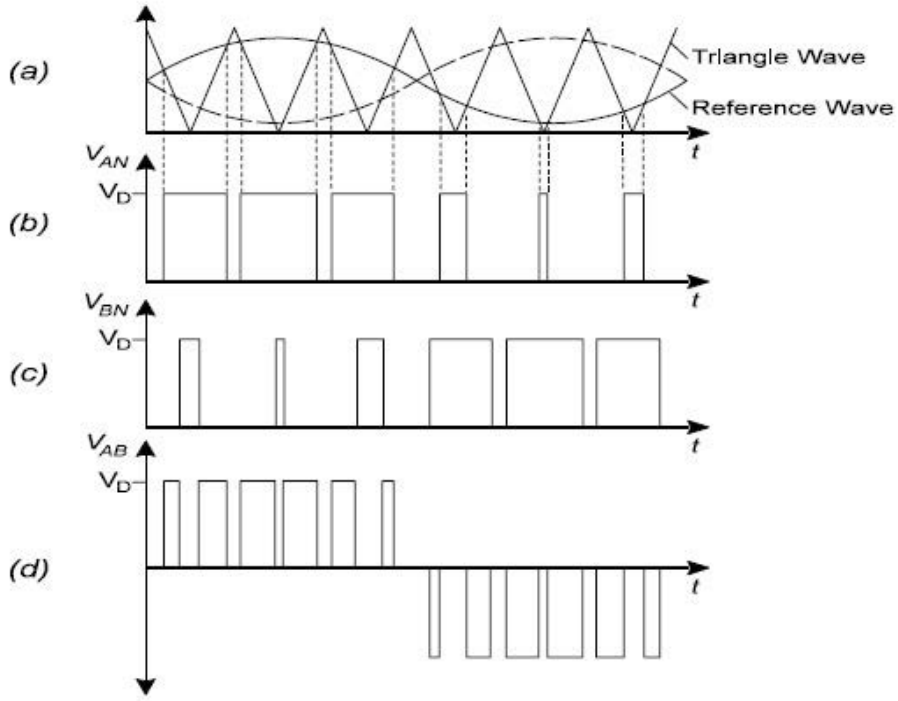

Fig.2.12. Principle of triangle intersection PWM

The technique using sine-triangle intersection is particularly suited for use with the older analogue control circuits, where the two reference waveforms were fed into a comparator and the output of the comparator was used to trigger the inverter switches. Modern *digital techniques* operate on the basis of a switching algorithm, for

example by producing triggering pulses proportional to the area under a part of the sine wave. In recent times, manufacturers have developed a number of different algorithms that optimize the performance of the output waveforms for AC induction motors. These techniques result in PWM output waveforms which are similar to those shown in Figure 2.12. The sine-coded PWM voltage waveform is a composite of a high frequency square wave at the pulse frequency (the switching carrier) and the sinusoidal variation of its width (the modulating waveform). It has been found that, for lowest harmonic distortion, the modulating waveform should be synchronised with the carrier frequency, so that is it should contain an integral number of carrier periods. This requirement becomes less important with high carrier frequencies of more than about twenty times the modulating frequency.

A three-phase inverter could be constructed from three inverters of the type shown in Figure 2.7. However, it is more economical to use a 6-pulse (three-leg) bridge inverter as shown in Figure 2.13.

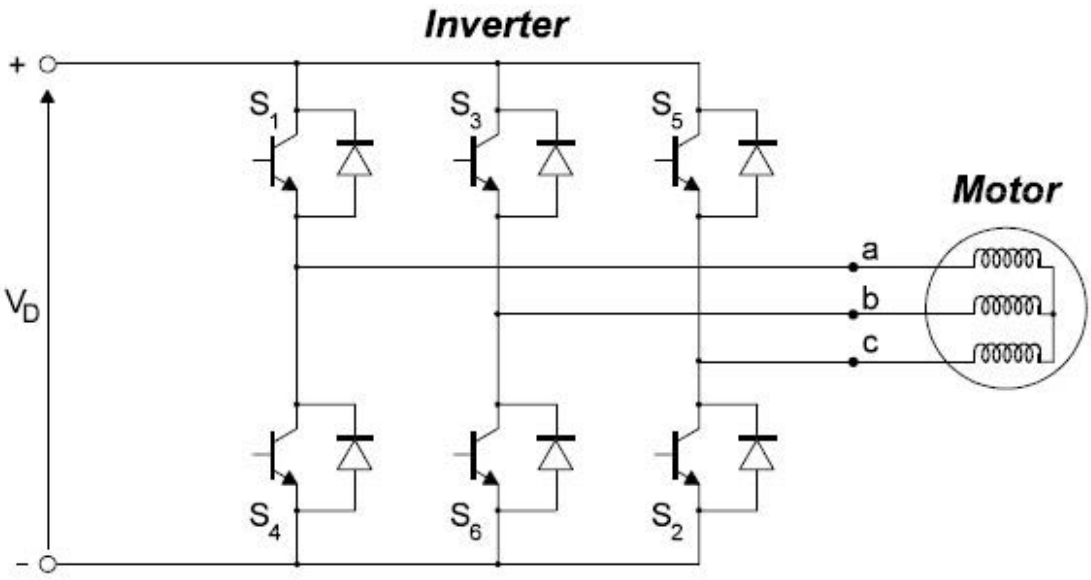

Fig.2.13. Three-phase inverter using gate controlled switches

The output voltage of a three-phase converter has a harmonic spectrum very similar to the single-phase square wave, except that the tripled harmonics (harmonics whose frequency is a multiple of three times the fundamental frequency) have been eliminated. In an inverter with a 3-phase output, this means that the third, 9th, 15th, and 21st, etc harmonics are eliminated. Manufacturers of AC frequency converters continue to work on the development of more efficient PWM algorithms in an attempt to improve the current waveform. The ultimate objective is a completely sinusoidal current, which produces no harmonic losses in the motor. These more advanced PWM algorithms have become possible because of the increased speed and power of microprocessors.

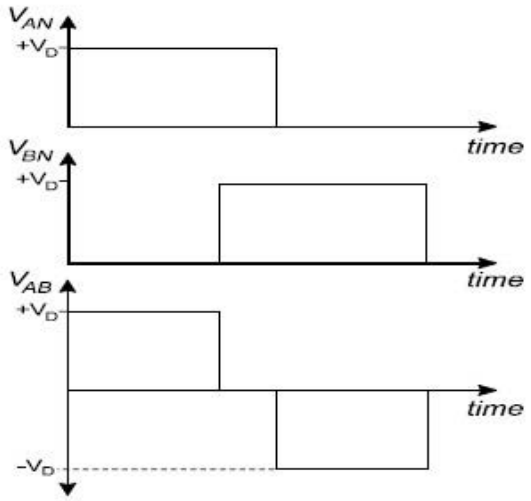

.

Fig.2.14. Quasi-square wave modulation output waveforms

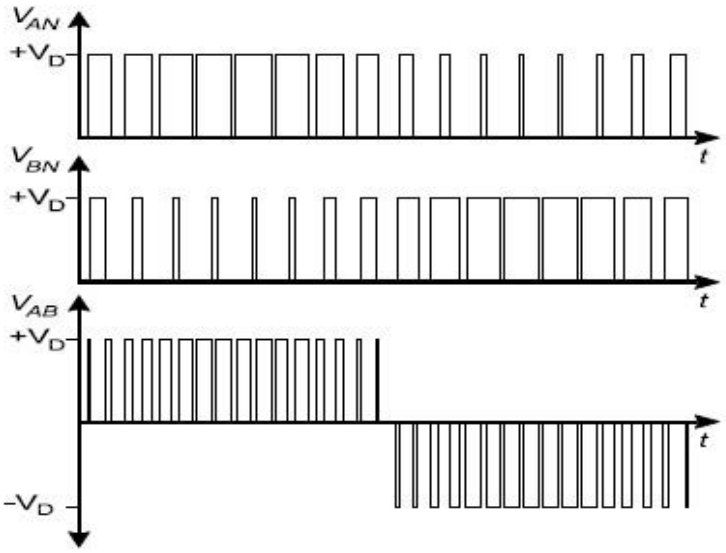

Fig.2.15. Output voltage waveform of a 3-phase sine coded PWM

The PWM DC/AC converter has been the main choice in the power electronics for a decade, because of its circuit simplicity and rugged control scheme. Typical applications for PWM DC/AC converter can be found in uninterruptible power systems, motor drives, and induction heating. Due to the switching losses and the limitations of semiconductor devices that are currently available, the switching frequency of PWM converter is usually around a few kilohertz when the power rating is tens of kilowatts. For that reason, a new inverter topology was developed; it gives either zero voltage or zero current during switching, to reduce switching power loss to a very low level. This new technique was soft.

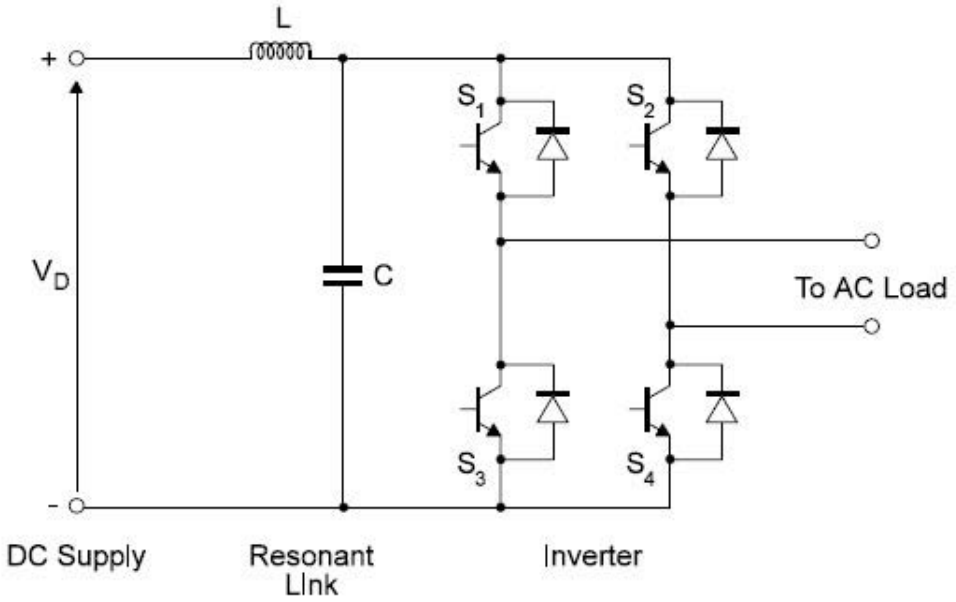

Fig.2.16. The topology of a single-phase resonant link soft-switch inverter

One of the possible designs for achieving this goal is the resonant link inverter, which is shown for a single-phase case in Figure 2.16. The front-end is identical to a normal hard switched inverter, except for the series inductor and shunt capacitor between the DC bus and the inverter stage. The circuit is controlled as follows:

- Assume that the capacitor is shortly discharged from the previous cycle of inverter operation.
- All inverter switches are turned ON at zero voltage, applying zero volts to the load and shorting out the capacitor. The inductor current then ramps up through the switches.
- When the inductor current reaches an appropriate level, one switch in each leg is opened (at zero voltage) to apply voltage to the load. The capacitor voltage then rings up to a value exceeding the supply while the

inductor current decreases. The oscillation continues with capacitor voltage now decreasing.

- When the capacitor voltage decreases to zero, the anti-parallel diodes clamp the capacitor voltage from going negative, in effect, placing a short-circuit across the capacitor and shortly discharging it.
- The process is repeated.

The supply across the inverter legs has the form of a series of pulses with the same waveform as the capacitor voltage as shown in Figure 2.17. The inverter legs must switch at one of the voltage zeros if the resonance is to be continued and low switching losses are to be achieved.

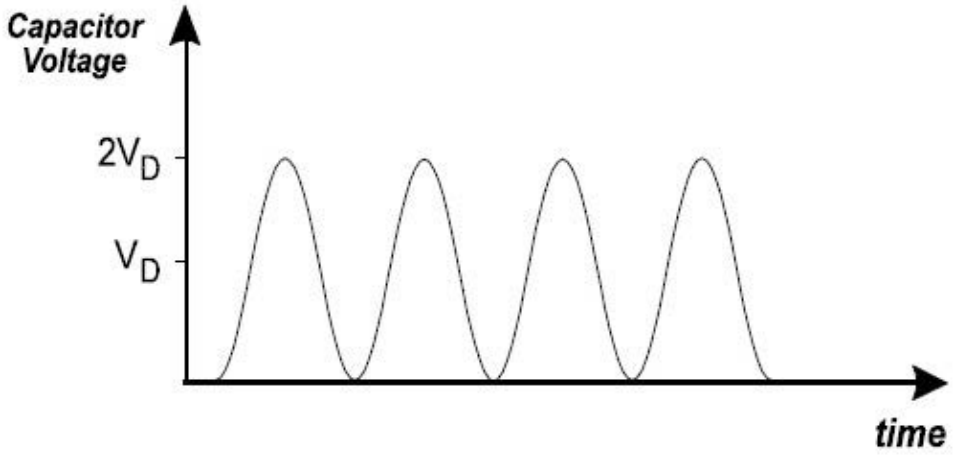

Fig.2.17. Resonant link inverter waveform at inverter leg

In the soft-switched topologies, a high-frequency resonant network is added to the conventional hard-switching PWM topology. The resonant network can be composed of only passive elements and or it can also have additional auxiliary diodes and/or switches. As a result, the switch voltage or current swings and crosses zero point, which thus creates the soft-switching conditions for the power devices.

Therefore, the switch waveforms are shaped by the resonant network such that the switching losses can be minimized, the switch stresses can be reduced, and EMI can be prevented. Therefore, depending on the chosen resonant network scheme, different shapes of voltage and current waveforms in the converter can be obtained. Based upon the location of the resonant network, soft-switching converters can be classified into three groups.

2.4.1.2.a. Load resonant DC–AC converter:

An LC resonant tank is added at the load side in a series, parallel, or in a combination of series and parallel LC schemes. Hence, the ZVS or ZCS condition can be produced for the active switches on the inverter bridge. The DC-bus waveform of the load resonant DC–AC converter is unaltered.

These converters can be generally classified as series resonant converters and parallel resonant converters. In series resonant topologies, the inverter bridge supplies a square-wave voltage to a resonant network that is connected in series with the inverter bridge. The load can be connected to the resonant network in series [2.47], parallel [2.48] or in a hybrid resonant configuration, such as series/parallel [2.49] parallel/series [2.50] and multi resonant [2.51]. In the parallel resonant converter, the inverter supplies a square-wave current into a resonant network that is connected in parallel with the inverter.

Since the resonant elements are connected in the main power transfer path, these converters suffer from high voltage and current ratings in every component. Because of this, series resonant converters have limitations at high power levels (at the 20-kHz/100-kW level, for example), due to the difficulty of implementing a compact, high-efficiency high-power resonant inductor [2.52]. However, load resonant converters can provide excellent output regulation by tuning the load closely to the

resonant frequency. In this case, the load power factor approaches one, and the voltage and current ratings of the power devices can be minimized, when compared to the un-tuned load case using PWM. However, if one is interested in extracting low-frequency AC from a high-frequency switched signal at the output of a DC–AC converter, it is convenient that the resonant network does not take part in the main power flow, and it is activated only as a means of creating the soft switching conditions during the switch state changes.

2.4.1.2.b. Resonant transition DC–AC converter

A resonant network is added to the inverter bridge, thereby creating the ZVS or ZCS conditions. The characteristic of the switches can also be part of the resonant scheme. The input DC bus is not altered.

In resonant transition DC–AC converters, the input bus voltage or current is fixed. The soft-switching condition is implemented by resonating the voltage and/or current of the inverter switches. Ideally, the resonant network should be activated only during the switching transition intervals, should make the resonance circulating energy be as low as possible and completely decoupled from the main power transfer to the load. The resonant network should operate according to the controller commanding signals, which are usually provided by a PWM-type controller. It is shown that the concepts of quasi-resonant [2.53-2.55] , resonant snubber [2.56] and soft-transition PWM conversion [2.57, 2.58] [zero-voltage transition and zero-current transition] are closely related, and that can be generally termed as resonant transition when they are applied to DC–AC conversion.

2.4.1.2.c. Resonant link DC–AC converter

The resonant network is connected between the input DC source and the inverter bridge. Thus, the input bus is oscillating in order to create the soft-switching conditions for the power devices. Therefore, the input buses of these resonant link converters are different from the conventional PWM system.

The resonant link DC–AC converters shift the resonant network from the inverter bridge to the DC bus. Depending on the resonant network configuration and the switching scheme, the resonant link DC–AC converters can be divided into two types:

- *Resonant AC-link DC–AC converter* - The link waveform can be either an alternating voltage or alternating current, in order to create ZVS or ZCS conditions for the inverter bridge. Hence, bidirectional switches should be used [2.59, 2.60]; and
- *Resonant DC-link DC–AC converter* - The link is a DC-biased oscillating waveform, whereby unidirectional switches can be implemented in the inverter bridge and with zero-voltage source or zero-current source conditions [2.61-2.65].

2.4.1.3. AC/AC converter

AC converter is that special type of converter that converts AC, of one voltage and frequency, to AC of another voltage and frequency, which are often variable. An AC frequency converter is a special type of AC converter.

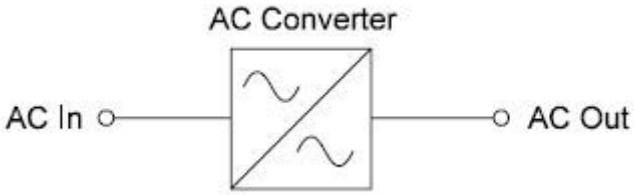

Fig.2.18. AC/AC converter

In a power electronic AC converter, it is common to use an intermediary DC link with some form of smoothing.

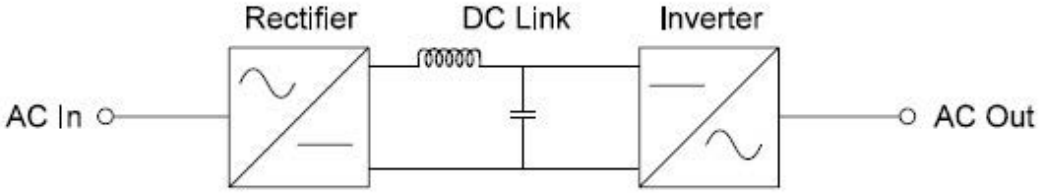

Fig.2.19. AC/DC/AC converter

A mains-friendly AC–AC converter with bidirectional power flow can be implemented by coupling the DC-link of a PWM rectifier and a PWM inverter. The DC-link quantity is then impressed by an energy storage element that is common to both stages: a capacitor C_{DC} for the voltage DC-link back-to-back converter (V-BBC) or an inductor L_{DC} for the current DC-link back-to-back converter (C-BBC).

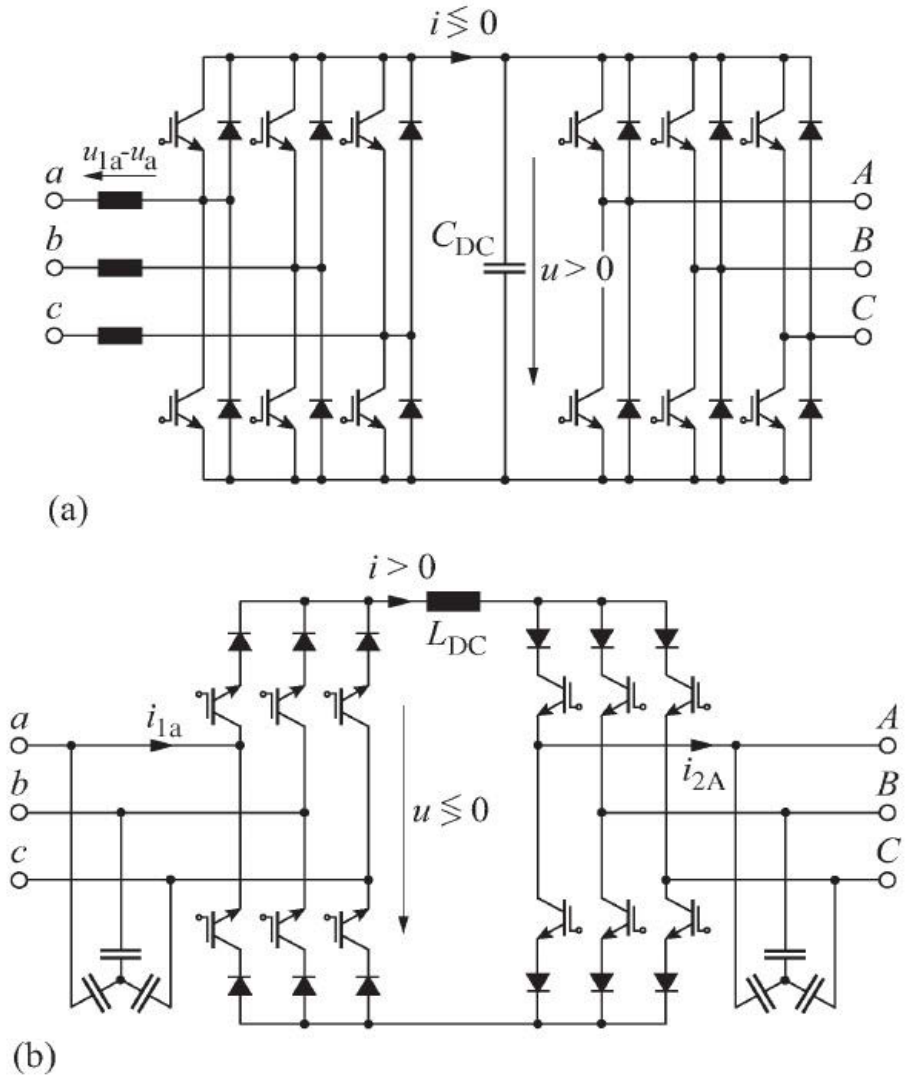

Fig.2.20. Basic three-phase AC–AC converter topologies with DC-link energy storage. (a) Voltage DC-link, (b) Current DC-link back-to-back converter

Due to the DC-link energy storage element, there is an advantage that both converter stages are, to a large extent, decoupled regarding their control for a typical sizing of the energy storage. Furthermore, a constant mains-independent input quantity exists for the PWM inverter stage, which results in a high utilization of the converter's power capability. On the other hand, the DC-link energy storage element can have a relatively large physical volume compared with the total converter volume, and when electrolytic capacitors are used for the DC-link of the V-BBC, the service

lifetime of the converter can potentially be reduced. In the case of the V-BBC, the PWM inverter stage is considered, and for the C-BBC, the PWM rectifier stage is considered [2.66, 2.67].

At first, all AC converter designs contain energy storage elements, such as inductance and capacitance, as well as the semiconductor power switches. The energy storage components result in extra losses, are bulky, and contribute to unreliability. The matrix converter attempts to eliminate these storage devices. The concept is very simple, consisting of a matrix of switches joining each of the three input lines to an output line. The output voltage waveform is made up of sections of the input as shown in the Figure 2.21 below. It has been demonstrated that the circuit can operate in all four quadrants with an input line current of any desired power factor.

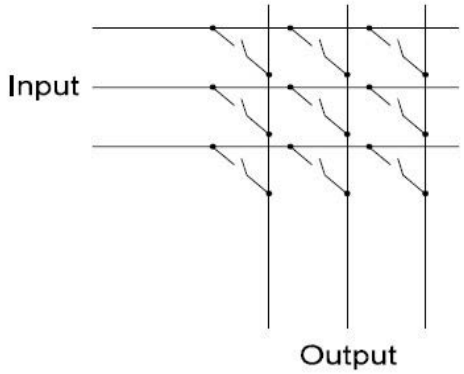

Fig.2.21. Matrix converter connection circuit

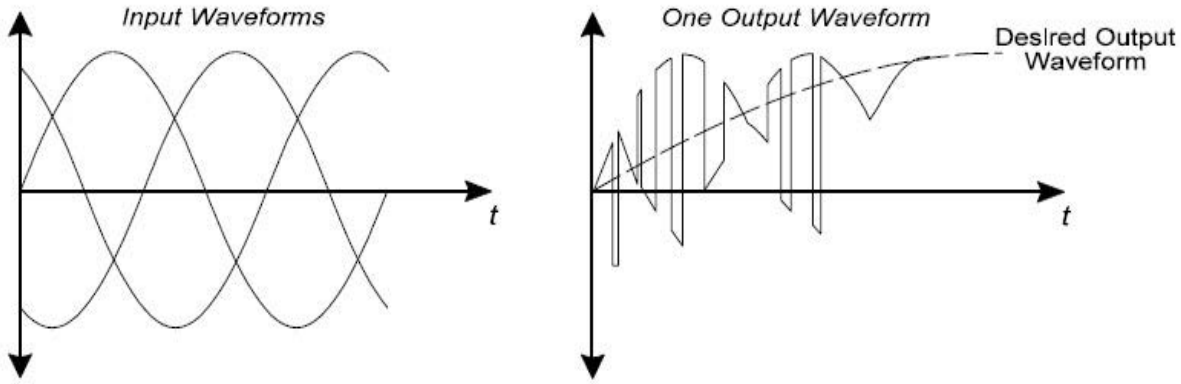

Fig.2.22. The input and output voltage waveforms of the matrix converter

2.4.1.4. DC/DC converter

DC converter is one that converts DC of one voltage to DC of another voltage.

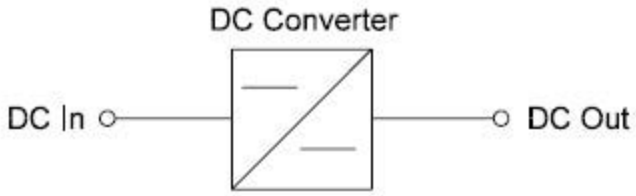

Fig.2.23. DC/DC converter

In a DC converter, it is common to use an intermediary AC link, usually with galvanic isolation via a transformer.

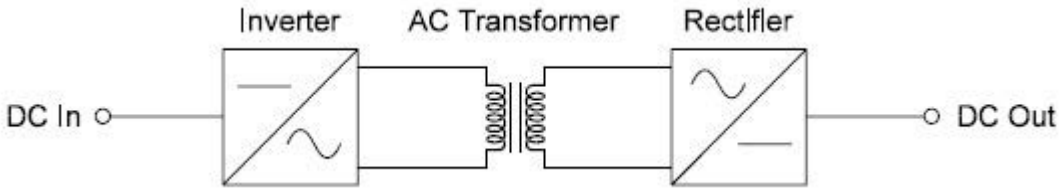

Fig.2.24. DC/AC/DC converter

2.4.1.5. Grid-connected power converters

Most of control methods for DGs nowadays use power converters as the interfaced devices not only to integrate RESs with power grid but also to approach different goals in controlling voltage or current of the grid. Here are some papers with different strategies to control these converters.

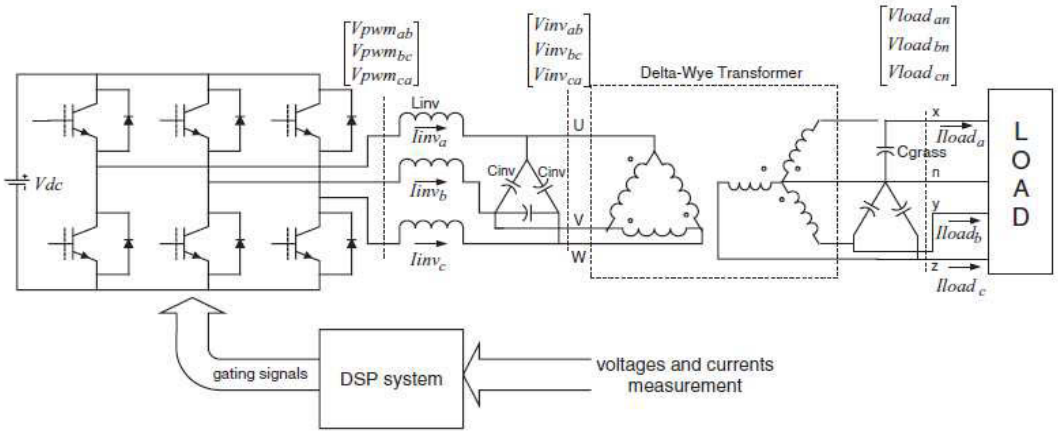

Fig.2.25. Power converter system

First of all, a controller with optimization methods was designed to stably coordinate multiple inverter-interfaced distributed generators and to control individual inverters against voltage and frequency disturbance on the island mode [2.68]. The DG controllers are composed of two controllers: DG coordination controllers and inverter-output controllers. The coordinate controllers need to calculate the output power references, whereas the inverter controllers should control the inverter-output voltage. Another method to control the voltage and current of the grid is the perfect robust servomechanism problem theory, which has been widely used all over the world [2.69-2.71], and a discrete-time sliding mode current controller. This method (seen in figure 2.25 above) consists of a typical three-phase PWM voltage inverter with *LC* output filter and a delta-wye transformer that acts both as a potential

transformer and electrical isolation to the load. A digital signal processor (DSP) system controls the operation of the power converter, providing required PWM gating signals to the power devices. In conclusion, this paper outlined the development of a digital control strategy for PWM inverters in DG systems. The power converter, as can be seen, can be used as not only as a controller but also as a grid-interfaced device.[2.72, 2.73]. Both of the two papers referenced above, [2.72, 2.73], propose a grid-interfacing power quality compensator with two inverters connected in shunt and series. The control of shunt inverter contains internal voltage/current regulation loops and external power control loops, which control real and reactive power flow by producing the desired command frequency ω, phase δ and positive-sequence voltage magnitude E. The series inverter is expected to supply zero real and reactive power to the grid system as it injects only negative-sequence voltage along the feeder, which now conducts only positive-sequence currents. This is a new grid-interfacing power quality compensator to be used with individual DG systems in a micro grid. To improve this research, another tasks will be considered, the stabilising of *V* and *f,* and application in WT sources, where the input power fluctuated wildly.

An overview, that consists of the main Distributed power generation system structures, PV, fuel cell system and WT as well, was introduced to provide an all-rounded look about the DG system [2.74]. About grid-side, the controller has some main tasks: control of active power generated to the grid, reactive power transfer between the DGs and the grid; control of DC-link voltage; ensure high quality of the injected power; grid synchronization. Then the converter consists mainly of two loops, current loop and voltage loop or power loop and voltage loop. Some power quality considerations and also some different implementation structures like *dq* and stationary and natural frame control structures were also mentioned [2.74]. In

addition, a conventional PI-controller, which was used for the boost DC/DC converters, was designed [2.75]. Beside that, a *d-q* transformer two-loop current control scheme is presented for the space vector PWM based inverter to control power delivered from the PV cell power system to the grid. A space vector PWM controller is designed for the inverter to satisfy voltage regulation. The input and output are DC rather than sinusoidal quantities, hence, enabling the controller to obtain a complete elimination of phase error between the reference and controlled currents.

2.4.1.6. Renewable energy storage control

Renewable energy, especially wind power and solar energy are not load following. The utilization of energy and power in industry, working and living may often be in at a different time of day compared to the available period of renewable energy, which is particularly true with wind energy that tends to be more available during off-peak hours in Europe. If, at some times, the grid cannot absorb the entire output of the generator, then output must be curtailed and the value of the excess power is effectively zero [2.76]. However, at other times, demand is so high that expensive generators are used to meet that demand then the price will be high as a result. Therefore, the storage of energy and power becomes a critical issue in the future, where renewable energy provides the major power supply for meeting a variety of needs.

The traditional objective of direct electricity storage was to optimize the match between demand and generation in a power plant but in the future, maybe this method will be essential and critical. For that reason, renewable energy needs to be stored as electricity or other forms of energy such as hydrogen, fuel, etc. [2.77, 2.78] in order to provide electricity needed without time restriction.

However, with the rising proportion of renewable energy nowadays, electricity storage such as batteries, capacitors… are facing some technical problems to match not only periods but also capacity. For example, the size of a central station wind farm was more than 2 MW, and lead-acid batteries have been used for many years and the maximum energy storage has reached 40MWh and this number with sodium sulphur batteries is 57 MWh in 2008 [2.77]. Increasing the capacitor of energy storage will be more difficult than investigating a novel method to control the micro grid that includes DGs, local loads and energy storages.

2.5. POWER FLOW CONTROL THEORY

The DG unit above consists of a DC bus powered by any DC source or AC source with a rectifier, a voltage source inverter (VSI), an *LC* filter stage, and a delta/*Y* type isolation transformer with secondary side filtering. The DG unit has a local load, linear or nonlinear, and is connected to the utility grid through a three-phase static switch. In island mode, the inverter conducts voltage control, where the load voltage V_{ABC} should track the given reference. In grid-connected mode, the DG unit conducts power control, where the output active power P and reactive power Q from the DG unit to the utility grid should be regulated to desired values P_{ref} and Q_{ref}.

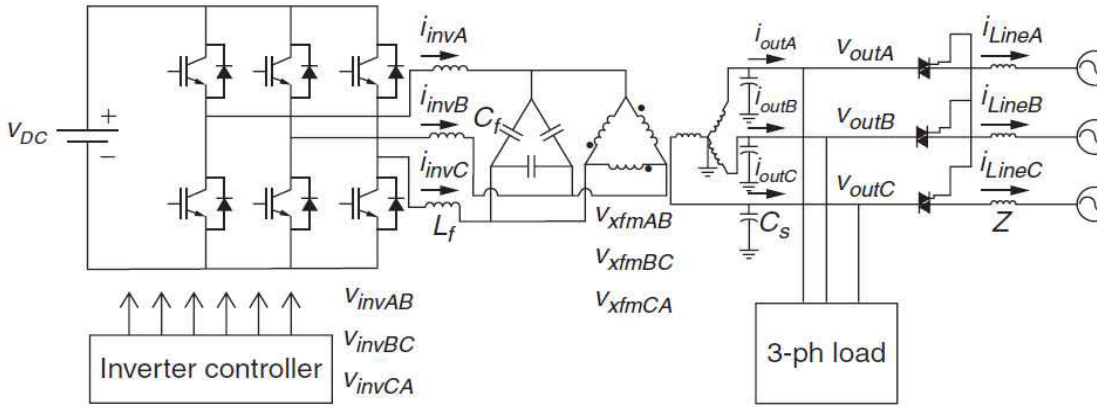

Fig.2.26. A grid-connected DG unit with local load.

With inverter control, both active and reactive power pumped into the utility grid from the DG units can be controlled. The proposed approach achieves decoupled *P* and *Q* control under grid-connected mode; an integral approach to conduct the power flow control has been developed to control *P* by adjusting the power angle and control *Q* by adjusting the filter capacitor voltage [2.79, 2.80]. It was indicated that both *P* and *Q* are affected by only adjusting one of *V* and δ (power angle) , which is so called coupling between *P* and *Q*. However, variations of *V* and δ have different levels of impact on *P* and *Q* as described in each paper.

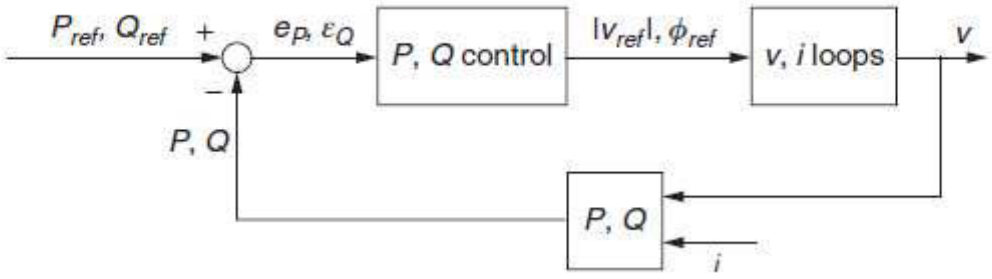

Fig.2.27. Block diagram of P, Q control.

In 1987, Kalaitzakis *et al* [2.81] first introduced the power control concept for synchronous generator paralleled with power system into the application of grid connected inverters, which states that active power P can be controlled by adjusting the phase angle of output voltage and reactive power Q can be controlled by adjusting the magnitude of output voltage. Since then, Chandorkar *et al.* [2.9] have developed an inverter control technique for line-interactive operation where P and Q can be separately controlled through closed-loop control, and Sedghisigarchi *et al.* [2.82] have performed a simulation research on P and Q dynamic control under reclosing operating condition although its control strategy is inadequately addressed and the transient response is slow.

Illindala *et al.* [2.11] presented a different power control strategy based on frequency and voltage drop characteristics of power transmission, which allows decoupling of and at steady state. In this method, power regulation errors are used to generate output voltage phase angle and magnitude changes respectively, which decouples and controls in steady state. Unfortunately, the presented simulation result does not show a satisfactory performance in response time which could be caused by low feedback gain and implies that higher gain may cause problems.

Since the DG unit uses a VSI with a strong voltage control, its output active and reactive power are determined by the unit's output voltage, including magnitude and phase angle, as stated in

$$P = E(V_{out} \sin\delta) / X \tag{2-1}$$

$$Q = \left(V_{out}^2 - V_{out} E \cos\delta\right) / X \tag{2-2}$$

where V_S is the equivalent main voltage, X is the equivalent line reactance where the resistance is ignored, and δ is the power angle – the phase angle difference between

V_{out} and E. Since the DG already exists, the task of the power controller is to generate the voltage command for the voltage controller based on the desired power value P_{ref} and Q_{ref} and actual value P and Q as illustrated in Fig. 3 above.

It is apparent that the desired DG unit output voltage V and the power angle δ can be calculated from (2-1) and (2-2) given desired P and Q values and system parameter X. If this is true, the power control problem is solved. However, in practical systems, the above approach is not feasible based on the existing techniques due to the following three reasons:

- Equations (2-1) and (2-2) show that the power system parameters, both *X* and *E* need to be known to solve the equations, which is difficult based on the existing approaches. Practically, the value of *X* may change due to the operation of the power system.
- Both *P* and *Q* are sensitive to variation of *X* since it appears in the denominators and especially when *X* is small. The greater the difference between the power system capacity and the DG's power rating, the less the value of *X* could be.
- Both equations are nonlinear and are difficult to solve in real time, which prevents the idea being implemented in practice.

Therefore, power control solutions requiring knowledge of *X* have not been practically used, and people tend to search for other solutions, which is an integral method. It can be observed from (2-1) and (2-2) that both *P* and *Q* will be affected by only adjusting one of *V* and δ and we have different levels of impact on *P* and *Q* as described in the following partial derivatives

$$\frac{\partial P}{\partial \delta} = \frac{V_{out}.E}{X} cos\,\delta \tag{2-3}$$

$$\frac{\partial P}{\partial V_{out}} = \frac{E}{X} sin\,\delta \tag{2-4}$$

$$\frac{\partial Q}{\partial \delta} = \frac{V_{out}.E}{X} sin\,\delta \tag{2-5}$$

$$\frac{\partial Q}{\partial V_{out}} = \frac{2V_{out} - Ecos\delta}{X} \tag{2-6}$$

With normalized *V, E* and *X,* it can be observed from (2-3)-(2.6) that, when $|\delta|$ is small and *V* is close to 1 which is true for large capacity power systems, $\partial P/\partial \delta$ is close to 1 and $\partial P/\partial V_{out}$ is close to 0 and conversely, $\partial Q/\partial \delta$ is close to 0 and $\partial Q/\partial V_{out}$ is close to 1. This fact indicates that P is more sensitive to δ and Q is more sensitive to V_{out}especially when the DG unit is connected to a large capacity system where the power angle δ is usually small. The different levels of sensitivity of *P* and Q to δ and V_{out} provide a chance to control *P* and Q relatively independently, not completely independently though. Based on the above analysis, an integral approach to conduct the power flow control can be developed to control *P* by adjusting δ and control Q by adjusting V_{out}. If the phase angle associated with the system voltage *E* is assumed to be 0, $\delta = \phi$ holds, where ϕ is the phase angle associated with is V_{out}. The voltage and phase angle references can be generated as

$$\phi_{ref} = \int \left(K_p \left(P_{ref} - P \right) + \omega_n \right) dt + \phi_0 \tag{2-7}$$

$$V_{ref} = \int K_Q \left(Q_{ref} - Q \right) dt + V_0 \tag{2-8}$$

where $\omega_n = 2\pi.60rad/s$ is the system nominal angular frequency, ϕ_0 and V_0 are the initial voltage and phase angle at the moment that the DG unit is connected to the grid from island mode. The integral power controller is illustrated in Fig. 2.28.

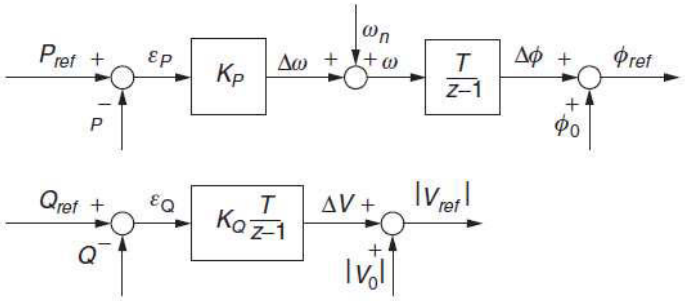

Fig.2.28. Power regulator for P and Q.

However, in recent years, as discussed earlier, the greatest potential market for DG is to enhance its important role in energy industry by creating more microgrids so as to minimize the transmission and distribution losses. Thus, the technologies for both energy storages and load following control in a microgrid are more promising than for one power grid of a state or a nation. However, this method requires its own control technique to maintain the stabilization of the frequency and power flow of the grid regardless of wild fluctuation of the wind and solar energy. Modern technology has made just a little study in this promising field of renewable energy [2.79, 2.83].

Several control schemes have been proposed for the power flow control of the microgrid converter. The classic linear controllers, which include two common methods, voltage oriented control (VOC) and direct control, have been the widely employed control strategies for power converters. Later on, more complex control techniques, such as fuzzy logic, and predictive control, were developed with the rapid evolution of digital signal processing capacity.

2.5.1. Voltage oriented control

Fig. 2.29 shows the classic block diagram of VOC. Since the line current vector, $i = i_d + ji_q$ is aligned with the phase voltage vector, $v = v_d + jv_q$, of the power line supplying the converter, the stationary *abc* system is transformed into the

dq system, and the active and reactive power of the converter output can be controlled by adjusting the reference value , i_d* and i_q*, of the quadrature component of i, [2.84, 2.85]. The current references are compared with the actual values, and the errors are then delivered to the proportional-integral (PI) controllers to produce the voltage references. Finally, the switching signals for individual phases of the rectifier are generated by a classic space vector modulator (SVM). VOC has various advantages including fixed switching frequency and being insensitive to the line inductance variation. However, the requirement of the decoupling term between active and reactive components and PI regulators results in a complex algorithm and compromised transient performance.

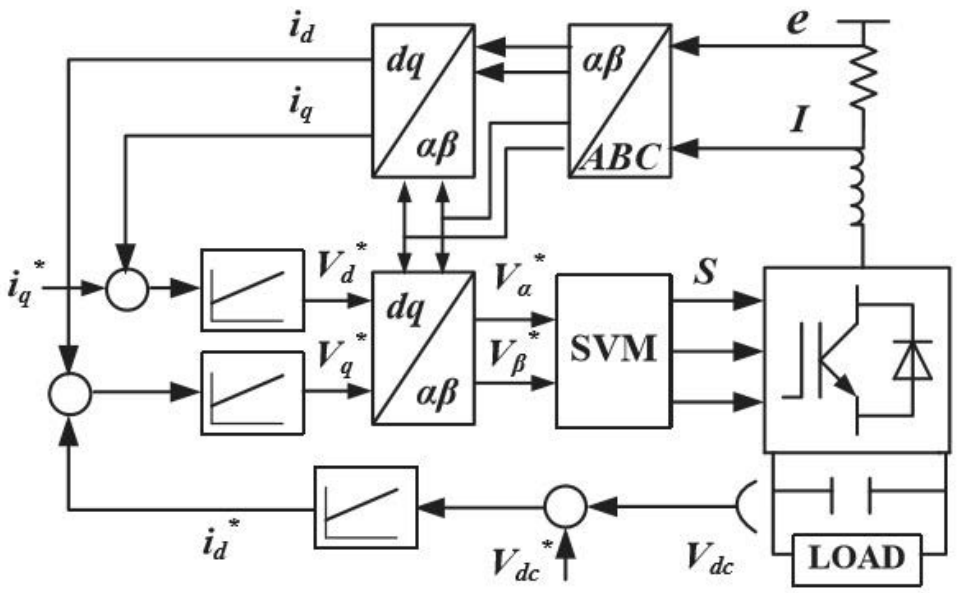

Fig.2.29. Block diagram of VOC

2.5.2. Direct power control

Another control method using linear control is direct power control (DPC). Among the existing direct control methods for power converter control, the DPC is one of the most commonly used methods. The conventional switching table-based

direct power control (SDPC) is derived from the original direct torque control (DTC) for AC machine drives [2.86, 2.87], and has now become one of the most popular control strategies, because of its excellent transient performance, robustness, and simplicity. In the SDPC, the converter switching states are determined using a switching table, which is built up from the output signals of hysteresis active and reactive controllers as well as the position of grid voltage vector or virtual-flux vector [2.88-2.94]. The referenced active and reactive power, P^* and Q^*, are delivered to two fixed bandwidth hysteresis comparators using the tracking errors between the estimated and referenced values of active and reactive power. The converter switching states are selected from a look-up switching table according to generated *dQ, dP* and the position of power source voltage, which is located in an α-β plane of 12 sectors. This algorithm is implemented in the stationary reference frame without involving any modulations or transformation systems. The major drawbacks are the variable switching frequency and large power ripples, and a high sampling frequency is required to obtain a satisfactory performance.

2.5.3. Fuzzy logic control

Fuzzy logic control has adaptive characteristics in nature, and can achieve robust response to a system with uncertainty, parameter variation, and load disturbance. It has been broadly used in the field of power electronics. Compared to the SDPC, this method selects the converter switching states by means of fuzzy logic rules using instantaneous errors of active and reactive power, εP and εQ, respectively.

2.5.4. Model predictive control

Recently, the concept of predictive control emerged as an attractive alternative for the control of electrical machines and power converters. Several kinds of control

methods have been developed under the name of predictive control. The most important types are the deadbeat control, model predictive control (MPC) and vector-sequence based predictive control (VPC). The deadbeat control uses a system model to predict the required reference voltage once every sampling period. This voltage is then generated using a modulator [2.95-2.103]. In the MPC, a system model is used to predict the behaviour of the variables over a certain time horizon, and a cost function is used as the criterion to select the optimal switching states [2.104-2.110]. The principle of the vector based predictive control is to force the system variables onto the pre-calculated trajectories, where several voltage vectors are typically used within each sampling period [2.111-2.117]. More recently, several multi-objective model-predictive control methods are also studied and applied for microgrid with PVs as well as WTs [2.118].

This thesis focuses on traditional VOC and MPC which will be present in the coming chapters.

2.6. CONCLUSION

This chapter reviewed the Vietnamese current power scheme, the characteristics to define a smart microgrid along with several control techniques that can be applied for a smart microgrid. It should be noted that Vietnam has a great potential of RESs, therefore smart microgrid is a very promising topic for researchers. A new smart microgrid structure will be proposed in Chapter 3 with several case studies for various Vietnamese scenarios. This literature review also highlighted the power flow control techniques for grid-connected inverters that will be further developed in the upcoming chapters.

REFERENCES

[2.1] R. H. Lasseter, "MicroGrids," in *Power Engineering Society Winter Meeting, 2002. IEEE*, 2002, pp. 305-308 vol.1.

[2.2] D. Guezgouz, D. E. Chariag, Y. Raingeaud, and J. C. Le Bunetel, "Modeling of Electromagnetic Interference and PLC Transmission for Loads Shedding in a Microgrid," *Power Electronics, IEEE Transactions on,* vol. 26, pp. 747-754, 2011.

[2.3] W. Fei, J. L. Duarte, and M. A. M. Hendrix, "Grid-Interfacing Converter Systems With Enhanced Voltage Quality for Microgrid Application 2014;Concept and Implementation," *Power Electronics, IEEE Transactions on,* vol. 26, pp. 3501-3513, 2011.

[2.4] S. Bolognani and S. Zampieri, "Distributed control for optimal reactive power compensation in smart microgrids," in *Decision and Control and European Control Conference (CDC-ECC), 2011 50th IEEE Conference on*, 2011, pp. 6630-6635.

[2.5] G. Mine, R. Borer, F. Kupzog, and H. Nishi, "Construction method of dynamic microgrid by using optimized grouping method," in *Industrial Informatics (INDIN), 2010 8th IEEE International Conference on*, 2010, pp. 780-785.

[2.6] L. Xiong, W. Peng, and L. Poh Chiang, "A Hybrid AC/DC Microgrid and Its Coordination Control," *Smart Grid, IEEE Transactions on,* vol. 2, pp. 278-286, 2011.

[2.7] J. M. Guerrero, J. C. Vasquez, J. Matas, V. de, x00F, L. G. a*, et al.*, "Hierarchical Control of Droop-Controlled AC and DC Microgrids 2014;A

General Approach Toward Standardization," *Industrial Electronics, IEEE Transactions on,* vol. 58, pp. 158-172, 2011.

[2.8] B. Enayati, A. K. Ziarani, and T. H. Ortmeyer, "An intelligent power flow controller for autonomous operation of islanded micro-grids," in *Industrial Electronics, 2008. IECON 2008. 34th Annual Conference of IEEE*, 2008, pp. 3033-3038.

[2.9] M. C. Chandorkar, D. M. Divan, and R. Adapa, "Control of parallel connected inverters in standalone AC supply systems," *Industry Applications, IEEE Transactions on,* vol. 29, pp. 136-143, 1993.

[2.10] A. P. S. Meliopoulos, G. Cokkinides, H. Renke, E. Farantatos, C. Sungyun, L. Yonghee*, et al.*, "Smart Grid Technologies for Autonomous Operation and Control," *Smart Grid, IEEE Transactions on,* vol. 2, pp. 1-10, 2011.

[2.11] M. Illindala and U. Venkataramanan, "Control of distributed generation systems to mitigate load and line imbalances," in *Power Electronics Specialists Conference, 2002. pesc 02. 2002 IEEE 33rd Annual*, 2002, pp. 2013-2018.

[2.12] M. Illindala and G. Venkataramanan, "Control of distributed generation systems to mitigate load and line imbalances," in *Power Electronics Specialists Conference, 2002. pesc 02. 2002 IEEE 33rd Annual*, 2002, pp. 2013-2018.

[2.13] R. Tirumala, N. Mohan, and C. Henze, "Seamless transfer of grid-connected PWM inverters between utility-interactive and stand-alone modes," in *Applied Power Electronics Conference and Exposition, 2002. APEC 2002. Seventeenth Annual IEEE*, 2002, pp. 1081-1086 vol.2.

[2.14] G. Escobar, P. Mattavelli, A. M. Stankovic, A. A. Valdez, and J. Leyva-Ramos, "An Adaptive Control for UPS to Compensate Unbalance and Harmonic Distortion Using a Combined Capacitor/Load Current Sensing," *IEEE Transactions on Industrial Electronics,* vol. 54, pp. 839-847, 2007.

[2.15] R. Majumder, A. Ghosh, G. Ledwich, and F. Zare, "Load sharing and power quality enhanced operation of a distributed microgrid," *IET Renewable Power Generation,* vol. 3, pp. 109-119, 2009.

[2.16] L. Yunwei, D. M. Vilathgamuwa, and L. Poh Chiang, "Microgrid power quality enhancement using a three-phase four-wire grid-interfacing compensator," *IEEE Transactions on Industry Applications,* vol. 41, pp. 1707-1719, 2005.

[2.17] S. Engelhardt, I. Erlich, C. Feltes, J. Kretschmann, and F. Shewarega, "Reactive Power Capability of Wind Turbines Based on Doubly Fed Induction Generators," *IEEE Transactions on Energy Conversion,* vol. 26, pp. 364-372, 2011.

[2.18] A. Camacho, M. Castilla, J. Miret, J. C. Vasquez, and E. Alarcon-Gallo, "Flexible Voltage Support Control for Three-Phase Distributed Generation Inverters Under Grid Fault," *IEEE Transactions on Industrial Electronics,* vol. 60, pp. 1429-1441, 2013.

[2.19] N. Pogaku, M. Prodanovic, and T. C. Green, "Modeling, Analysis and Testing of Autonomous Operation of an Inverter-Based Microgrid," *IEEE Transactions on Power Electronics,* vol. 22, pp. 613-625, 2007.

[2.20] E. Barklund, N. Pogaku, M. Prodanovic, C. Hernandez-Aramburo, and T. C. Green, "Energy Management in Autonomous Microgrid Using Stability-

Constrained Droop Control of Inverters," *IEEE Transactions on Power Electronics,* vol. 23, pp. 2346-2352, 2008.

[2.21] J. M. Guerrero, J. C. Vasquez, J. Matas, M. Castilla, and L. G. d. Vicuna, "Control Strategy for Flexible Microgrid Based on Parallel Line-Interactive UPS Systems," *IEEE Transactions on Industrial Electronics,* vol. 56, pp. 726-736, 2009.

[2.22] P. Palensky and D. Dietrich, "Demand Side Management: Demand Response, Intelligent Energy Systems, and Smart Loads," *Industrial Informatics, IEEE Transactions on,* vol. 7, pp. 381-388, 2011.

[2.23] V. Calderaro, C. N. Hadjicostis, A. Piccolo, and P. Siano, "Failure Identification in Smart Grids Based on Petri Net Modeling," *Industrial Electronics, IEEE Transactions on,* vol. 58, pp. 4613-4623, 2011.

[2.24] C. Cecati, C. Citro, and P. Siano, "Combined Operations of Renewable Energy Systems and Responsive Demand in a Smart Grid," *Sustainable Energy, IEEE Transactions on,* vol. 2, pp. 468-476, 2011.

[2.25] A. Vaccaro, G. Velotto, and A. F. Zobaa, "A Decentralized and Cooperative Architecture for Optimal Voltage Regulation in Smart Grids," *Industrial Electronics, IEEE Transactions on,* vol. 58, pp. 4593-4602, 2011.

[2.26] Y. Peizhong, A. Iwayemi, and Z. Chi, "Developing ZigBee Deployment Guideline Under WiFi Interference for Smart Grid Applications," *Smart Grid, IEEE Transactions on,* vol. 2, pp. 110-120, 2011.

[2.27] D. S. V. C. Gungor , T. Kocak and S. Ergut *Smart grid communications and networking*, 2011.

[2.28] L. Bin and V. C. Gungor, "Online and Remote Motor Energy Monitoring and Fault Diagnostics Using Wireless Sensor Networks," *Industrial Electronics, IEEE Transactions on,* vol. 56, pp. 4651-4659, 2009.

[2.29] C. Gezer and C. Buratti, "A ZigBee Smart Energy Implementation for Energy Efficient Buildings," in *Vehicular Technology Conference (VTC Spring), 2011 IEEE 73rd*, 2011, pp. 1-5.

[2.30] R. P. Lewis, P. Igic, and Z. Zhongfu, "Assessment of communication methods for smart electricity metering in the U.K," in *Sustainable Alternative Energy (SAE), 2009 IEEE PES/IAS Conference on*, 2009, pp. 1-4.

[2.31] A. Yarali, "Wireless Mesh Networking technology for commercial and industrial customers," in *Electrical and Computer Engineering, 2008. CCECE 2008. Canadian Conference on*, 2008, pp. 000047-000052.

[2.32] Z. Ming-Yue, "Transmission Characteristics of Low-Voltage Distribution Networks in China Under the Smart Grids Environment," *Power Delivery, IEEE Transactions on,* vol. 26, pp. 173-180, 2011.

[2.33] V. Paruchuri, A. Durresi, and M. Ramesh, "Securing powerline communications," in *Power Line Communications and Its Applications, 2008. ISPLC 2008. IEEE International Symposium on*, 2008, pp. 64-69.

[2.34] D. M. Laverty, D. J. Morrow, R. Best, and P. A. Crossley, "Telecommunications for Smart Grid: Backhaul solutions for the distribution network," in *Power and Energy Society General Meeting, 2010 IEEE*, 2010, pp. 1-6.

[2.35] M. Tou, K. Al-Haddad, G. Olivier, and V. Rajagopalan, "Analysis and design of single-controlled switch three-phase rectifier with unity power

factor and sinusoidal input current," *Power Electronics, IEEE Transactions on,* vol. 12, pp. 608-614, 1997.

[2.36] R. Wu, S. B. Dewan, and G. R. Slemon, "Analysis of a PWM AC to DC voltage source converter under the predicted current control with a fixed switching frequency," *Industry Applications, IEEE Transactions on,* vol. 27, pp. 756-764, 1991.

[2.37] E. H. Ismail, C. M. Oliveira, and R. W. Erickson, "A low-distortion three-phase multiresonant boost rectifier with zero-current switching," *Power Electronics, IEEE Transactions on,* vol. 13, pp. 718-726, 1998.

[2.38] S. Y. R. Hui and H. Chung, "Paralleling power converters for AC-DC step-down power conversion with inherent power factor correction," *Electric Power Applications, IEE Proceedings -,* vol. 146, pp. 247-252, 1999.

[2.39] T. C. Green, M. H. Taha, N. A. Rahim, and B. W. Williams, "Three-phase step-down reversible AC-DC power converter," *Power Electronics, IEEE Transactions on,* vol. 12, pp. 319-324, 1997.

[2.40] P. Vitor Fernao and J. F. Silva, "Three-phase single-stage four-switch PFC buck-boost-type rectifier," *Industrial Electronics, IEEE Transactions on,* vol. 52, pp. 444-453, 2005.

[2.41] C. T. Pan and T. C. Chen, "Step-up/down three-phase AC to DC convertor with sinusoidal input current and unity power factor," *Electric Power Applications, IEE Proceedings -,* vol. 141, pp. 77-84, 1994.

[2.42] Y. Lung-Sheng, L. Tsorng-Juu, and C. Jiann-Fuh, "Analysis and Design of a Novel Three-Phase AC–DC Buck-Boost Converter," *Power Electronics, IEEE Transactions on,* vol. 23, pp. 707-714, 2008.

[2.43] D. D. C. Lu, H. H. C. Iu, and V. Pjevalica, "A Single-Stage AC/DC Converter With High Power Factor, Regulated Bus Voltage, and Output Voltage," *Power Electronics, IEEE Transactions on,* vol. 23, pp. 218-228, 2008.

[2.44] C. Qiao and K. M. Smedley, "A topology survey of single-stage power factor corrector with a boost type input-current-shaper," *Power Electronics, IEEE Transactions on,* vol. 16, pp. 360-368, 2001.

[2.45] M. Daniele, P. K. Jain, and G. Joos, "A single-stage power-factor-corrected AC/DC converter," *Power Electronics, IEEE Transactions on,* vol. 14, pp. 1046-1055, 1999.

[2.46] J. F. Zhao, J. G. Jiang, and X. W. Yang, "AC-DC-DC isolated converter with bidirectional power flow capability," *Power Electronics, IET,* vol. 3, pp. 472-479, 2010.

[2.47] F. C. Schwarz, "A Method of Resonant Current Pulse Modulation for Power Converters," *Industrial Electronics and Control Instrumentation, IEEE Transactions on,* vol. IECI-17, pp. 209-221, 1970.

[2.48] N. Mapham, "An SCR Inverter with Good Regulation and Sine-Wave Output," *Industry and General Applications, IEEE Transactions on,* vol. IGA-3, pp. 176-187, 1967.

[2.49] R. L. Steigerwald, "A comparison of half-bridge resonant converter topologies," *Power Electronics, IEEE Transactions on,* vol. 3, pp. 174-182, 1988.

[2.50] V. Belaguli and A. K. S. Bhat, "Analysis and design of hybrid parallel-series resonant converter," in *Power Electronics Specialists Conference, 1996. PESC '96 Record., 27th Annual IEEE*, 1996, pp. 259-265 vol.1.

[2.51] S. Farhangi, U. Kirchenberger, and D. Schroeder, "Energy based closed form solution of ZCS multiresonant series-parallel converters," *Power Electronics, IEEE Transactions on,* vol. 11, pp. 285-291, 1996.

[2.52] R. L. Steigerwald, R. W. De Doncker, and H. Kheraluwala, "A comparison of high-power DC-DC soft-switched converter topologies," *Industry Applications, IEEE Transactions on,* vol. 32, pp. 1139-1145, 1996.

[2.53] R. Tymerski, V. Vorperian, and F. C. Y. Lee, "DC-to-AC inversion using quasi-resonant techniques," *Power Electronics, IEEE Transactions on,* vol. 4, pp. 381-390, 1989.

[2.54] B. S. Acharya, R. W. Gascoigne, and D. M. Divan, "Active power filters using resonant pole inverters," in *Industry Applications Society Annual Meeting, 1989., Conference Record of the 1989 IEEE*, 1989, pp. 967-973 vol.1.

[2.55] A. Kotsopoulos and D. G. Holmes, "A new soft-switched, thyristor-based, regenerative, quasi-resonant, current regulated inverter," *Industry Applications, IEEE Transactions on,* vol. 32, pp. 308-315, 1996.

[2.56] L. Jih-Sheng, "Resonant snubber-based soft-switching inverters for electric propulsion drives," *Industrial Electronics, IEEE Transactions on,* vol. 44, pp. 71-80, 1997.

[2.57] V. Vlatkovic, D. Borojevic, and F. C. Lee, "Soft-transition three-phase PWM conversion technology," in *Power Electronics Specialists Conference, PESC '94 Record., 25th Annual IEEE*, 1994, pp. 79-84 vol.1.

[2.58] V. Vlatkovic, D. Borojevic, F. Lee, C. Cuadros, and S. Gataric, "A new zero-voltage transition, three-phase PWM rectifier/inverter circuit," in *Power*

Electronics Specialists Conference, 1993. PESC '93 Record., 24th Annual IEEE, 1993, pp. 868-873.

[2.59] P. K. Sood and T. A. Lipo, "Power conversion distribution system using a high-frequency AC link," *Industry Applications, IEEE Transactions on,* vol. 24, pp. 288-300, 1988.

[2.60] S. K. Sul and T. A. Lipo, "Design and performance of a high-frequency link induction motor drive operating at unity power factor," *Industry Applications, IEEE Transactions on,* vol. 26, pp. 434-440, 1990.

[2.61] D. M. Divan, "The resonant DC link converter-a new concept in static power conversion," *Industry Applications, IEEE Transactions on,* vol. 25, pp. 317-325, 1989.

[2.62] G. Venkataramanan and D. M. Divan, "Pulse width modulation with resonant DC link converters," *Industry Applications, IEEE Transactions on,* vol. 29, pp. 113-120, 1993.

[2.63] J. He and N. Mohan, "Parallel resonant DC link circuit-a novel zero switching loss topology with minimum voltage stresses," in *Power Electronics Specialists Conference, 1989. PESC '89 Record., 20th Annual IEEE*, 1989, pp. 1006-1012 vol.2.

[2.64] G. Venkataramanan and D. M. Divan, "Control of pulse width modulated resonant DC link inverter," in *Industry Applications Society Annual Meeting, 1992., Conference Record of the 1992 IEEE*, 1992, pp. 737-743 vol.1.

[2.65] E. DaSilva, G. Ledwich, M. T. Aydemir, and T. A. Lipo, "Pulse width modulated series resonant converter," in *Industry Applications Society Annual Meeting, 1992., Conference Record of the 1992 IEEE*, 1992, pp. 744-749 vol.1.

[2.66] M. Baumann and J. W. Kolar, "Comparative evaluation of modulation methods for a three-phase/switch buck power factor corrector concerning the input capacitor voltage ripple," in *Power Electronics Specialists Conference, 2001. PESC. 2001 IEEE 32nd Annual*, 2001, pp. 1327-1332 vol. 3.

[2.67] M. H. Bierhoff and F. W. Fuchs, "Loss Minimized Pulse Width Modulation of IGBT Current Source Converters," in *IEEE Industrial Electronics, IECON 2006 - 32nd Annual Conference on*, 2006, pp. 1739-1744.

[2.68] C. Il-Yop, L. Wenxin, D. A. Cartes, E. G. Collins, and M. Seung-Il, "Control Methods of Inverter-Interfaced Distributed Generators in a Microgrid System," *Industry Applications, IEEE Transactions on,* vol. 46, pp. 1078-1088, 2010.

[2.69] M. N. Marwali and A. Keyhani, "Control of distributed generation systems-Part I: Voltages and currents control," *Power Electronics, IEEE Transactions on,* vol. 19, pp. 1541-1550, 2004.

[2.70] M. N. Marwali, J. Jin-Woo, and A. Keyhani, "Control of distributed generation systems - Part II: Load sharing control," *Power Electronics, IEEE Transactions on,* vol. 19, pp. 1551-1561, 2004.

[2.71] E. Davison and B. Scherzinger, "Perfect control of the robust servomechanism problem," *Automatic Control, IEEE Transactions on,* vol. 32, pp. 689-702, 1987.

[2.72] Y. W. Li, D. M. Vilathgamuwa, and P. C. Loh, "Microgrid power quality enhancement using a three-phase four-wire grid-interfacing compensator," in *Industry Applications Conference, 2004. 39th IAS Annual Meeting. Conference Record of the 2004 IEEE*, 2004, pp. 1439-1446 vol.3.

[2.73] L. Yun Wei, D. M. Vilathgamuwa, and L. Poh Chiang, "A grid-interfacing power quality compensator for three-phase three-wire microgrid applications," *Power Electronics, IEEE Transactions on,* vol. 21, pp. 1021-1031, 2006.

[2.74] F. Blaabjerg, R. Teodorescu, M. Liserre, and A. V. Timbus, "Overview of Control and Grid Synchronization for Distributed Power Generation Systems," *Industrial Electronics, IEEE Transactions on,* vol. 53, pp. 1398-1409, 2006.

[2.75] J. N. Reddy, M. K. Moorthy, and D. V. A. Kumar, "Control of grid connected PV cell distributed generation systems," in *TENCON 2008 - 2008 IEEE Region 10 Conference*, 2008, pp. 1-6.

[2.76] J. P. Barton and D. G. Infield, "Energy storage and its use with intermittent renewable energy," *Energy Conversion, IEEE Transactions on,* vol. 19, pp. 441-448, 2004.

[2.77] L. Peiwen, "Energy storage is the core of renewable technologies," *Nanotechnology Magazine, IEEE,* vol. 2, pp. 13-18, 2008.

[2.78] H. Oh, "Optimal Planning to Include Storage Devices in Power Systems," *Power Systems, IEEE Transactions on,* vol. 26, pp. 1118-1128, 2011.

[2.79] X. Yong, D. Jiamei, and M. Shuangbao, "Power flow control of a distributed generation unit in micro-grid," in *Power Electronics and Motion Control Conference, 2009. IPEMC '09. IEEE 6th International*, 2009, pp. 2122-2125.

[2.80] D. Min, M. N. Marwali, J. Jin-Woo, and A. Keyhani, "Power Flow Control of a Single Distributed Generation Unit," *Power Electronics, IEEE Transactions on,* vol. 23, pp. 343-352, 2008.

[2.81] K. C. Kalaitzakis and G. J. Vachtsevanos, "On the Control and Stability of Grid Connected Photovoltaic Sources," *Energy Conversion, IEEE Transactions on,* vol. EC-2, pp. 556-562, 1987.

[2.82] K. Sedghisigarchi and A. Feliachi, "Control of grid-connected fuel cell power plant for transient stability enhancement," in *Power Engineering Society Winter Meeting, 2002. IEEE*, 2002, pp. 383-388 vol.1.

[2.83] M. G. Molina and P. E. Mercado, "Power Flow Stabilization and Control of Microgrid with Wind Generation by Superconducting Magnetic Energy Storage," *Power Electronics, IEEE Transactions on,* vol. 26, pp. 910-922, 2011.

[2.84] J. Holz, "Pulsewidth modulation – a survey," *IEEE Trans. Ind. Electron.*, vol. 39, pp 410-420, Oct. 1992.

[2.85] M. P. Kazmierkowski, R. Krishnan, and F. Blaabjerg, Control in Power Electronics. London, U.K.: Academic, 2002.

[2.86] I. Takahashi and T. Noguchi, "A new quick-response and high efficiency control strategy of an induction machine," *IEEE Trans. Ind. Appl., vol. IA-22*, pp 820827, 1986.

[2.87] G. S. Buja and M. P. Kazmierkowski, "Direct torque control of PWM inverter-fed AC motor – a survey," *IEEE Trans. Ind. Electron.*, vol. 51, no. 4, pp. 744-757, August 2004.

[2.88] T. Ohnishi, "Three phase PWM converter/inverter by means of instantaneous active and reactive power control," in Proc. IEEE IECON, 1991, vol. 1, pp. 819824.

[2.89] Noguchi, H. Tomiki, S. Kondo and I. Takahashi, “Direct power control of PWM converter without power-source voltage sensors,” *IEEE Trans. Ind. Appl.*, vol. 34, pp 473-479, 1998.

[2.90] M. Malinowski, M. P. Kazmierkowski S. Hansen, F. Blaabjerg and G. D. Marques, “Virtual-flux-based direct power control of three-phase PWM rectifiers,” *IEEE Trans. Ind. Appl.,* vol. 37, no. 4, pp. 1019-1027, 2001.

[2.91] M. Malinowski, M. P. Kazmierkowski and A. M. Trzynadlowski, “A comparative study of control techniques for PWM rectifiers in AC adjustable speed drives,” *IEEE Trans. Power Electron*., vol. 18, no. 6, pp. 1390-1396, November 2003.

[2.92] A. Bouafia, J. P. Gaubert and F. Krim, “Analysis and design of new switching table for direct power control of three-phase PWM rectifier,” in *Proc. IEEE Int. Power Electronics and Motion Control Conf. EPE-PEMC*’ 08, pp. 1-6, 2008.

[2.93] J. Alonso-Martinez, J. Eloy-Garcia, and S. Arnaltes, “Table-based direct power control: A critical review for microgrid applications,” *IEEE Trans. Power Electron.*, vol. 25, no. 12, pp. 2949-2916, December 2010.

[2.94] A. Sato and Toshihiko Noguchi, “Voltage-source PWM rectifier – inverter based on direct power control and its operation characteristics,” *IEEE Trans. Power Electron*., vol. 26, no. 5, pp. 1559-1567, May 2011.

[2.95] P. Cortes, M. P. Kazmierkowski, R. M. Kennel, D. E. Quevedo and J. Rodriguez, “Predictive control in power electronics and dirves,” *IEEE Trans. Ind. Electron,* vol. 55, no. 12, pp. 4312-4324, December 2008.

[2.96] D. Zhi, L. Xu, and B. W. Williams, “Model-based predictive direct power control of doubly fed induction generators,” *IEEE Trans. Power Electron*., vol. 25, no. 2, pp. 341-351, Feb. 2010.

[2.97] A. Bouafia, J. P. Gaubert and F. Krim, “Predictive direct power control of threephase pulsewidth modulation (PWM) rectifier using space-vector modulation (SVM),” *IEEE Trans. Power Electron*., vol. 25, no. 1, pp. 228-236, January 2010.

[2.98] J. M. Espí, J. Castelló, R. García-Gil, G. Garcerá, and E. Figueres, “An adaptive robust predictive current control for three-phase grid-connected inverters,” *IEEE Trans. Ind. Electron*, vol. 58, no. 8, pp. 3537-3546, August 2011.

[2.99] Q. Zeng and L. Chang, “An advanced SVPWM-based predictive current controller for three-phase inverters in distributed generation systems,” *IEEE Trans. Ind. Electron*, vol. 55, no. 3, pp. 1235-1246, Mar. 2008.

[2.100] O. Kukrer, “Discrete-time control of voltage-fed three-phase PWM inverters,” *IEEE Trans. Ind. Electron*, vol. 11, no. 2, pp. 260-269, Mar. 1996.

[2.101] R. E. Betz, B. J. Cook, and S. J. Henriksen, “A digital current controller for three phase voltage source inverters,” in Conf. Rec. IEEE IAS Annu. Meeting, New Orleans, LA, Oct. 2003, pp. 722-729.

[2.102] Y. Nishida, O. Miyashita, T. Haneyoshi, H. Tomita, and A. Maeda, “A predictive instantaneous-current PWM controlled rectifier with AC-side harmonic current reduction,” *IEEE Trans. Ind. Electron*, vol. 44, no. 3, pp. 337-343, Jun. 1997.

[2.103] S.-M. Yang and C.-H. Lee, “A deadbeat current controller for field oriented induction motor drives,” *IEEE Trans. Power Electron*., vol. 17, no. 5, pp. 772778, Sep. 2002.

[2.104] P. Cortes, J. Rodriguez, P. Antoniewicz, and M. Kazmierkowski, “Direct power control of an AFE using predictive control,” *IEEE Trans. Power Electron.,* vol. 23, no. 5, pp. 2516-2523, September 2008.

[2.105] P. Cortés, G. Ortiz, J. I. Yuz, J. Rodríguez, S. Vazquez, and L. G. Franquelo, “Model predictive control of an inverter with output LC filter for UPS applications,” *IEEE Trans. Ind. Electron*., vol. 56, no. 6, pp. 1875-1883, February 2009.

[2.106] S. Kouro, P. Cortes, R. Vargas, U. Ammann and J. Rodriguez, “Model predictive control─A simple and powerful method to control power converters,” *IEEE Trans. Ind. Electron*., vol. 56, no. 6, pp. 1826-1838, June 2009.

[2.107] T. Geyer, G. Papafotiou, and M. Morari, “Model predictive direct torque control – Part I: concept, algorithm, and analysis*,” IEEE Trans. Ind. Electron.,* vol. 56, no. 6, pp. 1894-1905, June 2009.

[2.108] P. Cortes, J. Rodriguez, D. E. Quevedo, and C. Silva, “Predictive current control strategy with imposed load current spectrum,” *IEEE Trans. Power Electron.,* vol. 23, no. 2, pp. 612-618, March 2008.

[2.109] M. Preindl, E. Schaltz, and P. Thogersen, “Switching frequency reduction using model predictive direct current control for high-power voltage sources inverters,” *IEEE Trans. Ind. Electron*., vol. 58, no. 7, pp. 2826-2835, July 2011.

[2.110] M. A. Perez, J. Rodriguez, E. J. Fuentes, and F. Kammerer, "Predictive control of AC – AC modular converters," *IEEE Trans. Ind. Electron*., vol. 59, no. 7, pp. 2832-2839, July 2012.

[2.111] S. A. Larrinaga, M. A. Rodriguez, E. Oyarbide and J. R. T. Apraiz, "Predictive control strategy for DC/AC converters based on direct power control," *IEEE Trans. Ind. Electron*., vol. 54, pp. 1261-1271, June 2007.

[2.112] P. Antoniewicz, and M. P. Kazmierkowski, "Virtual-Flux-Based predictive direct power control of AC/DC converters with online inductance estimation," *IEEE Trans. Ind. Electron*., vol. 55, no. 12, pp. 4281-4390, December 2008.

[2.113] J. Hu and Z. Zhu, "Investigation on switching patterns of direct power control strategies for grid-connected DC – AC converters based on power variation rates," *IEEE Trans. Power Electron*., vol. 26, no. 12, pp. 3582-3598, December 2011.

[2.114] R. Morales-Caporal, and M. Pacas, "Encoderless predictive direct torque control for synchronous reluctance machines at very low and zero speed," *IEEE Trans. Ind. Electron*., vol. 55, no. 12, pp. 4408-4416, December 2008.

[2.115] G. Abad, M. A. Rodriguez, and J. Poza, "Two-level VSC based predictive direct power control of the doubly fed induction machine with reduced power ripple at low constant switching frequency," *IEEE Trans. Energy. Convers.*, vol. 23, no. 2, pp. 570-580, Jun. 2008.

[2.116] G. Abad, M. A. Rodriguez, and J. Poza, "Two-level VSC based predictive direct torque control of the doubly fed induction machine with reduced torque and flux ripples at low constant switching frequency," *IEEE Trans. Power Electron.*, vol. 23, no. 3, pp. 1050-1061, May. 2008.

[2.117] G. Abad, M. A. Rodriguez, and J. Poza, “Three-level NPC converter-based predictive direct power control of the doubly fed induction machine at low constant switching frequency,” *IEEE Trans. Ind. Electron*., vol. 55, no. 12, pp. 4417-4429, 2008.

[2.118] J.Hu, “Advanced Control in Smart Microgrids”, PhD Thesis, University of Technology Sydney 2013

CHAPTER 3. MICROGRID AND APPLICATION IN VIETNAM

3.1. INTRODUCTION

Based on the current scheme of Vietnamese power scenario and its renewable energy potential presented on Chapter two, to meet the demand in the upcoming years, the Vietnamese Government is trying to develop the national electrical system in both stability and capacity to ensure the supply throughout the country. However in the near future, both individual and industrial customer will have to face the chance of blackouts occurring. On the other hand, the potential of RES in Vietnam is plentiful with large amount of both wind and solar energy. Therefore the Vietnamese Government will have to overcome a great challenge with the years to come. This chapter will present a new structure of microgrid with the usage of RES, which are very abundant, along with several study cases about different power scales in Vietnam.

3.2. MICROGRID TOPOLOGY

3.2.1. Microgrid structure

The concept of microgrid, which is composed of DGs, renewable power generations, such as solar PVs, WTs and fuel cells, together with customer loads, energy storage devices and power converters, was introduced in the early 2000s [3.1] and developed throughout the world in the last decade as an effective means to integrate intermittent renewable power sources in power grids [3.2-3.5].

Various microgrid structures have been present in recent year. Depending on the scale and area properties, there are different types of microgrids:

- AC bus microgrids [3.6-3.13]
- DC bus microgrids [3.14-3.22]
- Hybrid AC/DC bus microgrids [3.23-3.28]

For example, a microgrid in a city household with the main power sources being PV cells and WT on top of the building generates electricity for electrical devices in the house of which the majority require 220 V AC power. For that reason, this microgrid should have a 220 V common AC bus for convenient use.

Fig. 3.1 (a) and (b) show the structures of two proposed microgrids with DC and AC buses, respectively. In these microgrids, the DG sources include AC sources such as WTs or biogas, and DC sources such as PV cells. Energy can be stored in battery cells, super capacitors or can be transformed into another form of energy for convenient storage. AC and DC loads are connected to the transmission bus through converters. In the grid-connected mode, the microgrid connects to the utility grid through a converter. When connected, this inverter controls the power flow between the microgrid and the utility grid. If not connected, the micro grid operates in the

island mode, in which the loads are supplied by DG sources and from the energy storage system (ESS).

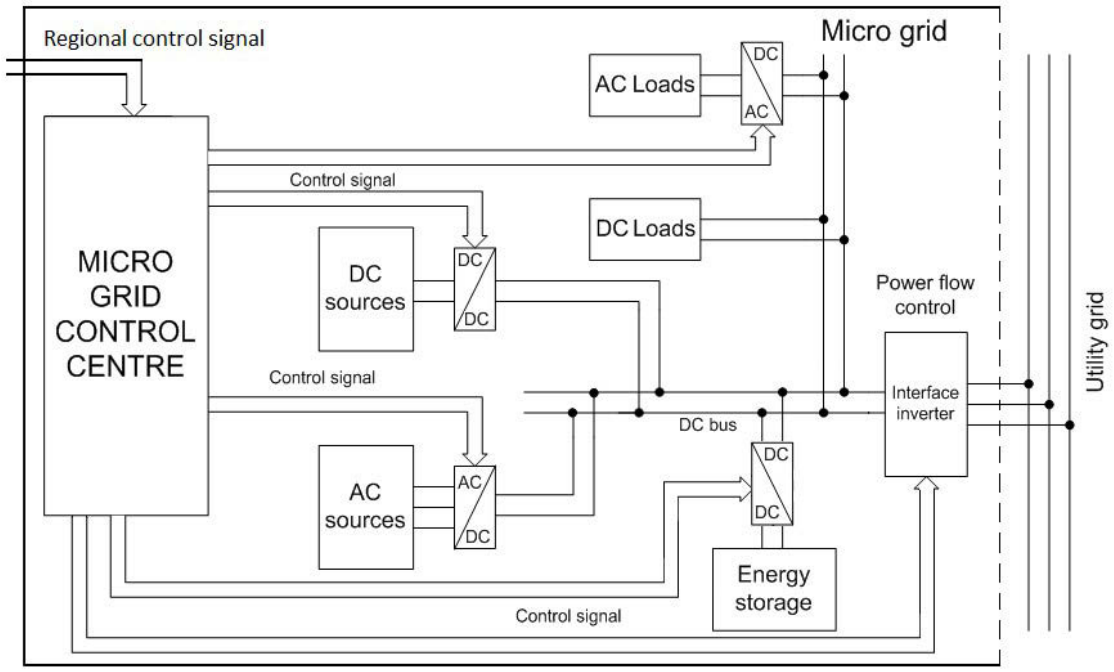

(a)

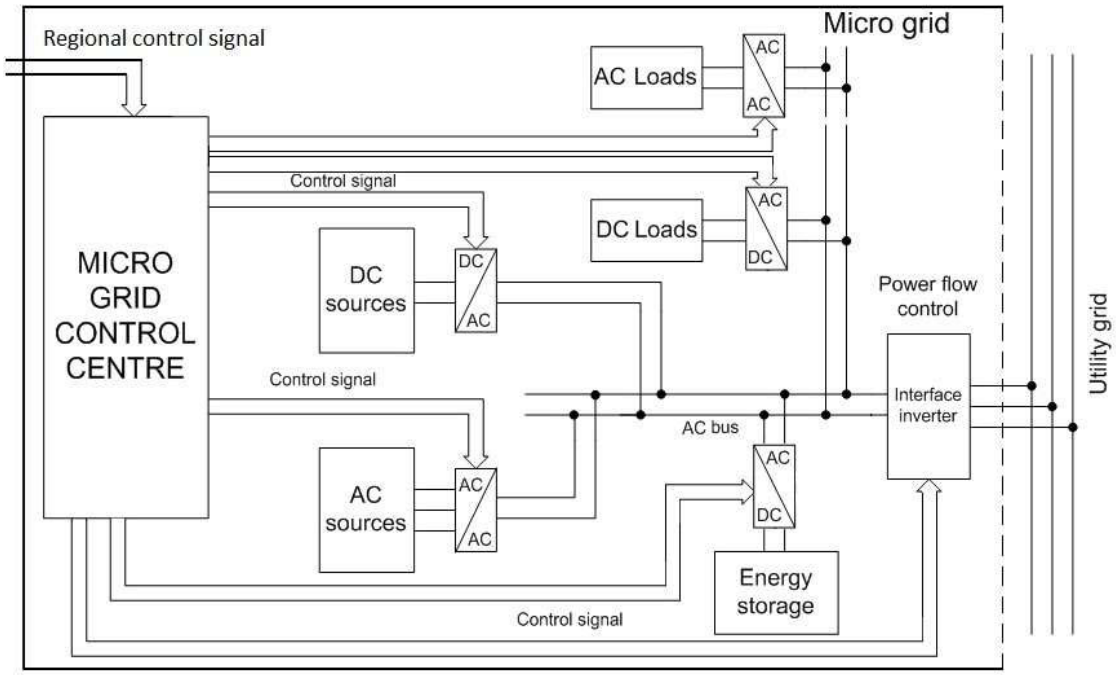

(b)

Fig.3.1 Structure of microgrid: (a) microgrid with DC common bus; (b) microgrid with AC common bus

3.2.2. Operation of microgrid

The microgrid control center sends and receives control signals from an external regional control center and from other devices in the microgrid. It controls the operation of every device and storage system. The ESS can be charged from the common bus in grid-connected mode or from DGs in the stand-alone mode. When a fault occurs, this energy storage can provide energy to support the bus voltage immediately. All AC and DC loads are connected to the common bus by power converters so that the performance can be improved. The microgrid uses droop or some other control methods to stabilize the voltage and frequency. A comprehensive study about the microgrid operation will be presented in Chapter 4.

3.3. MICROGRID TOPOLOGIES FOR DIFFERENT APPLICATIONS

Nowadays, many different areas have successfully applied a microgrid topology with various kinds of power DGs such as WTs, solar panels and diesel generations. In this thesis, several microgrid applications will be presented. Analysis including electrical reliability and power quality requirements, advantages and disadvantages will be carried out to determine the most suitable microgrid for each case.

3.3.1. A city building

Fig.3.2 shows as an example the power consumption of the Danish Embassy building in Vietnam. A city building has a strong grid with a low penetration of renewable energy because it is inconvenient for the user. For example, a university building cannot have an extremely large wind farm or WT on its top. However, it is

still possible to add DG to increase the reliability of the power system and reduce the cost of electricity by using diesel generators or PV cells on top of the building. Some loads are critical such as hospitals, and thus they need a power system with a relatively high reliability and good power quality. Normally, these kinds of loads always have back up power supplies such as diesel engine generators in order to operate when the grid supply is lost.

Overall, a city building must be provided with a sustainable power system with high reliability but it still can raise the percentage of renewable energy to reduce the electricity cost. For this reason, a microgrid with DER, which generates part of the electricity needed such as for lighting or air conditioning system, would be a smart choice. Therefore, a DC bus microgrid with distributed resources like PV panels and a small WT on the roof top is very suitable for this case.

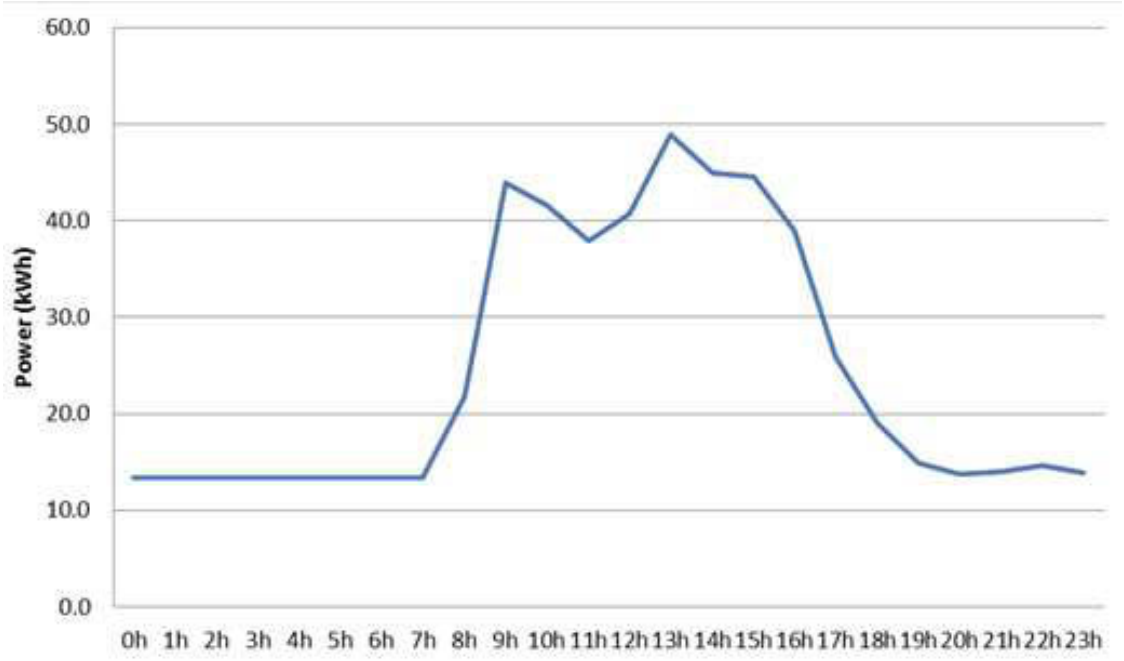

Fig.3.2. Power consumption of: Danish Embassy building in Vietnam.

3.3.2. A small town/village

Fig. 3.3 indicates the energy used in a small town. Normally, a small town or village, which is located far away from the conventional electrical grid, has a grid weaker than those in the cities, and is not attractive for energy investments. It also requires very low demand for sustainability of electrical service. However, this target has a greater potential for RESs such as large-scale wind farms or PV arrays. Therefore, it can provide a large amount of electricity to the grid.

A DC microgrid with clean energy resources, especial solar and wind energy is ideal in this case. The DC bus will bring more advantages to electrical quality and transmission and is more economical in comparison with an AC bus.

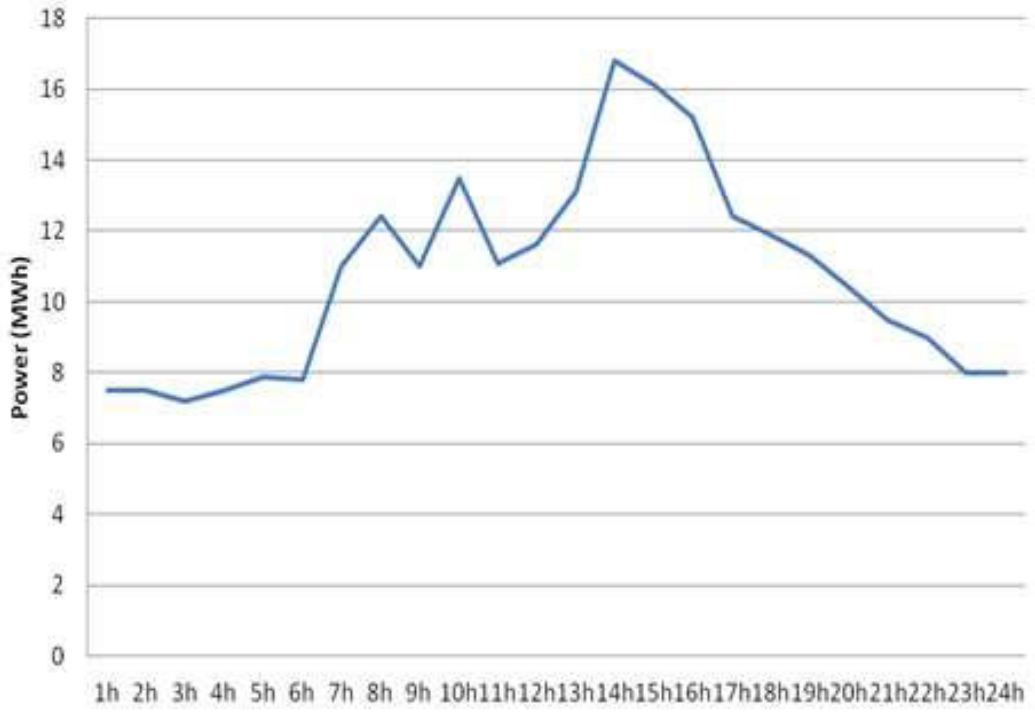

Fig.3.3. Power consumption of: a small town in Vietnam.

3.3.3. A factory far from grid

Fig.3.4 shows the power consumption of the Vinapipe steel factory. Similar to a small town or village, a Vietnamese factory is usually located in an area that is far from the conventional electrical grid. Then it also has a weak grid, but the energy demand is critical. Therefore, it certainly needs back up energy sources, such as diesel engine generators or WTs. A factory can operate like a stand-alone microgrid with DG or in grid-connected mode. One more advantage of a rural factory is that it has a lot of ground to place RES such as large WTs or PV arrays to increase the amount of renewable energy used. The investment cost is also an important factor when considering the operation of a factory. Therefore, it should increase the proportion of renewable energy.

In a factory, a DC microgrid is also suitable because of its demand for a grid with high reliability. Back-up generations and the battery energy storage will provide needed electricity in the stand-alone mode.

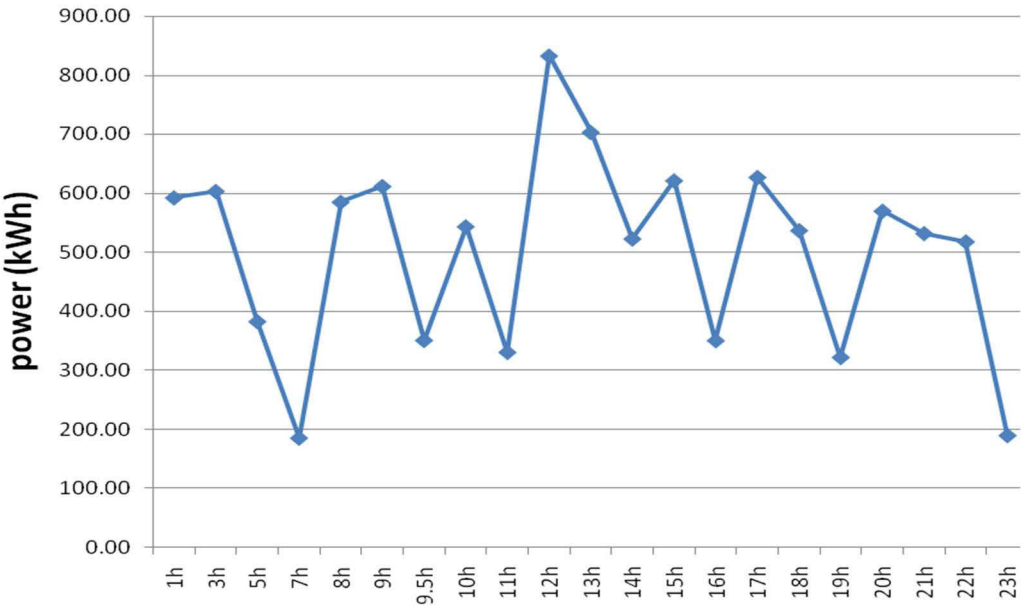

Fig.3.4. Power consumption of Vinapipe steel factory

3.3.4. A city household

Fig.3.5 shows the average electricity needed by a household in summer and winter.

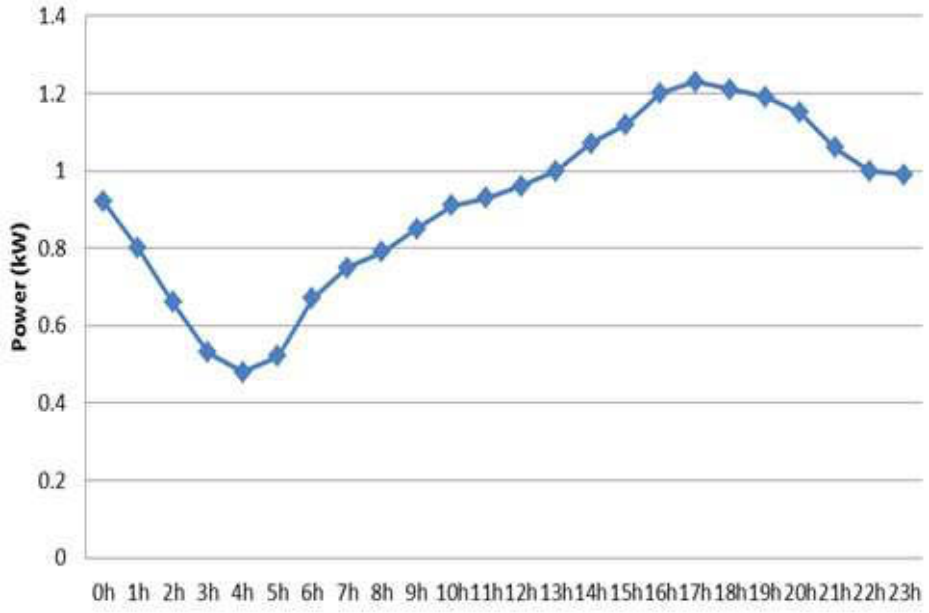

(a)

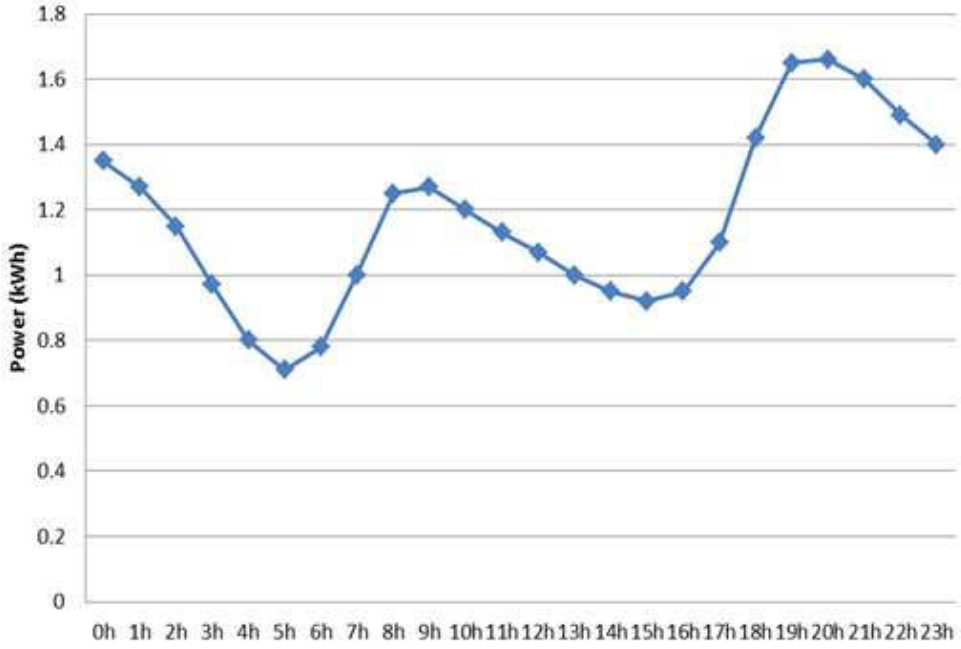

(b)

Fig.3.5. Average electrical consumption of a single Vietnamese household in: (a) winter, and (b) summer

A house in the city is limited in a fixed area, so that the size of renewable energy and DGs are very limited. For example, each small household in Sydney only can have PV arrays of 1.5 or 3 kW in each. The amount of electricity used is relatively small. Besides that, for a household, the electricity cost is a big concern. Therefore, to choose a suitable amount of RESs along with energy storage is very important. It helps not only the family reduce the money they have to pay but also the Government decrease the needs of energy in peak hours. Moreover, the reliability is important but not as much as critical loads. The power quality is not so important for a single household, and thus a microgrid with common AC bus can be used. Another reason to choose AC microgrid is that the majority of household devices use 220V AC power, and therefore an AC common bus is the best option in this case.

3.3.5. A rural farm

Like a small town or village, which is located relatively far away from the conventional electrical grid, a rural farm has an extremely weak grid and sometimes is isolated. The energy demand is not critical. It can operate as a stand-alone microgrid with a large number of DER like WTs, PV arrays or diesel generators. Electrical equipment for a farm may include both AC and DC devices, and thus either DC or AC microgrid can be applied in this area.

Assume that in the farm, it is possible to set up a great number of RES because of the large available area, especially wind and solar energy. Most electrical equipment in a farm uses the common 220 V AC power and some others the DC power. For that reason, a common 400 V DC bus is suitable in this case. For domestic devices like television, fridge, washing machine, computer, we use a DC-AC inverter to create a small AC bus inside the house for convenience.

Firstly, the WT with converter or PV cells establishes the low DC link with voltage regulation. Then a common 400 V DC grid is formed using a DC-DC boost converter as shown in Fig. 3.6.

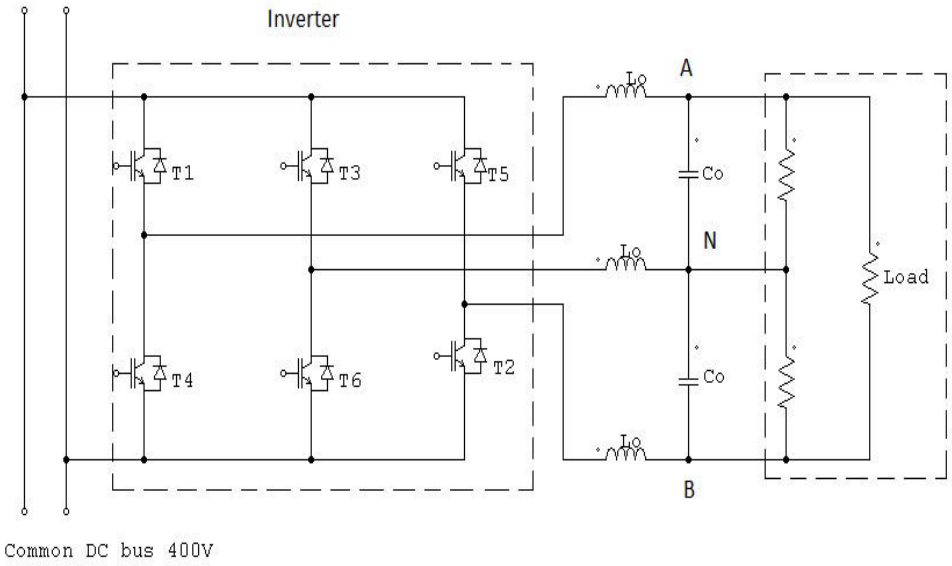

Fig.3.6. Single phase three wire load inverter

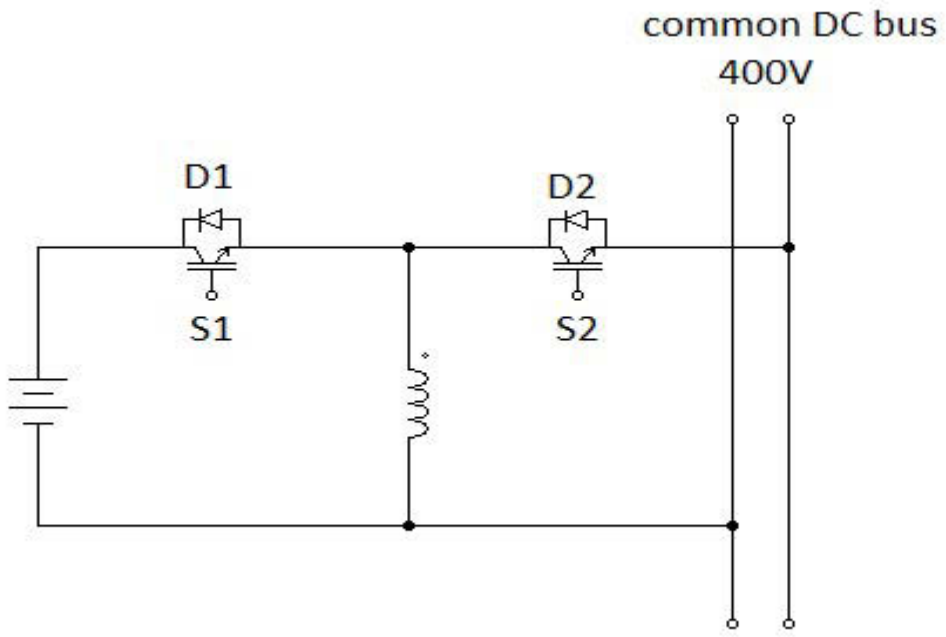

Fig.3.7. Bidirectional DC-DC converter

As to the power quality control of the microgrid system, the ESS, which should be the lead acid battery because of its low price, is established to maintain the common DC bus voltage. This battery bank is interfaced to the common 400 V DC grid by a bidirectional buck-boost converter as shown in Fig.3.7. During the charging mode, the battery is initially charged under a constant current with a set charging current. After the battery reaches the maximum voltage, the charging process is changed to constant voltage floating charging mode. When the main grid fails to provide the required electricity, the ESS can support the common DC bus voltage. The battery bank will discharge into the common DC grid at 400 V.

Depending on the appliances used, the common DC grid can provide 220 V AC sources for domestic devices by an Insulated Gate Bipolar Transistor (IGBT) inverter as shown in Fig.3.8. The two outer legs in the IGBT module are arranged to provide the 220 V AC voltage output, and the centre leg is used to maintain two balanced 110 V voltage outputs. As generally recognized, to achieve high performance of an inverter-fed plant, the control structured with inner current loop and outer voltage loop is usually adopted. To simplify the control mechanism, a robust voltage waveform control scheme for the developed inverter system without current loop is proposed. The waveform generated by the two outer legs of the IGBT module is handled by a master differential mode control scheme. The balance voltage, which is regulated via the PWM switching for the centre-leg IGBT, is handled by a slave common mode control scheme.

3.4. CONCLUSION

With the majority of rural farms in Vietnam, there is a large potential for the application of renewable energy. This case is very suitable for applying the microgrid topology because it has great potential for distributed energy which can satisfy most of the electrical demand. The details of a microgrid for this case will be presented in the next chapter.

REFERENCES

[3.1] R. H. Lasseter, "MicroGrids," in *Power Engineering Society Winter Meeting, 2002. IEEE*, 2002, pp. 305-308 vol.1.

[3.2] D. Guezgouz, D. E. Chariag, Y. Raingeaud, and J. C. Le Bunetel, "Modeling of Electromagnetic Interference and PLC Transmission for Loads Shedding in a Microgrid," *Power Electronics, IEEE Transactions on,* vol. 26, pp. 747-754, 2011.

[3.3] W. Fei, J. L. Duarte, and M. A. M. Hendrix, "Grid-Interfacing Converter Systems With Enhanced Voltage Quality for Microgrid Applications 2014;Concept and Implementation," *Power Electronics, IEEE Transactions on,* vol. 26, pp. 3501-3513, 2011.

[3.4] S. Bolognani and S. Zampieri, "Distributed control for optimal reactive power compensation in smart microgrids," in *Decision and Control and European Control Conference (CDC-ECC), 2011 50th IEEE Conference on*, 2011, pp. 6630-6635.

[3.5] G. Mine, R. Borer, F. Kupzog, and H. Nishi, "Construction method of dynamic microgrid by using optimized grouping method," in *Industrial Informatics (INDIN), 2010 8th IEEE International Conference on*, 2010, pp. 780-785.

[3.6] K. Jaehong, J. M. Guerrero, P. Rodriguez, R. Teodorescu, and N. Kwanghee, "Mode Adaptive Droop Control With Virtual Output Impedances for an Inverter-Based Flexible AC Microgrid," *Power Electronics, IEEE Transactions on,* vol. 26, pp. 689-701, 2011.

[3.7] P. C. Sekhar, S. Mishra, and R. Sharma, "Data analytics based neuro-fuzzy controller for diesel-photovoltaic hybrid AC microgrid," *Generation, Transmission & Distribution, IET,* vol. 9, pp. 193-207, 2015.

[3.8] S. Chakraborty and M. G. Simoes, "Experimental Evaluation of Active Filtering in a Single-Phase High-Frequency AC Microgrid," *Energy Conversion, IEEE Transactions on,* vol. 24, pp. 673-682, 2009.

[3.9] S. Chakraborty, M. D. Weiss, and M. G. Simoes, "Distributed Intelligent Energy Management System for a Single-Phase High-Frequency AC Microgrid," *Industrial Electronics, IEEE Transactions on,* vol. 54, pp. 97-109, 2007.

[3.10] H. Bevrani, F. Habibi, P. Babahajyani, M. Watanabe, and Y. Mitani, "Intelligent Frequency Control in an AC Microgrid: Online PSO-Based Fuzzy Tuning Approach," *Smart Grid, IEEE Transactions on,* vol. 3, pp. 1935-1944, 2012.

[3.11] K. T. Tan, P. L. So, Y. C. Chu, and M. Z. Q. Chen, "A Flexible AC Distribution System Device for a Microgrid," *Energy Conversion, IEEE Transactions on,* vol. 28, pp. 601-610, 2013.

[3.12] V. Nasirian, Q. Shafiee, J. M. Guerrero, F. L. Lewis, and A. Davoudi, "Droop-Free Distributed Control for AC Microgrids," *Power Electronics, IEEE Transactions on,* vol. 31, pp. 1600-1617, 2016.

[3.13] J. Rocabert, A. Luna, F. Blaabjerg, Rodri, x, and P. guez, "Control of Power Converters in AC Microgrids," *Power Electronics, IEEE Transactions on,* vol. 27, pp. 4734-4749, 2012.

[3.14] L. Baoquan, Z. Fang, Z. Yixin, and Y. Hao, "System Operation and Energy Management of a Renewable Energy-Based DC Micro-Grid for High Penetration Depth Application," *Smart Grid, IEEE Transactions on,* vol. 6, pp. 1147-1155, 2015.

[3.15] N. Eghtedarpour and E. Farjah, "Distributed charge/discharge control of energy storages in a renewable-energy-based DC micro-grid," *Renewable Power Generation, IET,* vol. 8, pp. 45-57, 2014.

[3.16] P. Shamsi and B. Fahimi, "Stability Assessment of a DC Distribution Network in a Hybrid Micro-Grid Application," *Smart Grid, IEEE Transactions on,* vol. 5, pp. 2527-2534, 2014.

[3.17] M. Davari and Y. A. R. I. Mohamed, "Robust Multi-Objective Control of VSC-Based DC-Voltage Power Port in Hybrid AC/DC Multi-Terminal Micro-Grids," *Smart Grid, IEEE Transactions on,* vol. 4, pp. 1597-1612, 2013.

[3.18] L. Sheng-yen, W. Li, L. Te-Ming, and A. V. Prokhorov, "Integration of Wind Power and Wave Power Generation Systems Using a DC Microgrid," *Industry Applications, IEEE Transactions on,* vol. 51, pp. 2753-2761, 2015.

[3.19] L. Nian, C. Qifang, L. Xinyi, L. Jie, and Z. Jianhua, "A Charging Strategy for PV-Based Battery Switch Stations Considering Service Availability and Self-

Consumption of PV Energy," *Industrial Electronics, IEEE Transactions on,* vol. 62, pp. 4878-4889, 2015.

[3.20] R. Majumder, "A Hybrid Microgrid With DC Connection at Back to Back Converters," *Smart Grid, IEEE Transactions on,* vol. 5, pp. 251-259, 2014.

[3.21] M. Kumar, S. C. Srivastava, S. N. Singh, and M. Ramamoorty, "Development of a control strategy for interconnection of islanded direct current microgrids," *Renewable Power Generation, IET,* vol. 9, pp. 284-296, 2015.

[3.22] C. Gavriluta, J. I. Candela, C. Citro, J. Rocabert, A. Luna, and P. Rodriguez, "Decentralized Primary Control of MTDC Networks With Energy Storage and Distributed Generation," *Industry Applications, IEEE Transactions on,* vol. 50, pp. 4122-4131, 2014.

[3.23] M. Hosseinzadeh and F. R. Salmasi, "Robust Optimal Power Management System for a Hybrid AC/DC Micro-Grid," *Sustainable Energy, IEEE Transactions on,* vol. 6, pp. 675-687, 2015.

[3.24] M. Hosseinzadeh and F. R. Salmasi, "Power management of an isolated hybrid AC/DC micro-grid with fuzzy control of battery banks," *Renewable Power Generation, IET,* vol. 9, pp. 484-493, 2015.

[3.25] L. Xiong, W. Peng, and L. Poh Chiang, "A Hybrid AC/DC Microgrid and Its Coordination Control," *Smart Grid, IEEE Transactions on,* vol. 2, pp. 278-286, 2011.

[3.26] L. Che, M. Shahidehpour, A. Alabdulwahab, and Y. Al-Turki, "Hierarchical Coordination of a Community Microgrid With AC and DC Microgrids," *Smart Grid, IEEE Transactions on,* vol. 6, pp. 3042-3051, 2015.

[3.27] L. Poh Chiang, L. Ding, C. Yi Kang, and F. Blaabjerg, "Autonomous Control of Interlinking Converter With Energy Storage in Hybrid AC–DC

Microgrid," *Industry Applications, IEEE Transactions on,* vol. 49, pp. 1374-1382, 2013.

[3.28] H. Jae-Sang, U. A. Khan, S. Woo-Ju, S. Jae-Kyu, L. Jong-Geon, K. Yong-Han*, et al.*, "Validity Analysis on the Positioning of Superconducting Fault Current Limiter in Neighboring AC and DC Microgrid," *Applied Superconductivity, IEEE Transactions on,* vol. 23, pp. 5600204-5600204, 2013.

CHAPTER 4. MICROGRID APPLICATION FOR RURAL FARMS IN VIETNAM

4.1. INTRODUCTION

Nowadays in Vietnam, 80% of people are living in the rural areas, which do not have a reliable utility grid. A majority of them are still doing agricultural works for living. In years to come, with the integration of advance technology as well as mechanized equipment, rural people will have to face the rising problem of power supply sooner or later. On the other hand, RESs are becoming more and more popular and recently lowering the energy burden in a number of countries all over the world. With a relative abundant potential of wind and solar energy resources, Vietnamese rural areas are very promising fields for smart micro grid applications. Chapter 3 presented numerous applications of smart microgrids with Vietnamese scheme. In each case, the suitable microgrids will be applied to cope with specific difficulties in order to help the customers with a relatively "weak" grid meet their electrical demands. In this chapter, a complete microgrid structure for a typical rural farm in Vietnam will be designed to not only maximize the electricity produced from renewable energy but also minimize the operating cost of the whole microgrid considering the energy price in Vietnam in the near future.

4.2. CASE STUDY OF A TYPICAL VIETNAMESE FARM

4.2.1. Current Vietnamese Power Scheme of A Rural Farm

Table 4-I illustrates the power demand in a Vietnamese rural farm in 2015. This number is projected to increase 10-15% annually to 15 kW in 2020 with the addition of some electrical equipment, such as water pump and heating lamp system, etc. Along with the progressive price system currently applied in Vietnam in Table 4-II, the total money each Vietnamese rural family has to pay for the energy in 2015 is around AUD 50, equivalent to 33% of the average income of Vietnamese people according to the record of 2016. Another factor to take into account is that in the last 5 years, the energy price in Vietnam increased 5% annually. It is clear that the economic problem which the Vietnamese rural people have to solve is getting harder especially with electricity.

Another major problem with the rural area is that the total amount of energy produced in Vietnam cannot meet its demand. For example, the Government had to cut off some non-critical loads during the peak-hours last year. In some reports from the local newspapers, each household in the countryside area had at least three days without electricity every month. In order to help the rural area, this thesis will design in detail a microgrid which can help increase the consumption of local RESs and lower the dependence on the main grid, and therefore increase the reliability and stability of the systems.

TABLE 4- I. A TYPICAL VIETNAMESE RURAL FARM POWER DEMAND IN 2015

No	Households	Power (W)	Amount	Total power(W)	Usage(h)	Energy(Wh)
1	Lamps Type 1 Type 2	 20 14	 5 3	 100 42	 6 2	 600 84
2	Televisions	340	2	680	3	2040
3	DVD	30	2	60	2	120
4	Computer	300	2	600	3	1800
5	Refrigerator	110	1	110	24	2640
6	Washing machine	300	1	300	2	600
7	Rice cooker Kitchen boiler	300 1000	1 1	300 1000	2 0.20	600 200
8	Heater/Air conditioner	500	1	500	7	3500
9	Fan	50	1	50	2	100
10	Laptop/Gadgets	50	4	200	3	600
					Total	12984

TABLE 4- II. CURRENT ENERGY PRICE IN VIETNAM 2016

	Price in Vnd	Price in Aus. cent
Division 1: 0-50 kWh	1.484	8.9
Division 2: 51-100 kWh	1.533	9.2
Division 3: 101-200 kWh	1.786	10.6
Division 4: 201-300 kWh	2.242	13.5
Division 5: 301-400 kWh	2.503	15.0
Division 6: more than 401 kWh	2.587	15.5

4.2.2. Proposed Microgrid Structure For A Rural Farm

Table 4-III illustrates the differences in efficiency of power converter when the electrical equipment is supplied with AC and DC power sources. It can be clearly seen in the table that most of the electrical devices will work better with DC power supply. Therefore, a microgrid with a DC bus is suitable for the rural farm. However, many of the household devices nowadays have the AC socket as primary manufactory setting; hence, the AC power supply brings more convenience to users. For this reason, the microgrid with the main DC bus and an extra AC bus for household devices and gadgets is the best solution. It will not only help obtain high efficiency through the microgrid but also be more user-friendly.

TABLE 4- III. POWER CONVERTER EFFICIENCY WITH AC AND DC POWER SUPPLIES

Equipment	Power (Watt)	Efficiency			
		AC		DC	
Flourescent Lamps	20	AC-DC-AC	0.70x0.87= 0.61	DC-AC	0.87
Lamps	20	AC-DC	0.70	DC-DC	0.87
Television	80	AC-DC	0.75	DC-DC	0.90
DVD	30	AC-DC	0.70	DC-DC	0.87
Ricecooker+Warmer	350	AC-DC-AC	0.79x0.92= 0.73	DC-AC	0.92
Laptop	60	AC-DC	0.75	DC-DC	0.90
Cellular	10	AC-DC	0.69	DC-DC	0.86
Iron	300		1.00	DC-AC	0.92
Air Conditioner	1000	AC-DC-AC	0.83x0.93= 0.77	DC-AC	0.93
Computer	300	AC-DC	0.78	DC-DC	0.92
Refrigerator	70	AC-DC-AC	0.75x0.90= 0.68	DC-AC	0.90
Washing Machine	370	AC-DC-AC	0.79x0.92= 0.73	DC-AC	0.92

Fig.4.1 illustrates two proposed structures of the microgrids that can be applied for the Vietnamese rural farm, with DC and AC common buses, respectively.

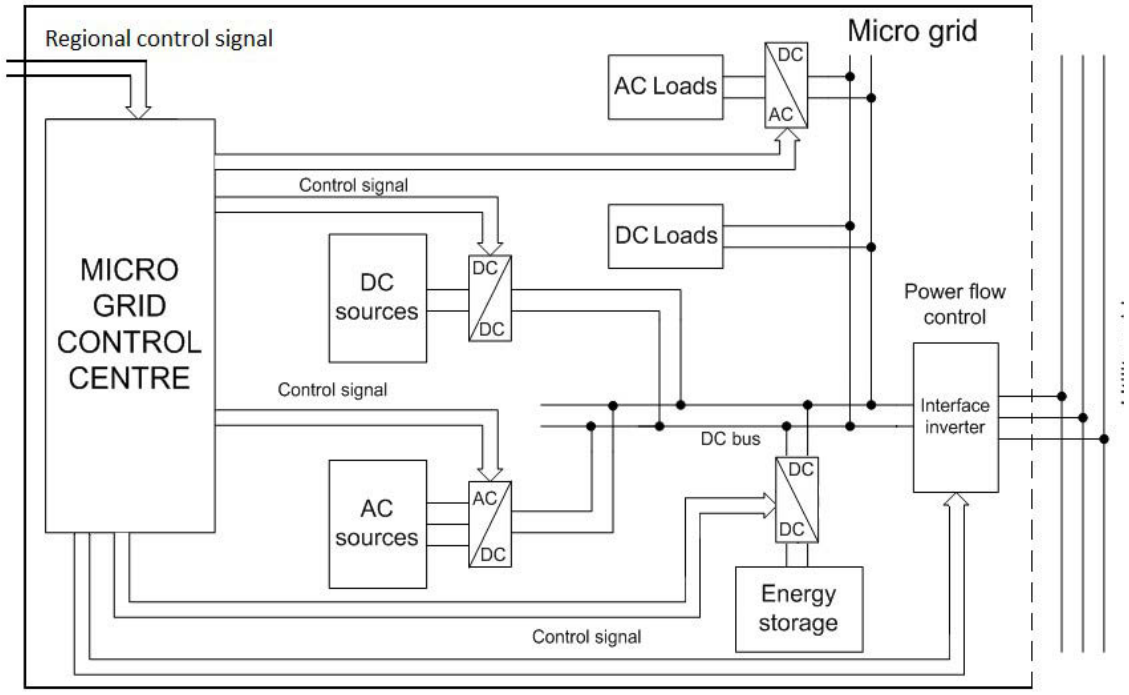

(a)

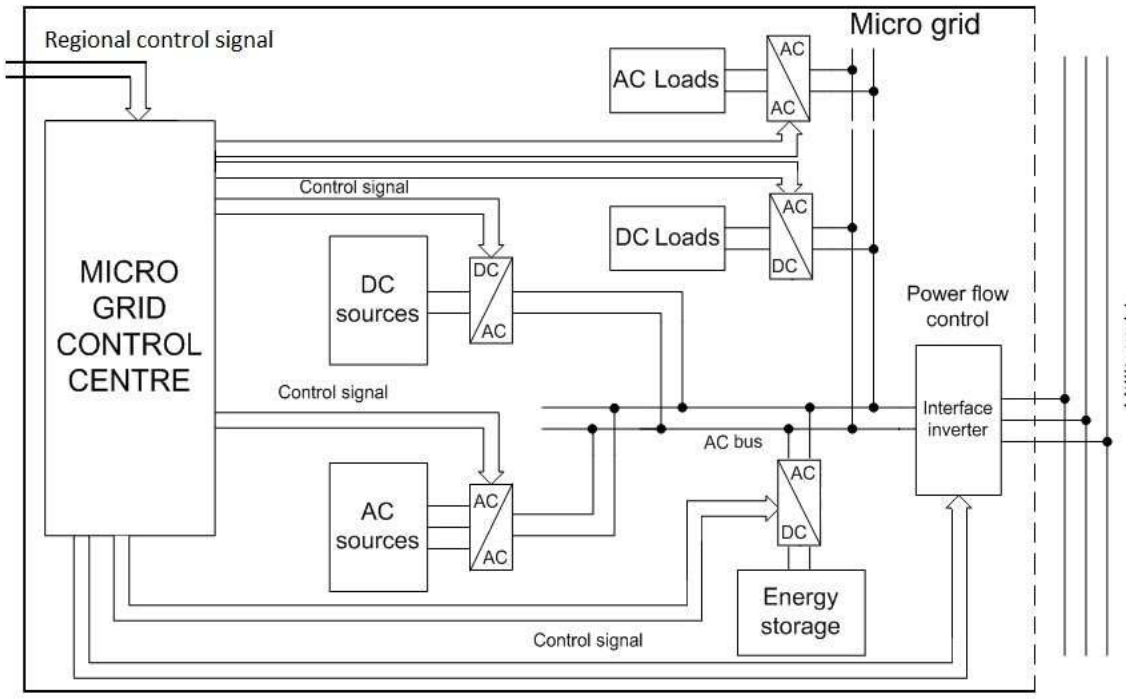

(b)

Fig.4.1. Structures of microgrids: (a) microgrid with DC common bus; (b) microgrid with AC common bus.

4.3. MICROGRID MODULAR DESIGN

With the structure of the chosen microgrid above, this section will describe in detail each component of the smart microgrid.

4.3.1. Modular Renewable and Distributed Energy Resources

4.3.1.1. Photovoltaic

The PV technology converts the solar energy directly into electrical energy by means of solar cells, which are usually manufactured and combined into modules that consist of 36 to 72 cells, depending on the output voltage and current of the module [4.1]. Additionally, the modules can also be grouped together in various quantities and configurations to form arrays with unique voltage and current characteristics [4.2], [4.3]. The performance of a PV array can be affected by many factors, such as the temperature, sun light strength, and shading, etc. This thesis will focus only on the mathematical model and the simulation model of PV cells and panels. Fig 4.2 shows the equivalent circuit of the ideal PV cell.

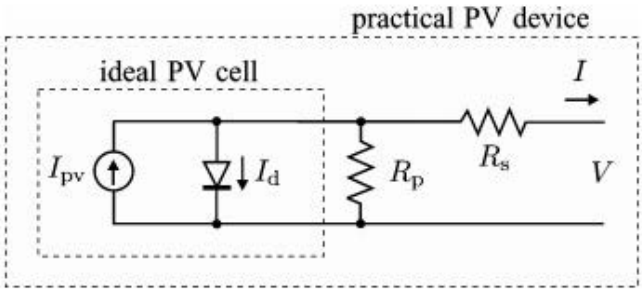

Fig.4.2.Single-diode model of the theoretical PV cell and equivalent circuit of a practical PV device including the series and parallel

According to the basic equation from the theory of semiconductors [4.4], the mathematic equation describes the *I–V* characteristic of the ideal PV cell is:

$$I = I_{pv,cell} - I_{0,cell}\left[exp\left(\frac{qV}{akT} \right) - 1 \right] \tag{4-1}$$

where $I_{pv,cell}$ is the current generated by the incident light, which is directly proportional to the solar irradiation, I_d the diode current, $I_{o,cell}$ the scale current of the diode, q the electron charge (1.60217646×10^{-19} C), k the Boltzmann constant (1.3806503×10^{-23} J/K), T (in Kelvin) the temperature of the *p–n* junction, and a the diode ideality constant. The net cell current I is composed of the light-generated current I_{pv} and the diode current I_d. The characteristic *I-V* of the PV cell is shown in Fig.4.3.

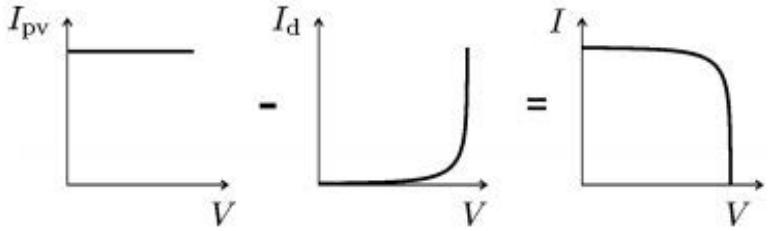

Fig.4.3. Characteristic *I–V* curve of the PV cell.

Practical arrays are composed of several connected PV cells and the observation of characteristics at PV array terminals requires the inclusion of additional parameters to the basic equation:

$$\begin{aligned} I &= I_{pv} - I_d \\ I_d &= I_o\left[exp\left(\frac{V + R_s I}{V_t a} \right) - 1 \right] - \frac{V + R_s I}{R_p} \end{aligned} \tag{4-2}$$

where I_{pv} and I_o are the PV and saturation currents of the array, $V_t = N_s kT/q$ is the thermal voltage of the array with N_s cells connected in series, R_s the equivalent series resistance of the array, and R_p the equivalent parallel resistance. Fig.4.4 shows a characteristic *I–V* curve of a practical PV cell.

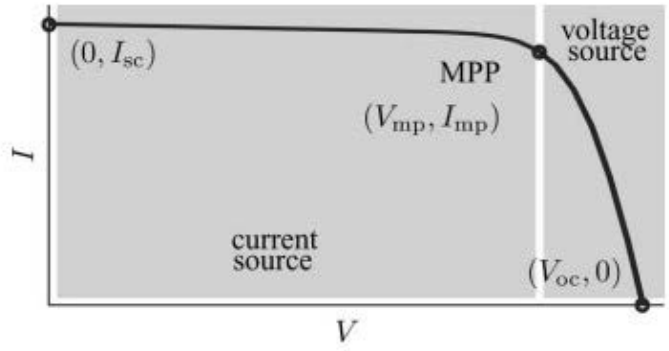

Fig.4.4. Characteristic I–V curve of a practical PV device and the three remarkable points: short circuit (0, Isc), MPP and open circuit (Voc,0)

The light-generated current of a PV cell depends linearly on the solar irradiation and is also influenced by the temperature [4.5] according to the following equation:

$$I_{pv} = \left(I_{pv,n} + K_I \Delta T\right)\frac{G}{G_n} \tag{4-3}$$

where $I_{pv,n}$ is the light-generated current under the nominal condition (usually 25ºC and 1000 W/m^2), $\Delta T = T - T_n$ (T and T_n being the actual and nominal temperatures), G (watts per square meters) the irradiation on the device surface, and G_n the nominal irradiation. The diode saturation current I_o and its dependence on the temperature may be expressed by:

$$I_0 = I_{0,n}\left(\frac{T_n}{T}\right)^3 exp\left[\frac{qE_g}{ak}\left(\frac{1}{T_n} - \frac{1}{T}\right)\right] \tag{4-4}$$

where E_g is the band gap energy of the semiconductor, E_g = 1.12 eV for the polycrystalline Si at 25ºC [4.6,4.7], and $I_{o,n}$ is the nominal saturation current:

$$I_{0,n} = \frac{I_{sc,n}}{exp\left(V_{oc,n} / aV_{t,n}\right) - 1} \tag{4-5}$$

The PV model described in the previous section can be improved if I_o is replaced by:

$$I_0 = \frac{I_{sc,n} + K_I \Delta T}{exp\left(\frac{V_{oc,n} + K_V \Delta T}{aV_t}\right) - 1} \tag{4-6}$$

where K_i and K_v are the current and voltage coefficients

This modification aims to match the open-circuit voltages of the model with the experimental data for a very large range of temperatures. This equation can simplify the model and cancel the model error of the open-circuit voltages, and consequently, in other regions of the *I–V* curve. The relation between R_s and R_p may be found by making $P_{max,m} = P_{max,e}$ and solving the resultant equation for R_s as shown by

$$P_{max,m} = V_{mp}\left\{I_{pv} - I_o\left[exp\left(\frac{q}{kT}\frac{V_{mp} + R_s I_{mp}}{N_s a}\right) - 1\right] - \frac{V_{mp} + R_s I_{mp}}{R_p}\right\} = P_{max,e} \tag{4-7}$$

$$R_p = \frac{V_{mp}\left(V_{mp} + R_s I_{mp}\right)}{V_{mp} I_{pv} - V_{mp} I_o\, exp\left(\frac{q}{kT}\frac{V_{mp} + R_s I_{mp}}{N_s a}\right) + V_{mp} I_o - P_{max,e}} \tag{4-8}$$

Equation (4-8) means that for any value of R_s there will be a value of R_p that makes the mathematical *I-V* curve cross the experimental (V_{mp}, I_{mp}) point. The goal is to find the value of R_s that makes the peak of the mathematical *P-V* curve coincide with the experimental peak power at the (V_{mp}, I_{mp}) point. This requires several iterations until $P_{max,m} = P_{max,e}$. It also should be noted that the photocurrent I_{pv} is proportional to the solar irradiation level *S* and the cell temperature according to (4-3). Tracking the maximum power point (MPP) of a PV array is usually an essential of a PV system, which will be implemented by a DC/DC converter. Since the PV power characteristic

is nonlinear, many maximum power point tracking (MPPT) methods have been developed and implemented over the years. Several methods are briefly introduced here:

- *Constant voltage method*: Normally the voltage at MPP is around 70% - 80% of the PV open-circuit voltage. Based on this experience, the MPP can be achieved by controlling the PV output voltage to a specified value [4.8]. This method is an approximate method.

- *Fixed duty cycle*: This method does not require any feedback, and the load impedance is adjusted only once for the MPP.

- *Beta method*: This method is to approximate the MPP through the equation of an intermediate variable β described as the following [4.9]:

$$\beta = ln\left(\frac{I_{pv}}{V_{pv}}\right) - cV_{pv} \tag{4-9}$$

where $c = (q/(\eta.K_B.T.Ns))$ is a constant that depends on the electron charge q, the quality factor of the junction panel η, the Boltzmann constant K_B, temperature T, and the number of PV cells in series N_s. The main drawback of this method is that the PV electrical parameters must be obtained.

- *Temperature method*: This method employs a low-cost temperature sensor and modifies the MPP algorithm function to maintain the right track of MPP and eliminate the deviation of the MPP due to the variation of temperature [4.10],[4.11].

- *Perturb and observe method (P&O):* The basic idea of the P&O method is to periodically increase or decrease the output terminal voltage of the PV cell and then compare the power obtained in the current cycle with the power of the previous one by checking the sign of dP/dV [4.12,4.13]. It is noted that in steady state, the operational point is not altered unless some changes in environmental conditions

happen. The key is to reduce the dP/dV to zero using a closed loop control performing the P&O based on PI.

In this section, the model of the PV cell is modeled in PSIM using the P&O method which is described in Figs.4.5 and 4.6. A DC/DC boost converter is used to boost the output voltage of the PV cell up to 48 V. Table 4-IV shows the parameters of the simulation.

The input of the PV system will be the daily temperature *T* and irradiation *s*. Fig 4.7 shows a typical solar irradiation (W/m^2) and temperature in September in north of Vietnam. Figs.4.8 and 4.9 show the simulation results of output power of the MPPT implemented and voltage of the PV model after the DC/DC boost converter.

With these results, the smart microgrid with PV can be modelled using the output power from the simulation of PV in PSIM.

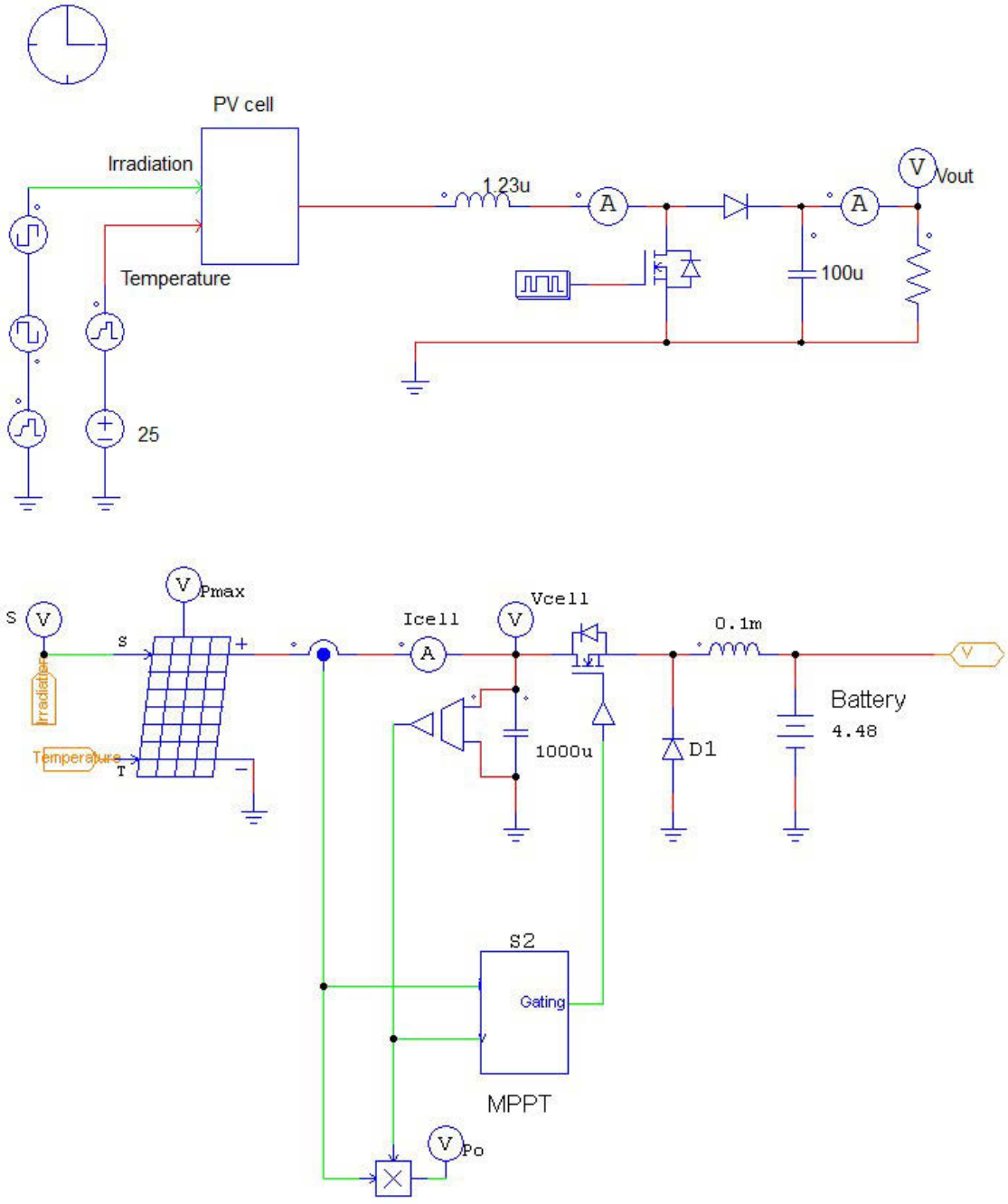

Fig.4.5. Array of PV cells module in PSIM

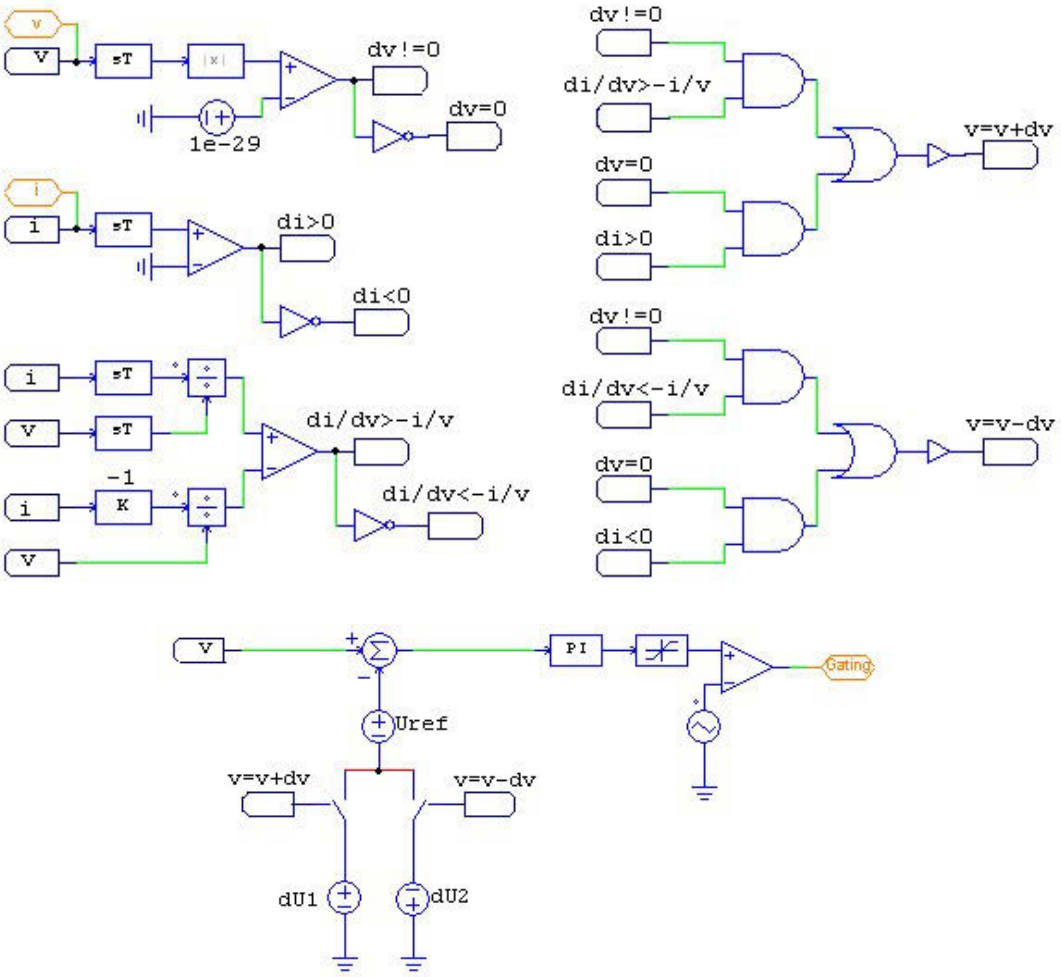

Fig.4.6. Perturb and observe method with PI in PSIM

TABLE 4- IV. PARAMETERS OF PSIM SIMULATION PV ARRAY MODULE

Number of cells	N_s	36
Standard light intensity	S_o	1000
Reference temperature	T	25 ºC
Series resistance	R_s	0.008 Ω
Shunt resistance	R_{sh}	1000 Ω
Short circuit current	$I_{sc,0}$	3.8 A
Saturation current	$I_{s,0}$	2.16×10^{-8} A

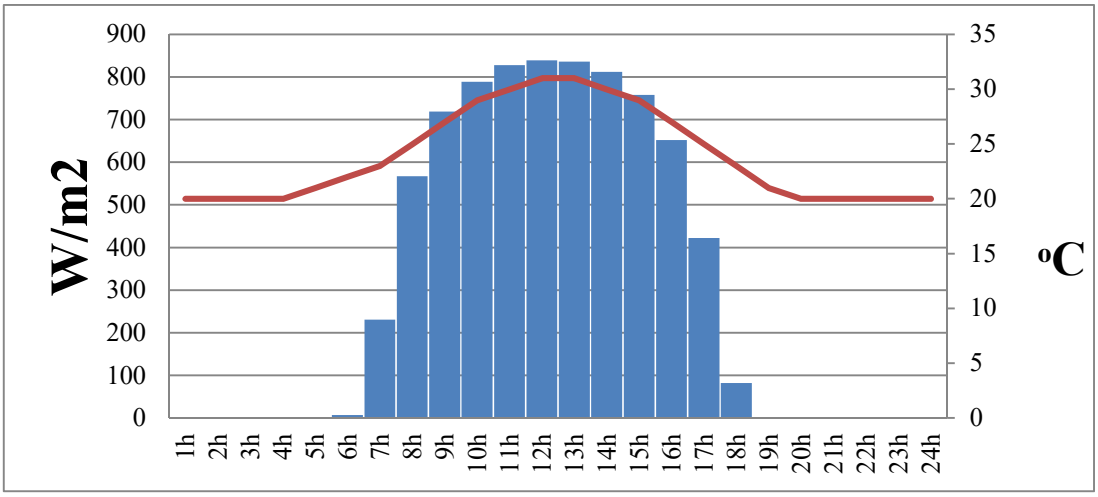

(a)

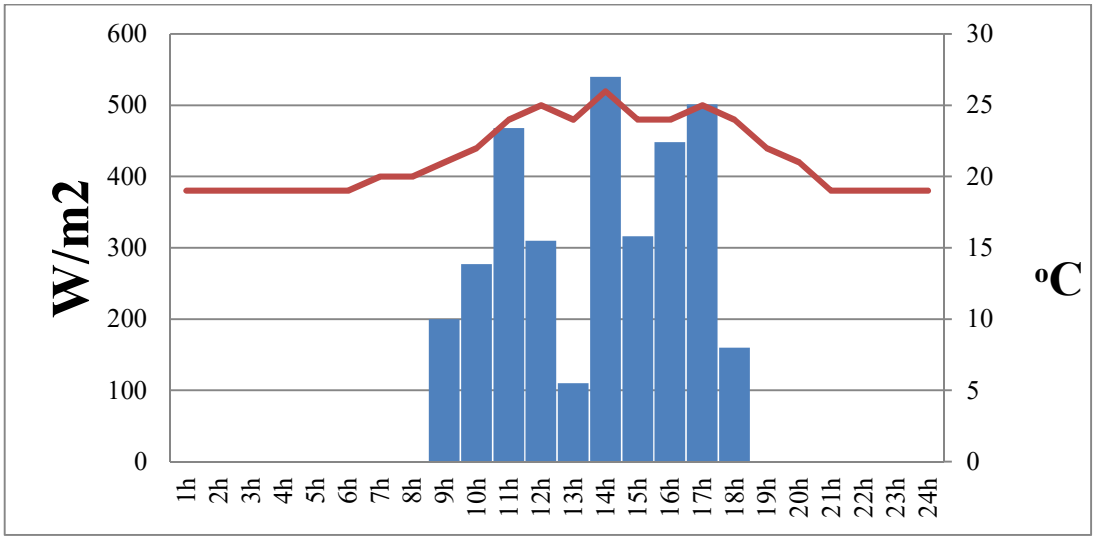

(b)

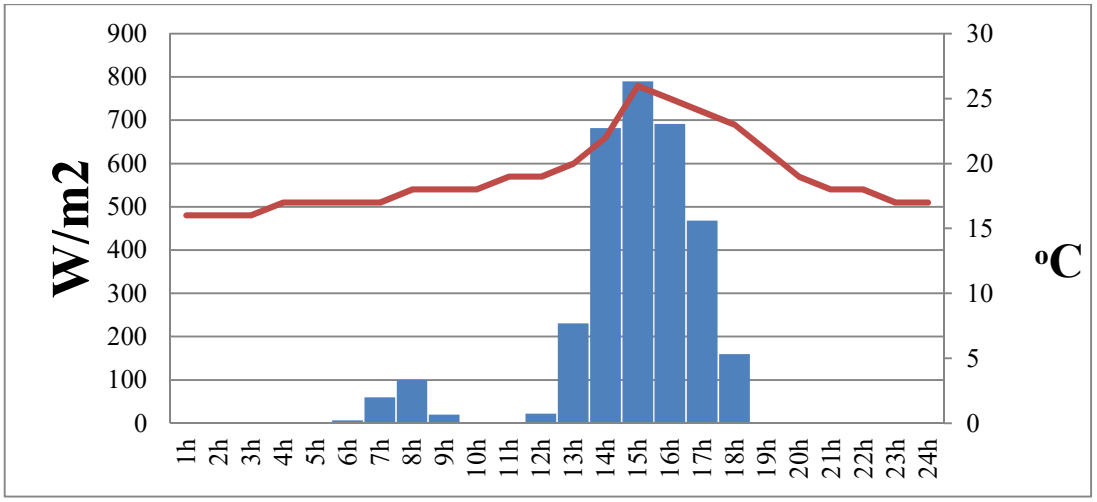

(c)

Fig.4.7. Solar irradiation and temperature of an example day in September in the north of Vietnam with (a) sunny day (b) cloudy day (c) rainy day

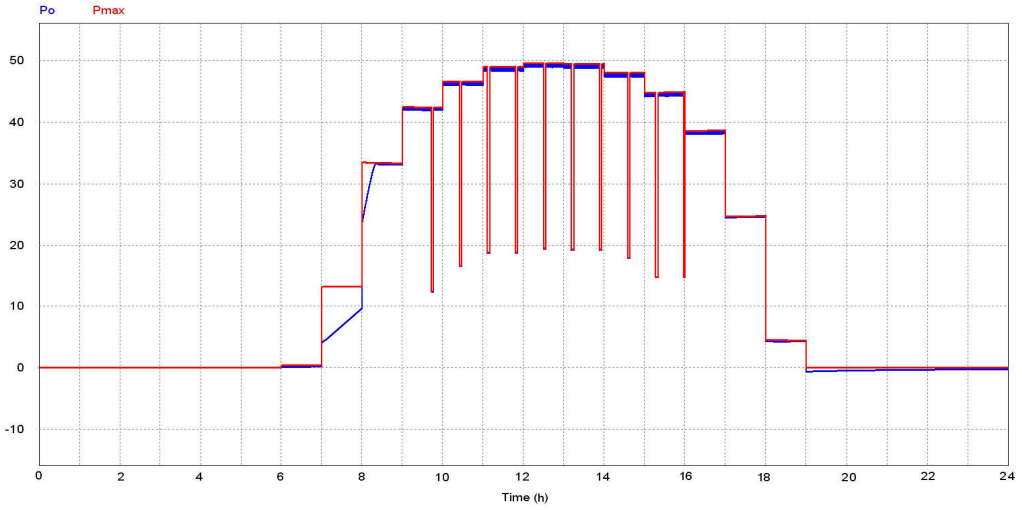

(a)

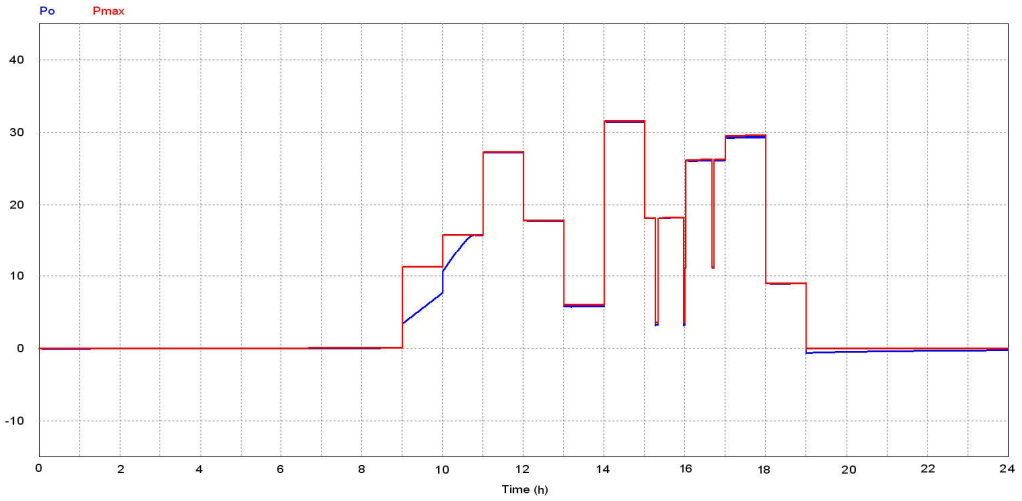

(b)

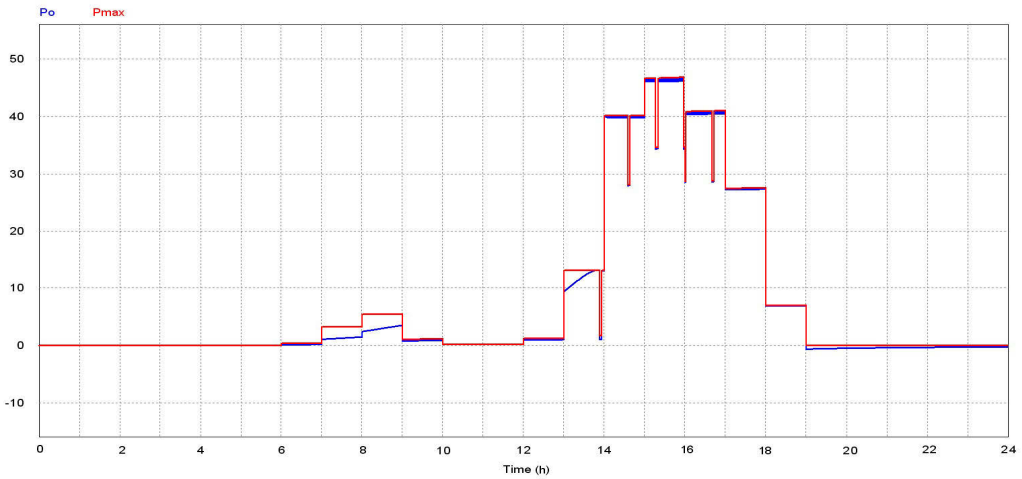

(c)

Fig.4.8. Output power of the PV cell rated 60 W in (a) perfect condition weather without rain (b) cloudy weather possibility 50%, rain possibility 30% (c) rain possibility 80%, and cloudy weather possibility 10%

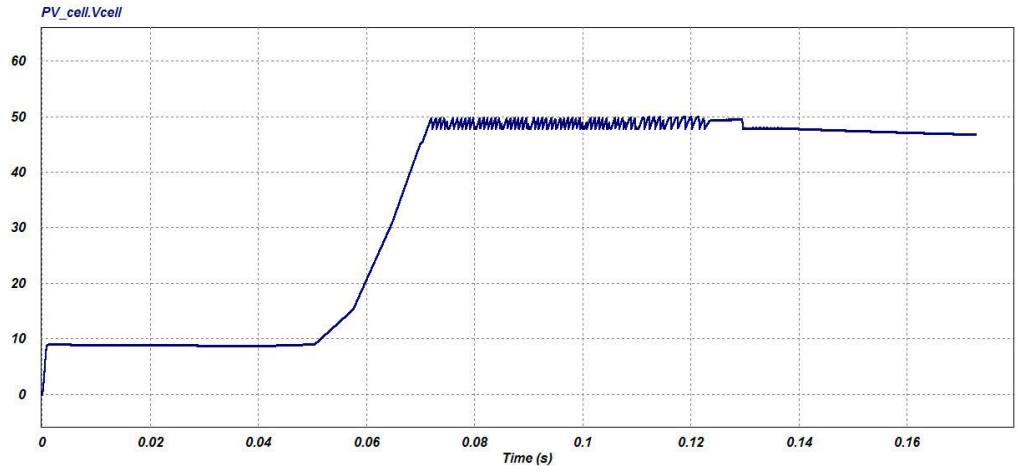

Fig.4.9. Output voltage of PV array after DC/DC boost converter to 48 V.

4.3.1.2. Wind Turbine

Wind energy has become one of the most promising and fastest growing energy resources in the world and the cost of electricity from wind energy has been reduced steadily in recent years. The wind power installed capacity has increased from about 40,000 MW in 2003 to 59,091 MW in 2006 all over the world and that number is expected to grow well over 1,260,000 MW by 2020, which will be sufficient for 12% of the world's electricity consumption [4.14]. Three important issues to be mentioned in wind energy generation system are the reliability, efficiency and cost [4.15]. Besides that, the power quality improvement, and automated fault ride-through have become the main research topic of wind system nowadays.

For a horizontal axis WT, the amount of power that WT is capable of producing is given by:

$$P = 0.5\rho A C_p v^3 \tag{4-10}$$

where P is the power available in watts, ρ the mass density of air, A the cross-sectional of air flow of interest, v the instantaneous free-stream wind velocity, and C_p

the power coefficient, which is a function of the tip speed ratio (TSR) λ and the blade pitch angle β. The TSR is defined as

$$\lambda = R\frac{\omega}{v} \tag{4-11}$$

where ω is the turbine rotational speed and R the turbine radius.

Fig.4.10 shows the relationship between the output power P and the rotational speed ω. For different wind speeds, there is only one specific λ at which C_p is maximum. This is why the rotational speed should be regulated to achieve MPPT. In general, wind power generation uses either fixed speed or variable speed turbines which can be characterised into these following types [4.16]:

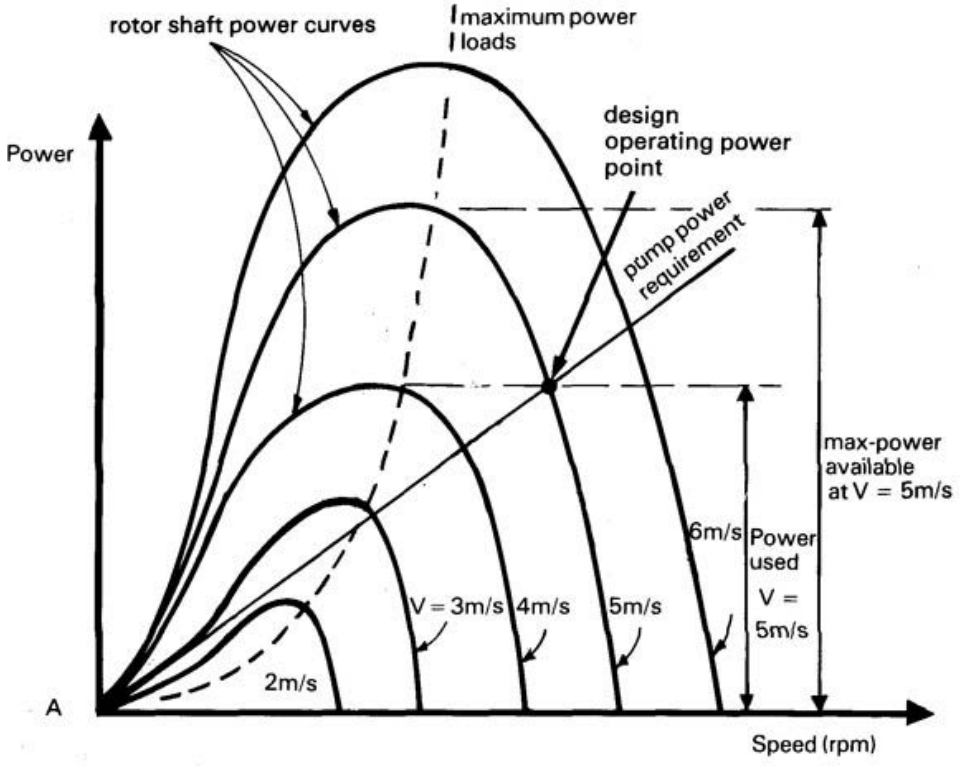

Fig.4.10. The power of a wind rotor as a function of rotational speed for different wind speed

- Fixed speed WTs or constant speed constant frequency system (CSCF): In such a system, an asynchronous squirrel-cage induction generator (SCIG) is directly

connected to the grid via a transformer as shown in Fig.4.11. The so-called “fix speed WT” comes from the point that the rotational speed of the WT cannot be automatically controlled and will only differ by the wind speed.

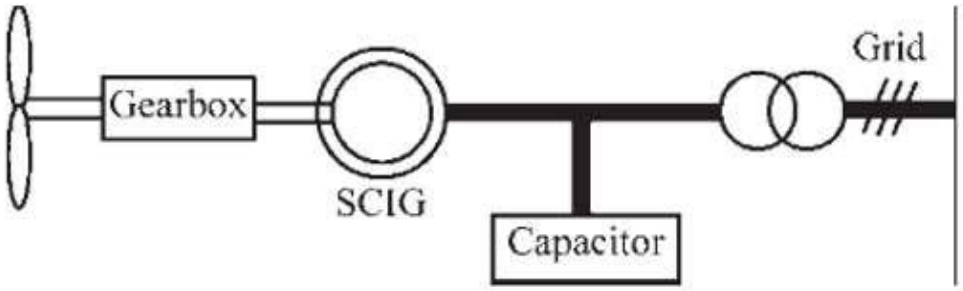

Fig.4.11. CSCF system with squirrel-cage induction generator

This type of WT needs a switch to prevent motoring operation during low wind speeds, and also suffers a major drawback of reactive power consumption subsequently there is no reactive power regulation. Besides, this type of WT transfers the wind variations to mechanical instabilities and further converts these into electrical power oscillations due to the fact that there are no speed or torque control loops. These electrical power oscillations can lead to an effect in the case of a weak grid. Also, the operating speeds are determined by choosing the number of generator poles and/or the gear ratio. The smaller generator is used in low winds and the larger one in high winds [4.17].

- Partial variable speed WT with variable rotor resistance: This type of turbines uses a wound rotor induction generator (WRIG) directly connected to the grid. The controlled resistances are connected in series with the rotor phase windings of the generator. In this way, the total rotor resistances can be regulated, and thus the slip and output power can be controlled. Due to the limitation of serial resistance sizes, the variable speed range is usually small, typically 0-10% above the synchronous speed [4.16].

- Variable speed WT with partial scale power converter: This arrangement, known as the doubly-fed induction generator (DFIG) concept, uses a variable speed controlled WT. The stator phase windings of the DFIG are directly connected to the grid, while the rotor phase windings are connected to a back-to-back converter via slip rings as in shown Fig.4.12.

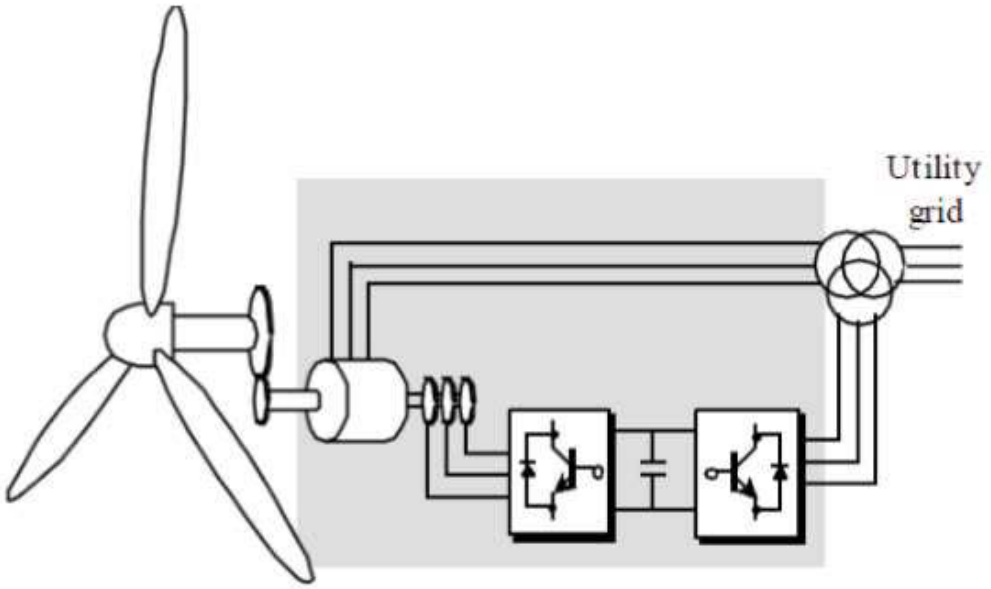

Fig.4.12. Doubly fed wound rotor induction generator system

The power converters could control the rotor frequency and thus the rotor speed. The power rating of the power converters is typically rated 20% around the rated power since the rotor of the DFIG would only deal with the slip power [4.18]. The smaller rating of the power converters makes this concept eye-catching from a cost-effective viewpoint. Besides, this type of WTs can also achieve the desired reactive power compensation.

- Variable speed WT with full scale power converter: Fig.4.13 shows the structure of a permanent magnet synchronous machine (PMSM) with a full-scale power converter. The stator phase windings are connected to the grid through a full-scale power converter.

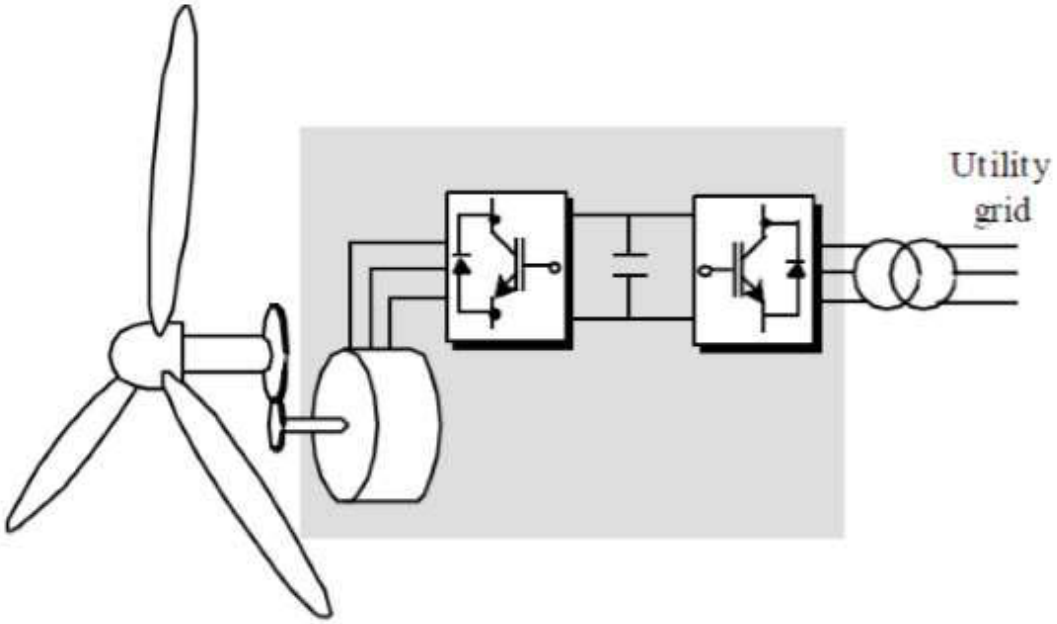

Fig.4.13. Permanent magnet synchronous generator (PMSG) system

The PMSM has several advantages [4.19], such as:

(a) The PMSM can achieve full speed regulation;

(b) The PMSM makes it possible to avoid a gearbox; and therefore, there are no mechanical stress issues when experiencing wind gusts;

(c) The PMSM does not need the slip-rings and brushes; and hence, less maintenance will be needed. Therefore, a PMSM-based WT will be more stable than a DFIG-based one, and

(d) The PMSM can also attain the active and reactive power control. The control schemes are relatively simple and easy to implement.

Although there are still some disadvantages [4.20], such as high loss due to power converters, high harmonic components, and the size limitation because of the use of multi-pole generators, etc., the PMSM is still suitable for small systems like a rural farm. Therefore, the microgrid designed in this project will use a PMSM WT.

The phase *a* voltage of a wye-connected PMSM with surface mounted magnets can be expressed as:

$$u_a = R_a i_a + \frac{d\psi_a}{dt} \tag{4-12}$$

where u_a is the voltage, R_a the stator winding resistance, i_a the current, and ψ_a the flux linkage of phase *a,* respectively. The phase *a* flux linkage, ψ_a, can be further described as

$$\psi_a = (L_{a\sigma} + L_{aao})i_a + M_{ab}i_b + M_{ac}i_c + \psi_M \cos(\theta_r + \varepsilon) \tag{4-13}$$

where $L_{a\sigma}$ is the leakage inductance corresponding to the flux that links only phase *a* winding, L_{aao} the component of self-inductance corresponding to the flux that links not only the phase *a* winding but also the windings of the other two phases, M_{ab} and M_{ac} are the mutual inductance between phase *a* and phases *b* and *c*, respectively, ψ_M the permanent magnet flux linkage, θ_r the angle between the reference point and the north pole of the permanent magnet, and ε the angle between phase *a* and the reference.

The *d*-*q* model of PMSG in synchronous reference frame is shown in Fig. 3.6. The *d* and *q*-axes voltages of PMSG can be given by

$$\begin{aligned} u_d &= i_d R_s + \omega\psi_d - p\omega\psi_q \\ u_q &= i_q R_s + \omega\psi_q + p\omega\psi_d + p\omega\psi_M \end{aligned} \tag{4-14}$$

where ψ_d and ψ_q are the *d* and *q*-axes stator flux linkages, i_d and i_q the *d* and *q*-axes stator currents. The *d*-*q* model of PMSG in synchronous reference frame is shown in Fig.4.14.

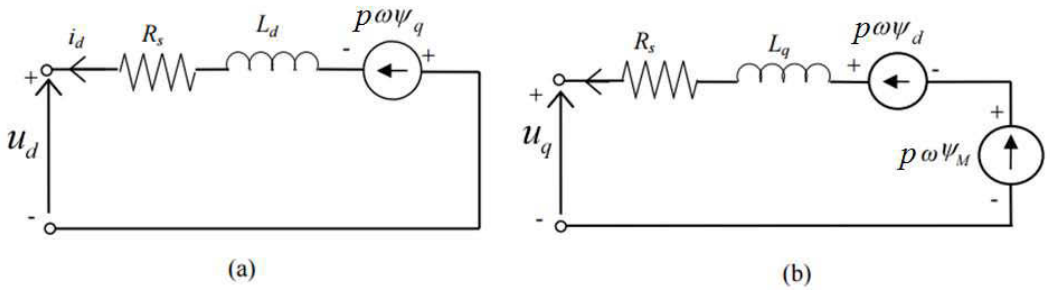

Fig.4.14. *d-q* model of PMSG in synchronous reference frame (a) d-axis equivalent circuit (b) q-axis equivalent circuit

For a PMSM with the chosen reference angle, the flux linkage and the torque produced from an electrical machine modelled in the rotating reference frame can be expressed as

$$\begin{aligned} \psi_d &= L_d i_d \\ \psi_q &= L_q i_q \\ \psi_M &= M i_f \end{aligned} \tag{4-15}$$

$$T = \frac{m}{2} p\left[(\psi_q + \psi_M) i_d - \psi_d i_q \right] \tag{4-16}$$

where m is the number of phases and p the number of pole pairs.

By substituting (4-15) into (4-16) the torque equation for a PMSM with surface mounted magnets becomes

$$T = -\frac{m}{2} p(\psi_M i_q + (L_d - L_q) i_d i_q) = -\frac{m}{2} p\psi_M i_q \tag{4-17}$$

It is apparent that the torque is composed of the "excitation torque" (occurring between i_q and the permanent magnet ψ_M) and "reluctance torque" due to the saliency (difference in the *d*-axis and *q*-axis inductances). For the surface mounted magnet PMSM, $L_d = L_q$ because the stator inductances are independent of rotor position, the torque of the WT is then controlled by controlling the current i_q. Normally, if the wind speed is below the rated number, the generator torque control is active while the blade

pitch is typically held at the constant angle that captures the most power. Otherwise, if the wind speed is above the rated number, the generator torque is typically held constant while the blade pitch control is active. The PSIM simulation in this section uses PMSM model which is shown in Fig.4.15.

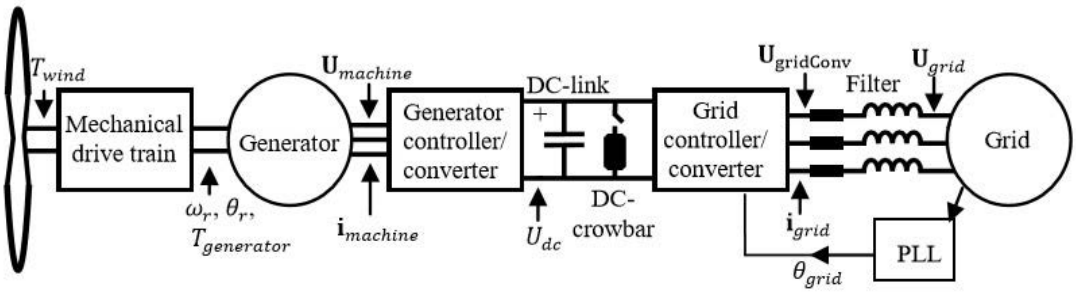

Fig.4.15. An overview of the PMSM wind turbine power generating system together with the measured quantities

With the PMSM as renewable energy of the smart microgrid, the DC link in Fig.4.15 is the DC bus of the microgrid. Fig.4.16 presents the PSIM simulation model of PMSM. The input of the system will be the wind speed, and the output is the power from the WT. The speed regulation and DC voltage controller of the simulation model are described in Fig.4.17. As seen in (4-20), for a PMSM the torque is proportional to the current, so the generator-side converter of PMSM model in the PSIM software controls the current in the α-β reference frame with a PI controller. If the WT is connected to the grid, the purpose of the grid-side converter is to deliver the energy from the DC-link to the grid. In real-time systems, there are always delays and other disturbances, so in order to make the system more redundant, a DC-link voltage controller is added to cope with energy offsets that may occur. Fig.4.18 shows the result of the torque and DC-link voltage control of PMSM WT model in PSIM software.

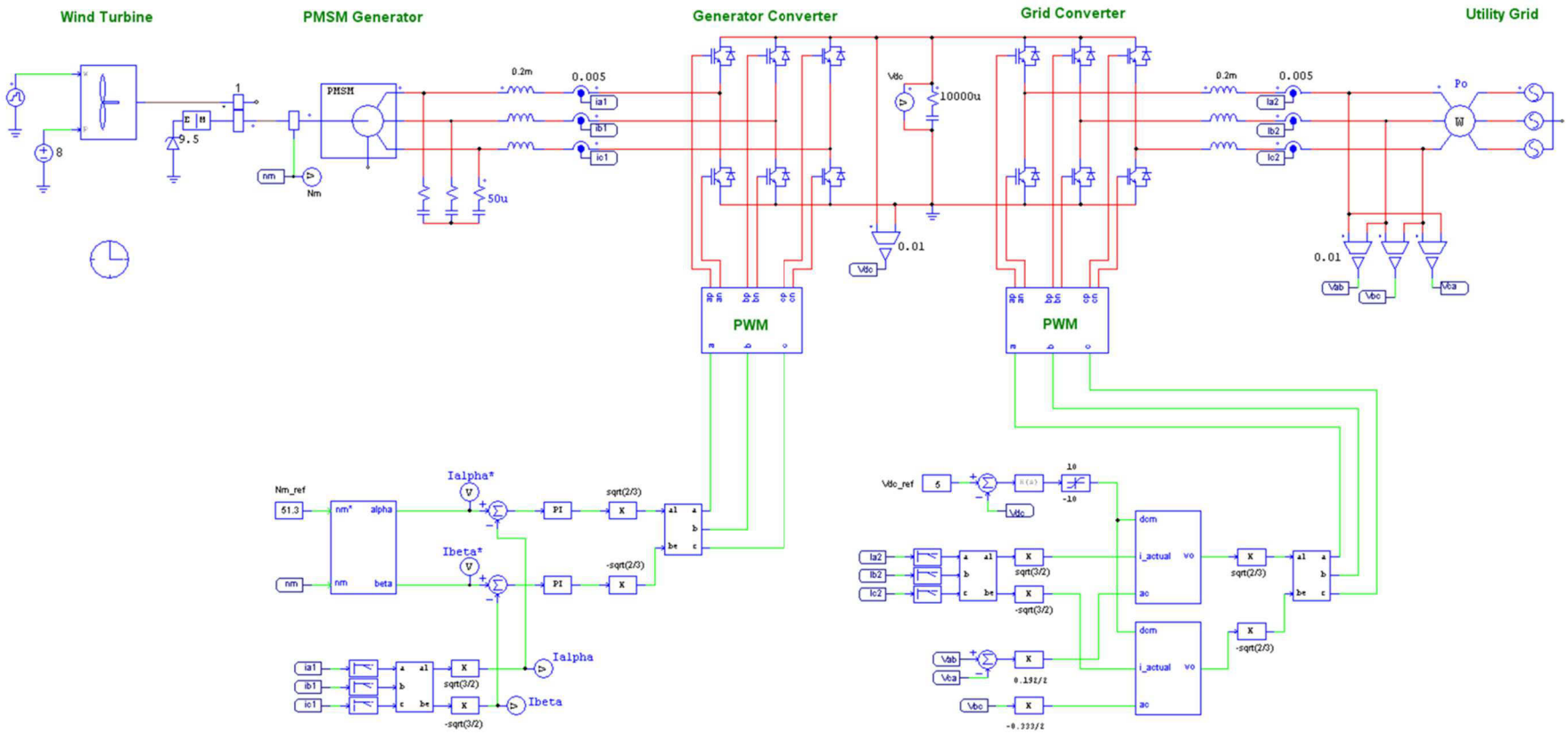

Fig.4.16.PSIM model of PMSM wind turbine

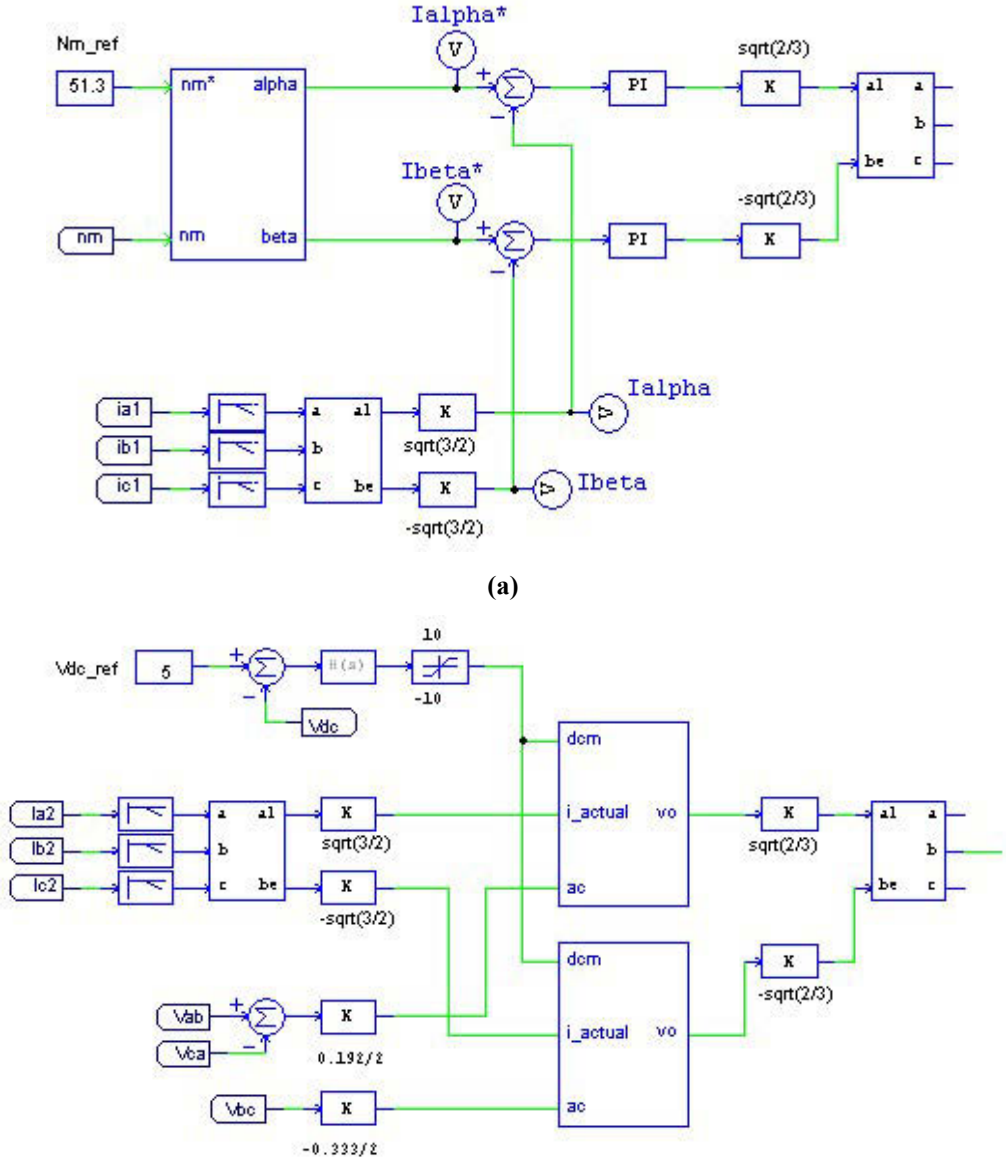

Fig.4.17. Speed regulated (a) and DC voltage control (b) of PMSM model

Table 4-V illustrates the parameters of the simulation in PSIM software.

TABLE 4- V. PARAMETERS OF THE SIMULATION

Rated output power	P	2 kW
Base wind speed	v_{min}	3.5 m/s
Rated wind speed	v	8 m/s
Machine stator resistance	R_s	0.0125 Ω

d-axis inductance	L_d	0.001 H
q-axis inductance	L_q	0.001 H
Machine torque constant	K_i	5.308 N.m/A peak
Machine pole pairs	p	5
Inductor in buck converter	L	500 µH
Capacitor in buck converter	C	300 µF

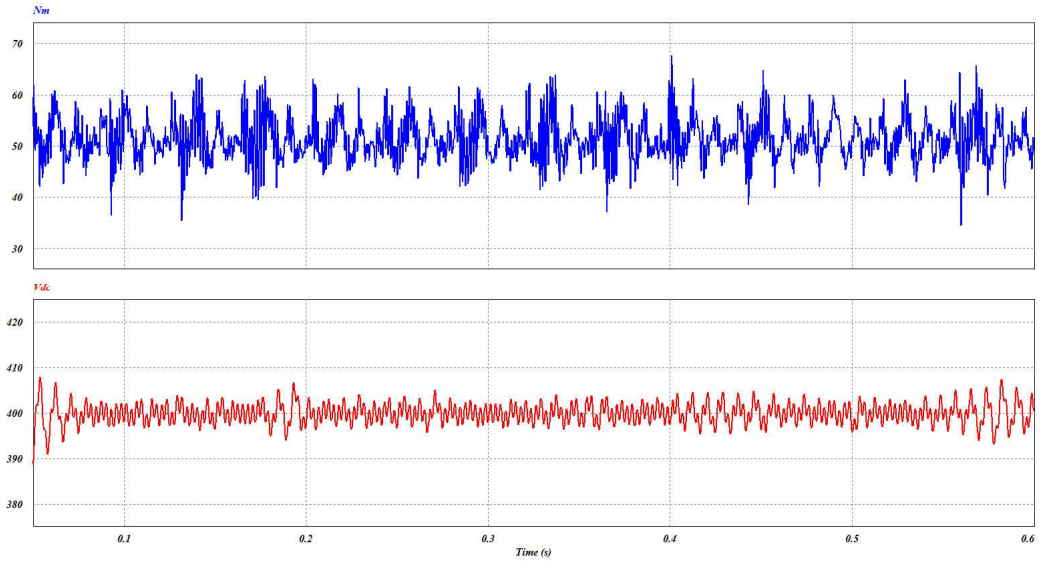

Fig.4.18. Simulation results of Torque *Nm* and DC output voltage at V = 400 V DC.

Fig.4.19 (a) shows the actual wind speed information measured in a wind farm during a day [4.21] with obvious fluctuation. Using this wind speed as the input of the system, the obtained power output of a wind power system of 2 kW PMSM is shown in Fig.4.19 (b).

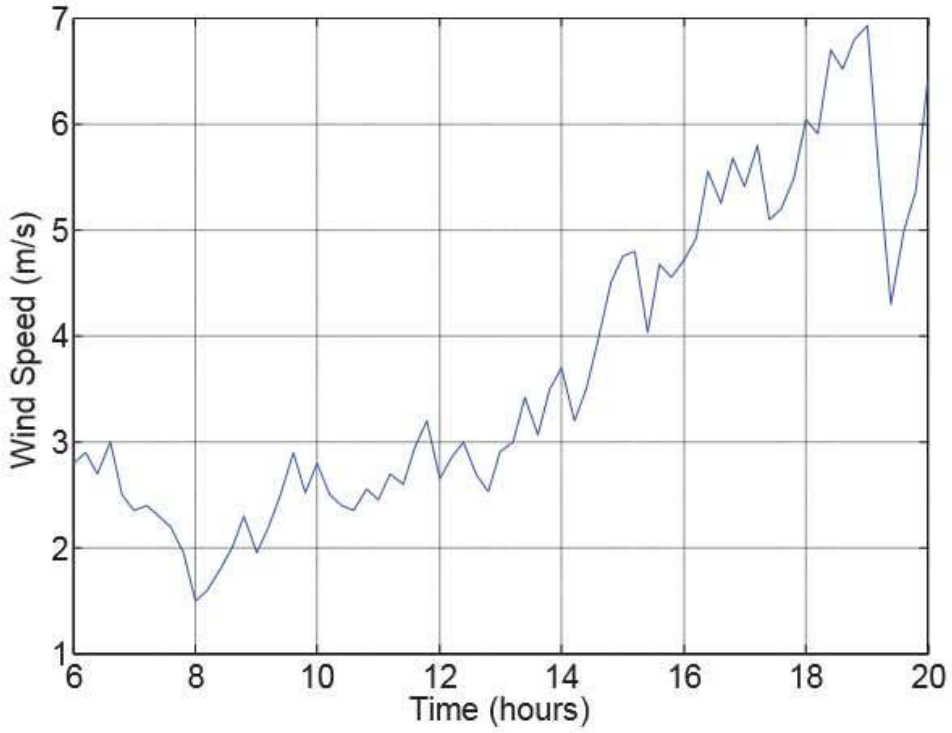

(a)

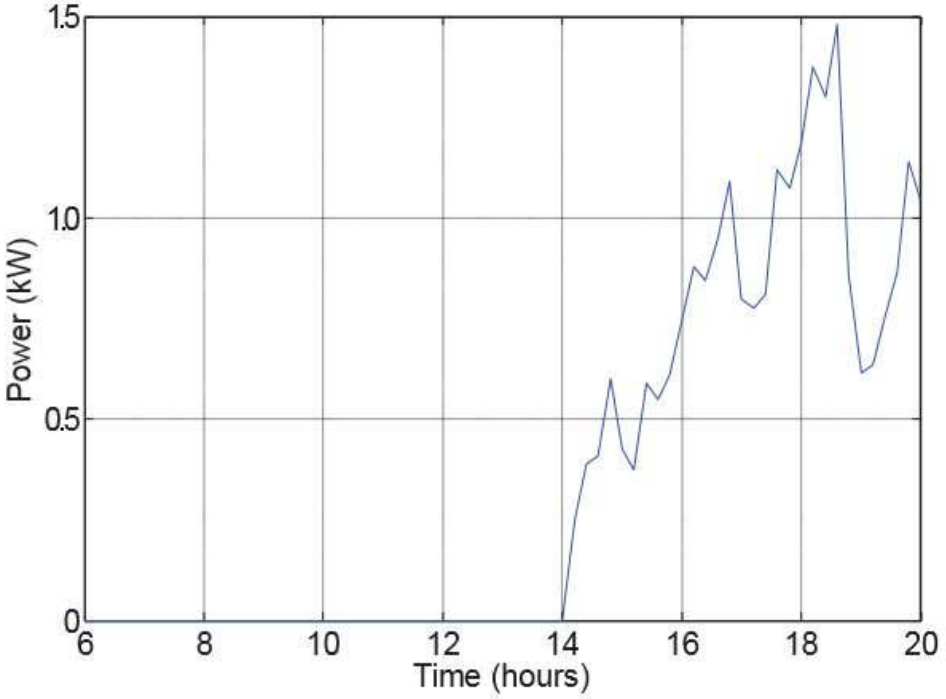

(b)

Fig.4.19. Wind speed (a) and Power output (b) of 2 kW PMSM system

4.3.1.3. Other distributed power generator

In a smart microgrid, other disturbed energy sources can also be used such as PEM fuel cells, and diesel generators, etc. Although the diesel generator is not renewable and clean, and maybe expensive to install and operate, the diesel generator or other distributed energy resources are quite essential sometimes, especially when the power output from the RESs cannot meet the demand of critical loads and the main grid is not available. This section will not go into detail of other type of DGs as they are optional.

4.3.2. Model of Energy Storage System

The battery bank is used as the energy storage device here to absorb the surplus power from the energy sources when the power generated is greater than the power consumed, and deliver it back in the opposite situation. The equivalent model of battery model is shown in Fig.4.20. Normally the manufacturer prevents intensive use of the batteries and also protects them from a deep discharging or overcharging. The batteries can support a specified peak current, but smooth operation is strongly recommended by the manufacturer for expanding lifetime of the battery. The data of the state of charge (SOC) from the battery bank is measured and sent to the control centre.

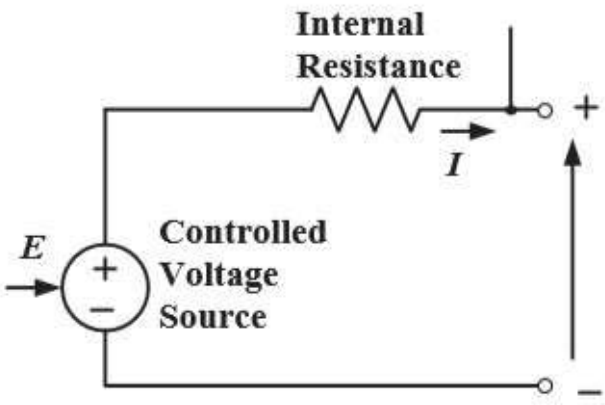

Fig.4.20. Equivalent circuit of battery bank

4.3.3. Model of Loads

The load profile is taken from the actual electricity power consumption of a Vietnamese household during a day with power consumption from all the electric appliances including lights, personal computers (PCs), and air conditioners, etc. Fig.4.21 shows the load profile during a day. It can be observed that the load profile features an obvious fluctuation with peak power consumption at 12:00 – 13:00 and 20:00 – 22:00, respectively.

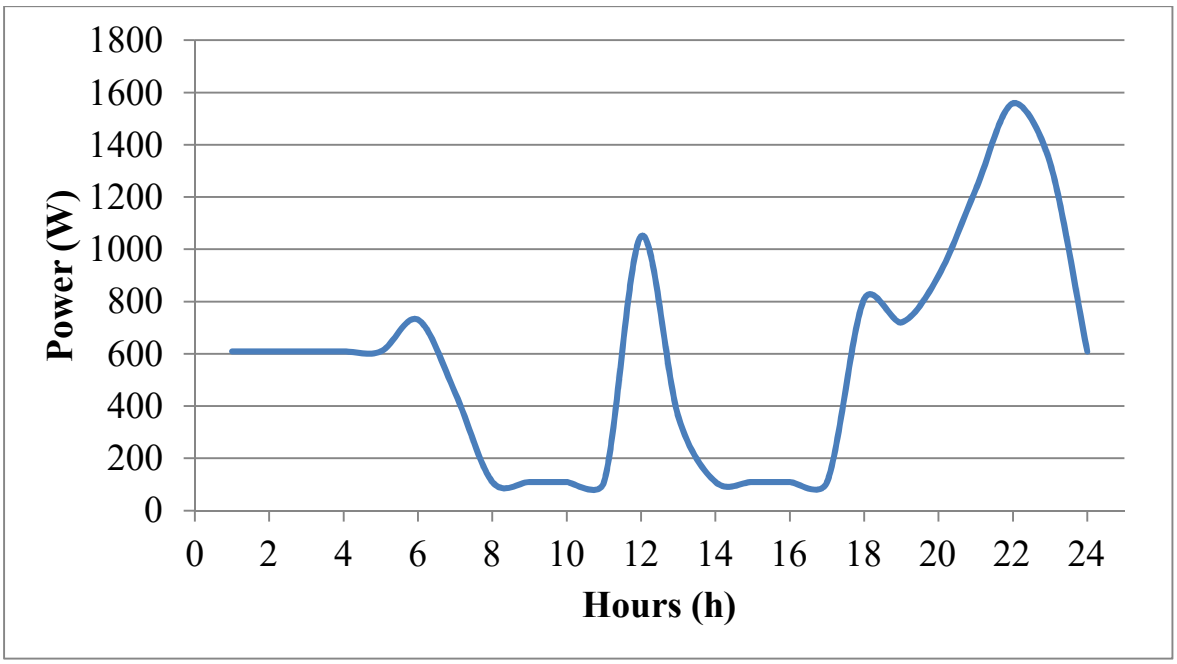

Fig.4.21. Daily average load profile of Vietnamese household

With such a fluctuation of load profile as well as power output from renewable energy, it seems that it is impractical to connect the renewable power generation units directly to the loads because not only the power output of energy sources themselves oscillate but also the load demand varies all the time. Therefore, the utilization of battery bank becomes essential since it can absorb the power fluctuation thus mitigating the power mismatch.

4.4. SMART MICROGRID OPERATION AND MODEL PREDICTIVE CONTROL TOPOLOGY

As mentioned early in this chapter, the Vietnamese main grid is quite unreliable and unstable. Therefore, the term of “smart microgrid” introduced in this section is proposed to cope with all the difficulties that Vietnamese rural people have to face. Firstly, the smart microgrid can operate in both islanded and grid-connected modes. During the time that the main grid is off, the local energy resources is the only power supply for the loads, and the smart microgrid is expected to be a well-controlled small system that can maximize the output of the RESs while still maintaining to provide high-quality power to the local loads. When connected to the main grid, the smart microgrid will minimize its operational cost and provide/absorb the desired active and reactive power to/from the utility grid. This grid thus can be thought of as a platform to meet the demand of both sides: main grid and end user sides [4.22-4.24]

In general, the newly introduced smart microgrid in this chapter will have the following features:

- Smart infrastructure: the microgrid structure consists of both DC main bus and AC sub-bus will take advantages in both user-friendly characteristics of 220 V AC bus [4.25-4.29] with small household devices such as air conditioning system, and personal gadget devices, etc. and power efficiency optimization of DC bus [4.30-4.34].

- Smart communication system: the smart microgrid will interface with the main grid through a grid-connected inverter, which will be studied in the upcoming

chapter. It also communicates with all the power converters inside the microgrid to provide control signal as well as gathering all the data needed through the smart control center. In this chapter, the smart control center is built up using MATLAB/Simulink to exchange data through the serial communication. Then the control command is sent from the software to control all the power converters inside the smart grid.

- Smart control and power management system: the main objective of the smart microgrid for the rural farm is to ensure the supply of high-quality power to the local loads while minimizing the operational cost by using local RES. Moreover, when there is a demand from the main grid, the smart microgrid should be able to provide the desirable active and reactive power through the grid-connected inverter. It is commonly necessary to use an ESS to smooth the gap between power generation and power consumption within the microgrid.

In the section below, firstly, the smart micro operation in islanded mode and grid-connected mode will be described. After that, the MPC scheme for smart microgrid will be applied to optimize the operation of the system.

4.4.1. Voltage Control For DC Microgrid

There are two types of voltage control methods that are commonly used to control the DC voltage in microgrids: the master-slave (MS) and voltage droop control. The MS method depends on the communication between the interface converters. The master converter controls the voltage of the DC bus and sends reference signals to other converters. In the voltage droop control, the DC bus voltage measured at the points of coupling of the converters is used to calculate the amount of energy that each load or source will consume or supply. The block diagrams of the

voltage droop control and MS control are illustrated in Figs.4.22. (a) and (b), respectively.

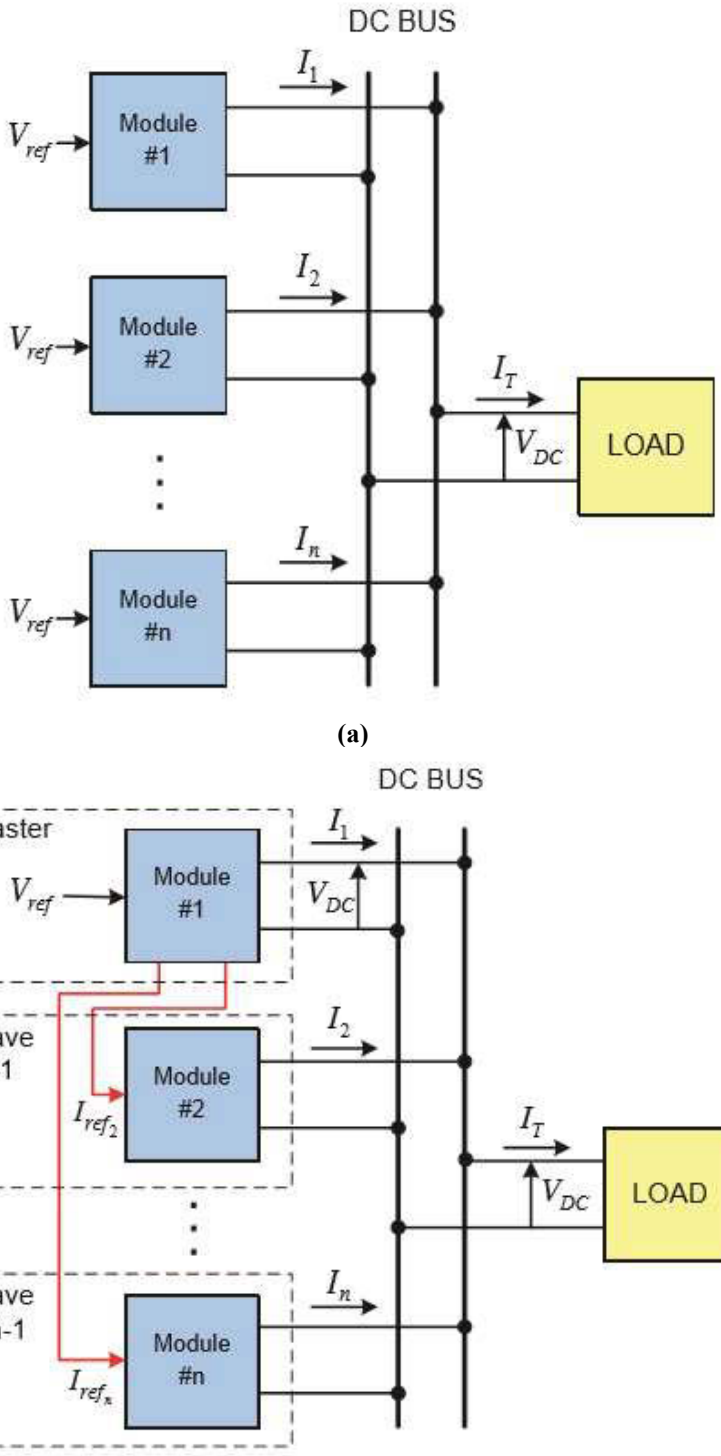

Fig.4.22. Block diagram of (a) voltage droop control

(b) master-slave control

In [4.34], five different methods including the droop control and four other control methods that need some level of communication are presented. In [4.36] and [4.37], some improvements in the voltage droop control using adaptive control and integral controllers were proposed to reduce the steady state errors. In [4.38], a methodology is applied to assure the power sharing between different sources with converters of the same power rating.

In Fig.4.22.(b), the master block, which is the microgrid control centre, will control the voltage of the DC bus and send the signal to the other slave RES blocks. This control scheme requires fast communication channels since the reference currents for the slave converters are provided by the microgrid control. It fits perfectly with the smart microgrid infrastructure and its smart communication system. However, the loss of communication link or malfunctioning of microgrid control centre can shut down the whole system [4.35], [4.39]. To avoid this, the smart micro grid should be able to work during a fault mode with voltage droop control method applied.

4.4.2. Grid-Connected Mode

4.4.2.1. Description

In the grid-connected mode, the grid-connect power converter acts as a rectifier to transfer the 220 V AC from the main grid into 400 V DC bus of the microgrid. The local loads are supplied by both RES and the main grid. The smart microgrid will operate according to the following conditions:

- If the load demand is smaller than power output from the RES:

+ case 1: SOC of ESS < 80%: load is supplied by RES; the power from RES will be stored in ESS.

+ case 2: SOC of ESS > 80%: load is supplied by RES, the rest power from RES will be sending back to main grid.

- If the load demand is greater than power output from the RES:

+ case 1: SOC of ESS > 20%: load is supplied by both RES and ESS.

+ case 2: SOC of ESS < 20%: load is supplied by RES and main grid.

The power converter of the RES should be able to connect the local RES to the common 400 V DC bus with MPPT applied all the time.

4.4.2.2. Numerical simulation

Using the data from each module of RES and the load profile, the system is simulated using MATLAB/Simulink, and the results of power output and load demand are shown in Figs.4.23 and 4.24.

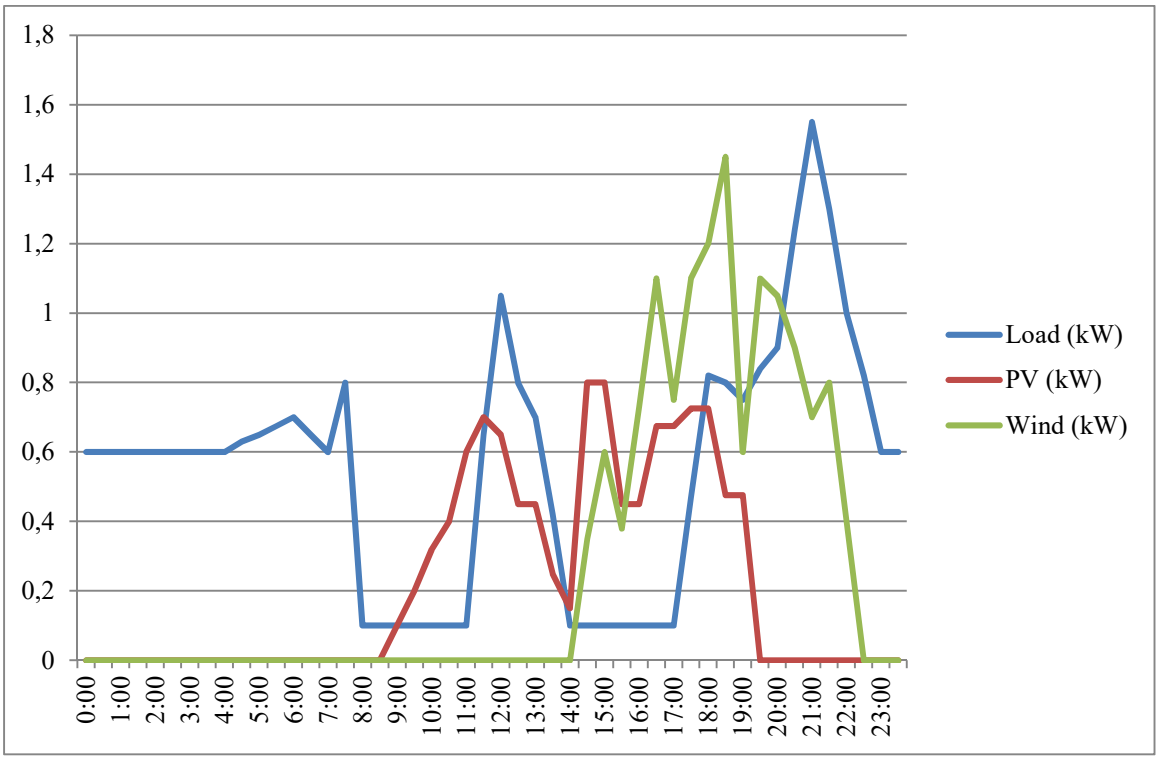

Fig.4.23. Power output from RES and load profile of a cloudy day in Vietnam

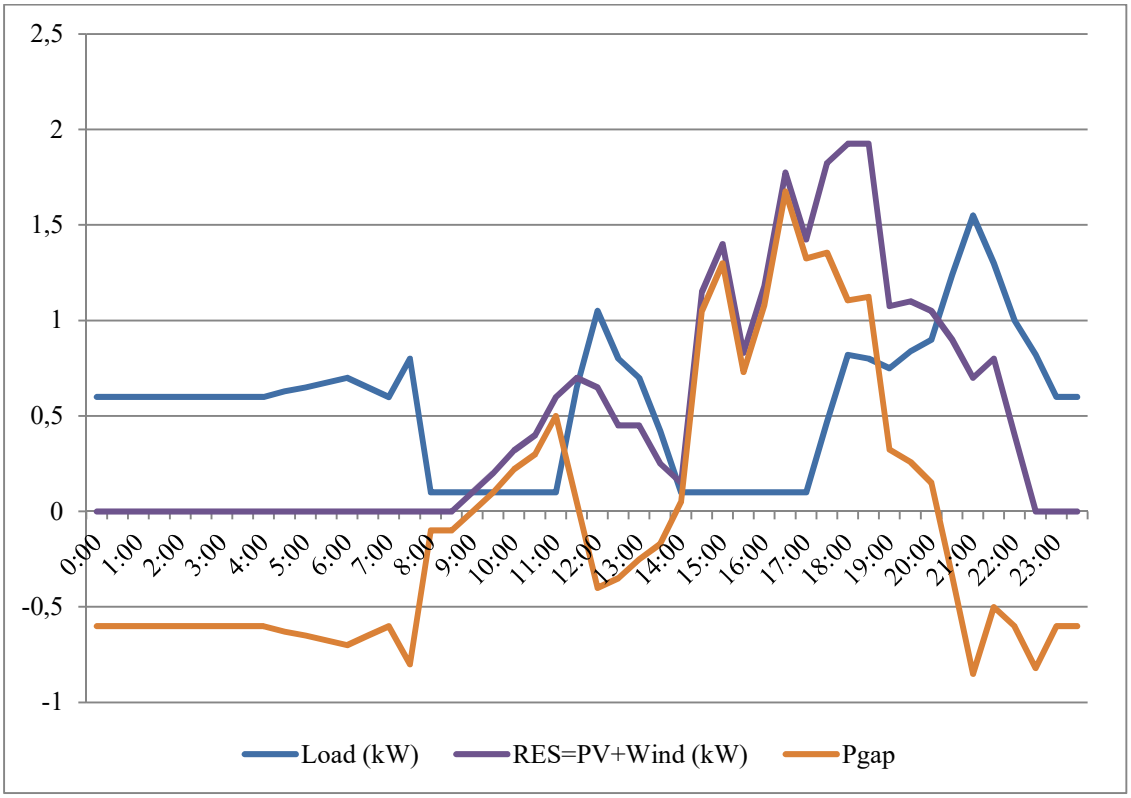

Fig.4.24. Power output from RES and power gap of Pres and PL

Fig.4.24 shows the gap between the output power P_{res} and load demand P_L: $P_{gap} = P_{res} - P_L$. This gap will be smoothed by power received from the main grid if $P_{gap} < 0$ kW or will be stored in ESS if $P_{gap} > 0$. The total energy stored in ESS and SOC of the battery bank capacity 5kWh is illustrated in Fig.4.25.

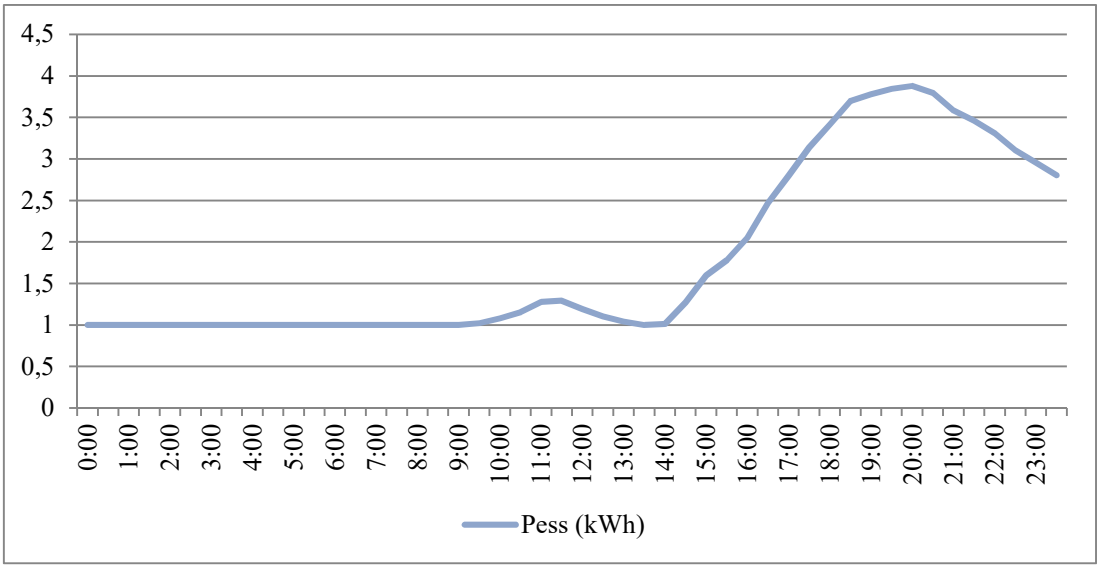

(a)

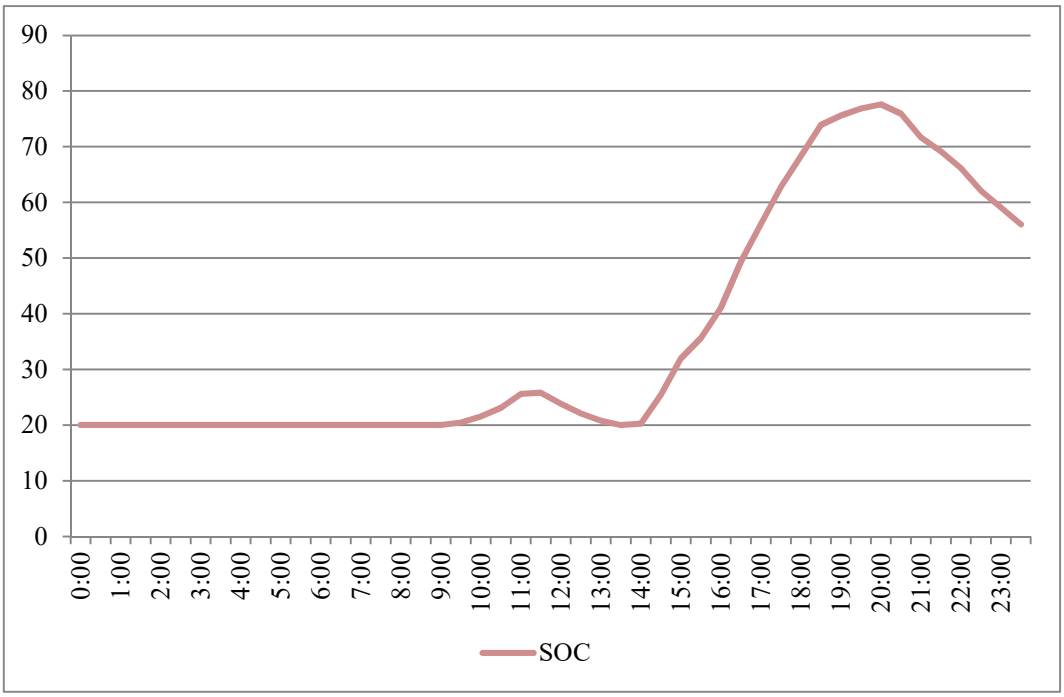

(b)

Fig.4.25. ESS total power and SOC during a day

4.4.3. Islanded mode

4.4.3.1. Description

When the smart microgrid is not connected to the main grid, the RES and ESS supply the local loads. The non-critical loads will be shut down if the RES and ESS

cannot provide enough power to the system. If the RES output power is still smaller than the demand of critical loads, the diesel generator will be used. The system will operate as the following:

- If the load demand is smaller than output power from RES, the rest power will be stored in ESS.

- If the load demand is greater than output power from RES:

+ case 1: SOC > 20%: load is supplied by both RES and ESS.

+ case 2: SOC < 20%: non-critical load will be shut down until output power from RES meets load demand.

+ case 3: SOC < 20%, non-critical load will shut down but critical load demand is still greater than RES output power: other DGs will be used.

4.4.3.2. Numerical simulation

Using the statistical from the previous section, suppose that the SOC of ESS in the previous section is 55.6% at the end the day, when there will be a power outage for the whole day next sunny day. The system simulation results are shown in Fig.4.26.

It can be noticed that during 3 AM – 6 AM, there is no power from RES and the ESS of the battery bank is 1 kWh which has the minimum SOC of 20%, the load will be shut down or the diesel generator will be used to meet the load demand during this time.

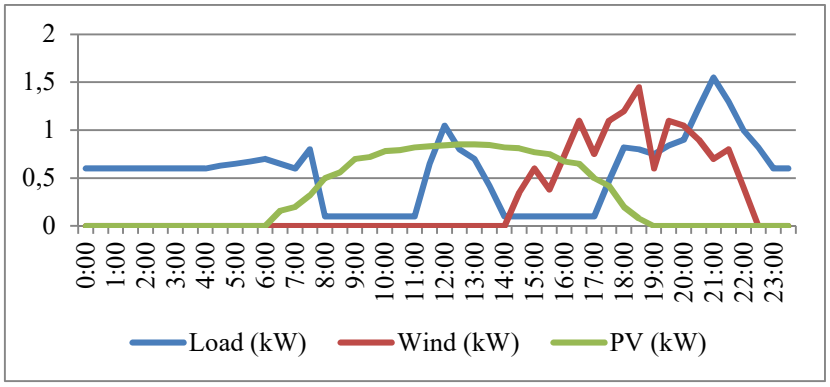

(a)

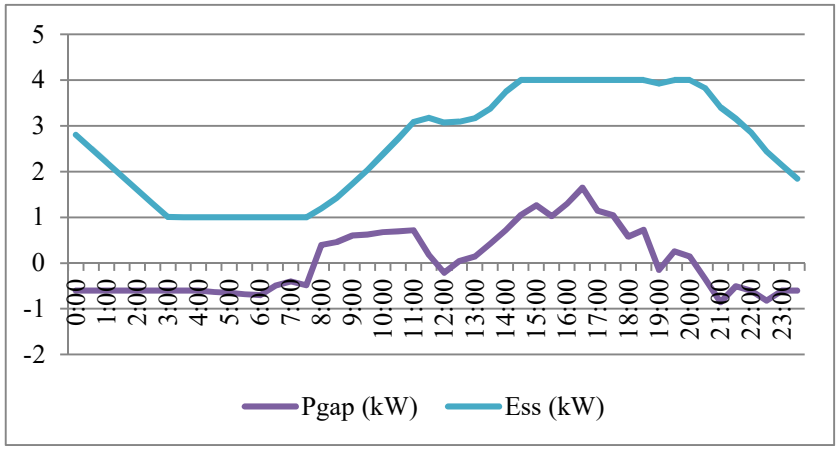

(b)

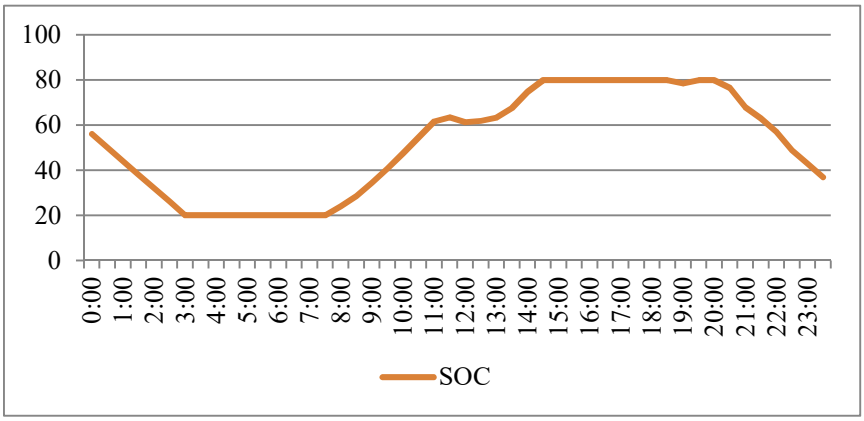

(c)

Fig.4.26. Results of (a) Power output from RES and load demand (b) power gap and energy stored in ESS (c) SOC of battery bank during islanded mode

4.4.4. Proposed Model Predictive Control For Smart Microgrid Operation

Most of the previous work in microgrids control mainly focuses on a two-parallel-DG based system, and the droop control method is generally used to control the inverters for autonomous power sharing between DGs. However, with the MS control, it is generally necessary to combine different kinds of DG sources, loads and energy storage units in order to ensure both long-term and short-term energy storage, and thus to bridge the gap between the power generation and power consumption within the microgrid. Hysteresis band control [4.40] and fuzzy control [4.41,4.42] are also employed in some development projects, due to their simple formulation control rules.

Recently, the MPC has been widely adopted in industries. There are several notable works regarding MPC implementation in MGs including energy scheduling on a hydrogen-based MG without batteries [4.43], renewable energy power management with battery storage in a water desalination plant [4.44], plug-in RES with battery storage [4.45], and hybrid modelling control for a PV-fuel cell power plant [4.46]. The electrical power transferred to the network and stored in ESS are the control variables that are considered. In this section, the MPC control strategy will be applied to control the whole smart-microgrid to optimize the power flows inside the microgrid and between the microgrid and the main grid with active and reactive power control when needed.

Define the power generated by RES as P_{RES} including P_{PV} from PV cell and P_{WIND} from WT, the total load demand as P_L. The power to be received from or transferred to the grid can be expressed as

$$P_{GRID} = P_L - P_{RES} = P_L - P_{PV} - P_{WIND} \quad (4\text{-}18)$$

With all the data available, the microgrid control centre can calculate all the output power as well as the demand from the load. The essential part of the MPC for smart microgrid is how to minimize the cost function for the power of the day:

$$\sum F_{net} = \sum_{k=1}^{n} C_{net,k} E_{net,k} \quad (4\text{-}19)$$

where $C_{net,k}$ and $E_{net,k} = P_{net,k}.t$ are the cost and power purchased from the grid during fixed time, respectively. Currently in Vietnam, the money received by selling power to the grid is zero that means $P_{net} = P_{GRID}$ if $P_{GRID} > 0$ and $P_{net} = 0$ if $P_{GRID} < 0$. Therefore, the most important control target is to determine the optimal operation with the lowest purchasing cost.

According to the characteristics of PV and WT in the previous section, the rated power of the PV is 1.5 kW and the rated power of the WT is 2 kW corresponding to the rated power generated and no load. In contrast, the maximum grid power is 1.6 kW for the load peak with no power from RES and minimum is -3.5 kW with no load and maximum power output from both PV and WT. The constraints aforementioned can be written for the control problem formulation as:

$$P_{L,\min} = 0kW \le P_L \le 1.6kW = P_{L,\max} \quad (4\text{-}20)$$

$$P_{RES,\min} = 0kW \le P_{RES} \le 3.5kW = P_{RES,\max} \quad (4\text{-}21)$$

$$P_{GRID,\min} = -3.5kW \le P_{GRID} \le 1.6kW = P_{GRID,\max} \quad (4\text{-}22)$$

Another constraint that needs to be taken into consideration is the protection of the battery from over charging and deep discharging, which can be implemented by setting the SOC as

$$SOC_{\min} = 20\% \le SOC \le 80\% = SOC_{\max} \quad (4\text{-}23)$$

The operational cost function is defined as

$$\begin{aligned} min \sum F_{net} &= \sum_{k=1}^{n} C_{net,k} E_{net,k} \\ &= \sum_{k=1}^{n} (C_{k,L} E_L - \alpha C_{k,PV} E_{PV} - \beta C_{k,Wind} E_{Wind}) + \delta_k SOC \end{aligned} \tag{4-24}$$

The weighting factors, α and β, can be determined based on the installation and operational cost of the PV and WT, respectively. The meaning of cost function $\sum F_{net}$ is that every factor of the microgrid will take into account the operational cost, including the price of electricity during the day. The surplus power generated can be fed to the utility grid rather than stored in the battery bank during those periods when the electricity market price is higher than the cost of PV and WT. Currently in Vietnam, there is no policy for people to sell electricity back to the grid so that the only target of this cost function is to maximize the power output from the RES. But in the near future, maybe there will be some changes in the market price to catch up with other developed countries like Australia.

According to AGL, the electricity price in NSW for residential is:

- Domestic time of use peak 2pm - 8pm: 50.33 cents per kWh
- Domestic time of use off peak 10pm - 7am: 11.07 cents per kWh
- Domestic time of use shoulder: 19.89 cents per kWh
- Solar feed-in tariff options: 20 cents per kWh exported

Applying these figures in the cost function of the example in section 4.4.2.1, we can have the results shown in Fig.4.27.

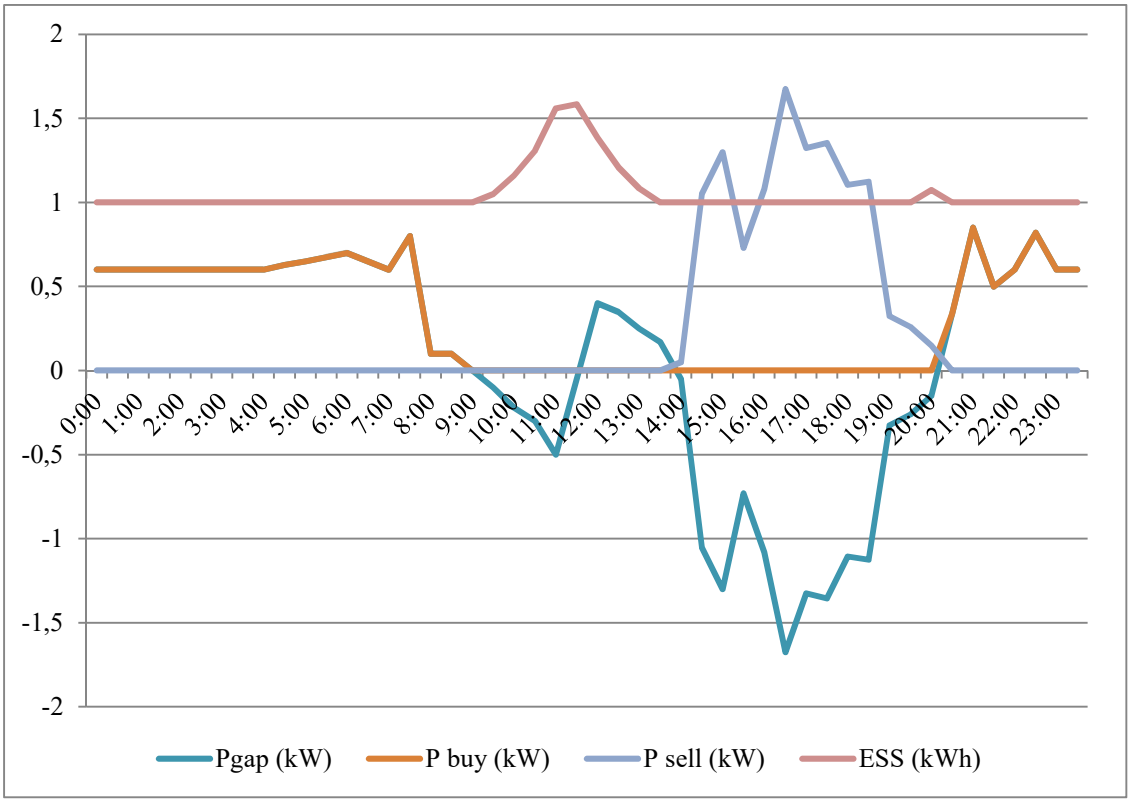

Fig.4.27. Power flow chart of smart microgrid with cost function applied

As can be seen in Fig.4.27, during the peak hour from 14:00 to 20:00, although the output power of the RES is greater than the load demand, the energy will not be store in ESS but to feed back to the grid for feed-in tariff money, the SOC of ESS maintain at minimum level of 20%. During the off-peak hours, because the rate of the electricity is nearly equal to the feed-in tariff rate, the energy will be charged and discharged from ESS if needed. For the rest of the day, the load is supplied by the main grid. The total cost function of this scheme is calculated as

$$\begin{aligned}
\sum F_{net} &= F_{shoulder} + F_{off-peak} - F_{sell} \\
\sum F_{net} &= \sum E_{shoulder}.C_{shoulder} + \sum E_{off-peak}.C_{off-peak} - \sum E_{sell}.C_{sell} \\
\sum F_{net} &= 1.145 \times 19.69 + 6.1625 \times 11.07 - 5.765 \times 20 \\
\sum F_{net} &= -24.536075(cents)
\end{aligned} \tag{4-25}$$

where $\sum E_{shoulder}$ = 1.145 kWh is the total energy purchased in shoulder hours from the grid, $\sum E_{off\text{-}peak}$ = 6.1625 kWh the total energy purchased in off-peak hours and $\sum E_{sell}$ = 5.765 kWh the total energy that sell to the grid.

In section 4.4.2.1 case study, without the application of the cost function above, the total energy that purchased from the grid should be $\sum E_{grid}$ = 1.5425 kWh, which is purchased during off-peak hours. So the total money that has to be paid to the electricity provider in section 4.4.2.1 case study should be:

$$F = 1.5425 \times 11.07 = 17.075475(cents) \tag{4-26}$$

Result from equation (4-25) with the cost function applied means the smart microgrid will actually receive 24.50 cents by selling electricity to the main grid, well below the result from equation (4-26) where the cost function is ignored.

4.5. CONCLUSION

This chapter has designed in detail a smart microgrid with its optimal power flow control. The module of each microgrid component is designed and simulated in PSIM software. The microgrid operation, both in grid-connected and islanded mode, is then described. Finally, a MPC concept for smart microgrid operation is proposed, where the power components generated by distributed energy sources, consumed by the load, stored by the ESS, and injected to the utility grid have been taken into account in the operational cost function. This MPC strategy along with its cost function in this section is very important in the future for the Vietnamese scenario. In order to control the power flow between the smart microgrid and utility grid, the structure and control of the grid-interfaced inverter will be study in the next chapter.

REFERENCES

[4.1] W. Kramer. S. Chakraborty, B. Kroposki, and H. Thomas, *Advanced Power Electronic Interfaces for Distributed Energy Systems – Part 1: Systems and Topologies*, Technical Report, NREL/TP-581-42672, March 2008.

[4.2] K. H. Hussein, I. Muta, T. Hoshino, and M. Osakada, "Maximum photovoltaic power tracking: An algorithm for rapidly changing atmospheric conditions," *Proc. Inst. Elect. Eng., Gen., Transm., Distrib.,* vol. 142, no. 1, pp. 59–64, 1995.

[4.3] A. Yazdani and P. P. Dash, "A control methodology and characterization of dynamics for a photovoltaic (PV) system interfaced with a distribution network," *IEEE Trans. Power. Delivery.,* vol. 24, no. 3, pp. 1538–1551, 2009.

[4.4] H. S. Rauschenbach, Van Nostrand Reinhold, "Solar cell array design handbook", 1980.

[4.5] Balakrishna S., Nabil A., Rajamohan G., Kenneth A. S., Ling C. J., "The Study and Evaluation of MPPT Systems", in *Proc. of International Conference on Energy and Environment*, Malaysia, 2006

[4.6] J. Hyvarinen and J. Karila, "New analysis method for crystalline silicon cells" In *Proc. 3rd World Conference on Photovoltaic Energy Conversion*, v. 2, p. 1521–1524, 2003

[4.7] N. Pongratananukul and T. Kasparis, "Tool for automated simulation of solar arrays using general-purpose simulators" in *Proc. IEEE Workshop on Computers in Power Electronics*, p. 10–14, 2004.

[4.8] A. Pandey, N. Dasgupta, and A. K. Mukerjee, "A simple single-sensor MPPT solution", *IEEE Trans. Power. Electron*., vol. 22, no. 6, pp. 698-700, 2007.

[4.9] S. Jain and V. Agarwal, “A new algorithm for rapid tracking of approximate maximum power point in photovoltaic systems,” *IEEE Power. Electron. Lett*., vol. 2, no. 1, pp. 16-19, 2004.

[4.10] M. Park and I. A. Yu, “Study on the optimal voltage for MPPT obtained by surface temperature of solar cell,” in *Proc. IEEE IECON*., 2004, pp. 2040-2045.

[4.11] R. F. Coelho, F. M. Concer, and D. C. Martins, “A MPPT approach based on temperature measurements applied in PV systems,” in *Proc. IEEE ICSET*., 2010, pp. 1-6.

[4.12] N. Femia, G. Petrone, G. Spanuolo, and M. Vitelli, “Optimization of perturb and observe maximum power point tracking method,” *IEEE Trans. Power Electron.*, vol. 20, no. 4, pp. 963-73, 2005.

[4.13] T. Esram and P. L. Chapman, “Comparison of photovoltaic array maximum power point tracking techniques,” *IEEE Trans. Energy Convers*., vol. 22, no. 2, pp. 439-449, 2007.

[4.14] S. Sawyer and A. Zervos, "Global Wind 2011 Report," Global Wind Energy Council, 2012

[4.15] S. Rahman, "Smart grid expectations [In My View]," Power and Energy Magazine, IEEE, vol. 7, pp. 88, 84-85, 2009.

[4.16] Bijaya Pokharel, “Modeling, Control and Analysis of a Doubly Fed Induction Generator Based Wind Turbine System with Voltage Regulation”, Tennessee Technological University, Master thesis, December 2011

[4.17] S. Soter and R. Wegener, "Development of Induction Machines in Wind Power Technology," in *Electric Machines & Drives Conference, 2007. IEMDC '07. IEEE International, 2007, pp. 1490-1495.*

[4.18] G. Boardman, J. Zhu, and Q. P. Ha, "Dynamic and steady state modelling of brushless doubly fed induction machines," in *IEEE Proceedings of the Fifth International Electrical Machines and Systems Conference (ICEMS),* 2001, pp. 412-416.

[4.19] S. Muller, M. Deicke and Rik W. De Doncker, "Doubly fed induction generator systems for wind turbines", *IEEE Industry Applications Magazine, Vol*. 8, No. 3, pp. 26-33, May/June 2002.

[4.20] S. Hao, Y. Zhang, X. Li, and Y. Yuan, "Equivalent wind speed model in wind farm dynamic analysis," in Proc. *IEEE Electric Utility Deregulation and Restructuring and Power Technologies Conf., 2011, pp. 1751–1755*.

[4.21] S. Benelghali, M. E. H. Benbouzid and J. F. Charpentier, "Comparison of PMSG and DFIG for Marine Current Turbine Applications", *XIX International Conference on Electrical Machines*, pp. 1-6, Rome, September 2010.

[4.22] J. Wang, A. Q. Huang, W. Sung, Y. Liu, and B. J. Baliga, "Smart grid technologies," IEEE Magazine Ind. Electron., pp. 16-23, June, 2009.

[4.23] E. J. Coster, J. M. A. Myrzik, B. Kruimer and W. L. Kling, "Integration issues of distributed generation in distribution grid," Proceedings of the IEEE., vol. 99, no. 1, pp. 28-39, 2011.

[4.24] K. Moslehi and R. Kumar, "A reliability perspective of the smart grid," IEEE Trans. Smart Grid., vol. 1, no. 1, pp. 57-64, 2010.

[4.25] S. Chakraborty and M. G. Simoes, "Experimental Evaluation of Active Filtering in a Single-Phase High-Frequency AC Microgrid," *Energy Conversion, IEEE Transactions on,* vol. 24, pp. 673-682, 2009.

[4.26] S. Chakraborty, M. D. Weiss, and M. G. Simoes, "Distributed Intelligent Energy Management System for a Single-Phase High-Frequency AC Microgrid," *Industrial Electronics, IEEE Transactions on,* vol. 54, pp. 97-109, 2007.

[4.27] H. Bevrani, F. Habibi, P. Babahajyani, M. Watanabe, and Y. Mitani, "Intelligent Frequency Control in an AC Microgrid: Online PSO-Based Fuzzy Tuning Approach," *Smart Grid, IEEE Transactions on,* vol. 3, pp. 1935-1944, 2012.

[4.28] K. T. Tan, P. L. So, Y. C. Chu, and M. Z. Q. Chen, "A Flexible AC Distribution System Device for a Microgrid," *Energy Conversion, IEEE Transactions on,* vol. 28, pp. 601-610, 2013.

[4.29] V. Nasirian, Q. Shafiee, J. M. Guerrero, F. L. Lewis, and A. Davoudi, "Droop-Free Distributed Control for AC Microgrids," *Power Electronics, IEEE Transactions on,* vol. 31, pp. 1600-1617, 2016.

[4.30] P. Shamsi and B. Fahimi, "Stability Assessment of a DC Distribution Network in a Hybrid Micro-Grid Application," *Smart Grid, IEEE Transactions on,* vol. 5, pp. 2527-2534, 2014.

[4.31] M. Davari and Y. A. R. I. Mohamed, "Robust Multi-Objective Control of VSC-Based DC-Voltage Power Port in Hybrid AC/DC Multi-Terminal Micro-Grids," *Smart Grid, IEEE Transactions on,* vol. 4, pp. 1597-1612, 2013.

[4.32] L. Sheng-yen, W. Li, L. Te-Ming, and A. V. Prokhorov, "Integration of Wind Power and Wave Power Generation Systems Using a DC Microgrid," *Industry Applications, IEEE Transactions on,* vol. 51, pp. 2753-2761, 2015.

[4.33] L. Nian, C. Qifang, L. Xinyi, L. Jie, and Z. Jianhua, "A Charging Strategy for PV-Based Battery Switch Stations Considering Service Availability and Self-

Consumption of PV Energy," *Industrial Electronics, IEEE Transactions on,* vol. 62, pp. 4878-4889, 2015.

[4.34] R. Majumder, "A Hybrid Microgrid With DC Connection at Back to Back Converters," *Smart Grid, IEEE Transactions on,* vol. 5, pp. 251-259, 2014.

[4.35] Shiguo Luo, Zhihong Ye, Ray-Lee Lin, and F. C Lee. A classification and evaluation of paralleling methods for power supply modules. In Proceedings of Power Electronics Specialists Conference, volume 2, pages 901–908, 1999.

[4.36] Jung-Won Kim, Hang-Seok Choi, and Bo Hyung Cho. "A novel droop method for converter parallel operation." *IEEE Transactions on Power Electronics*, 17(1):25–32, Jan 2002.

[4.37] P. Karlsson. "*Analysis, Design and Control for a Renewable Energy System."* PhD thesis, Department of Industrial Electrical Engineering and Automation, Lund University, Sweden, 2002.

[4.38] M. Mahmoodi, G.B. Gharehpetian, M. Abedi, and R Noroozian. "Control systems for independent operation of parallel dg units in dc distribution systems." In *Proceedings of IEEE International Power and Energy Conference*, pages 220–224, Nov 2006.

[4.39] Juanjuan Sun. "*Dynamic Performance Analyses of Current Sharing Control for DC/DC Converters.*" PhD thesis, Faculty of the Electrical and Computer Engineering, Virginia Polytechnic Institute and State University, 2007.

[4.40] Ø. Ulleberg., "The Importance of Control Strategies in PV-hydrogen Systems", *Solar Energy*, no 76, pp. 323-329, 2001.

[4.41] A. Bilodeau, K. Agbossou, "Control analysis of renewable energy system with hydrogen storage for residential applications", *Journal of Power Sources*, no 162, pp. 757–764, 2006.

[4.42] E.M. Stewart et al., "Modeling, analysis and control system development for the Italian hydrogen house", *International Journal of Hydrogen Energy*, pp. 16381646, 2009.

[4.43] P. L. Zervas, H. Sarimveis, J. A. Palyvos, and N. C. G. Markatos, "Model-based optimal control of a hybrid power generation system consisting of photovoltaic arrays and fuel cells," *Journal of Power Sources,* no. 181, pp. 327-338, 2008.

[4.44] W. Qi, J. Liu, and P. D. Christofides, "Supervisory predictive control for longterm scheduling of an integrated wind/solar energy generation and water desalination system," *IEEE Trans. Control Systems Technology*., vol. 20, no. 2, pp. 504-512, 2012.

[4.45] M. Khalid, "A model predictive control approach to the problem of wind power smoothing with controlled battery storate," *Renewable Energy*, pp. 1520-1526, 2010. [4.45] A. Del Real, A. Arce, C. Bordons, "Hybrid model predictive control of a twogenerator power plant integrating photovoltaic panels and fuel cell," *46 IEEE Conference on Decision and Control*, New Orleans, 2007.

[4.46] L. Wang, M. P. Polis, G. G. Yin, W. Chen, Y. Fu, and C. C. Mi, "Battery cell identification and SOC estimation using string terminal voltage measurements," *IEEE Trans. Vehicular Technology.*, vol. 61, no. 7, pp. 2925-2935, 2012.

CHAPTER 5. FEEDBACK AND FEEDBACK PLUS FEEDFORWARD CONTROL OF GRID CONNECTED INVERTER

5.1. INTRODUCTION

In the previous chapter, a three-phase inverter is implemented to transfer active and reactive power between the microgrid and the utility grid. The VSC with an output L-type or LCL-type filter is commonly used. The LCL-type filters, though superior in terms of filter size and weight, introduces undesirable high-frequency resonances in the output current. Passive damping of those resonances would cause power losses, whereas the active damping often requires measurement of multiple signals used in a complicated control method.

In general, the methods for three-phase grid-connected inverters are implemented in either stationary domain [5.1, 5.2] or synchronous reference domain [5.3-5.6]. The rotating frame can avoid the coupling terms and also the possibility of controlling harmonics, but suffers from the higher order control, more complicated design, sensitivity of the design to the grid frequency [5.7], and digital implementation difficulties known for resonant controllers [5.8]. The great advantage of the synchronous reference method is in mapping the AC variables into DC

quantities and thus, it is possible to employ simple PI controllers. A side effect of this transformation is, however, the introduction of mutual coupling terms into the model equations. Conventionally, input decoupling terms are used to decouple the active and reactive power control loops, and simple PI controllers are used.

The suppression of the injected grid current harmonics is an important aspect of the power quality issues [5.3]. IEEE STD 1547-2009 gives the limitation of injected grid current harmonics.

The control of active and reactive power has been widely understood and applied in rectifiers, grid-connection inverters of PV fuel cells, and distributed power generation systems [5.9-5.13]. This chapter presents several methods to control the grid-interfacing inverter for a microgrid with a DC bus[5.14]. This inverter has the following tasks:

(a) To control the active and reactive power transfer between the microgrid and the utility grid and

(b) To ensure high quality of the injected power.

In this chapter, the system is modelled in the *d-q* rotating frame and therefore the active and reactive power can be controlled separately by controlling the *d* and *q* axis current components, I_d and I_q . In the first place, the real and reactive power will be controlled at the same time by the traditional PI control. The disadvantages of the traditional PI control will be indicated and the new control scheme of PI control plus feedforward will be proposed to improve the control performance.

Simulations of the system with both PI control and PI plus feedforward control will be presented in this chapter. A prototype of the system was built to verify the result of the method.

5.2. ACTIVE AND REACTIVE POWER CONTROL OF GRID-CONNECTED INVERTER IN MICROGRID

5.2.1. Model In The Stationary Frame And Synchronous D-Q Frame

Figs.5.1 and 5.2 show the structure of the microgrid and its grid-interfaced inverter studied in this thesis, respectively. Assume that under the normal condition, using the droop control method within the microgrid, the DC bus voltage of the microgrid can be described as a DC source. A standard three-phase VSI with an L filter connects the microgrid to the utility grid, where L and R are the inductor and resistor, respectively.

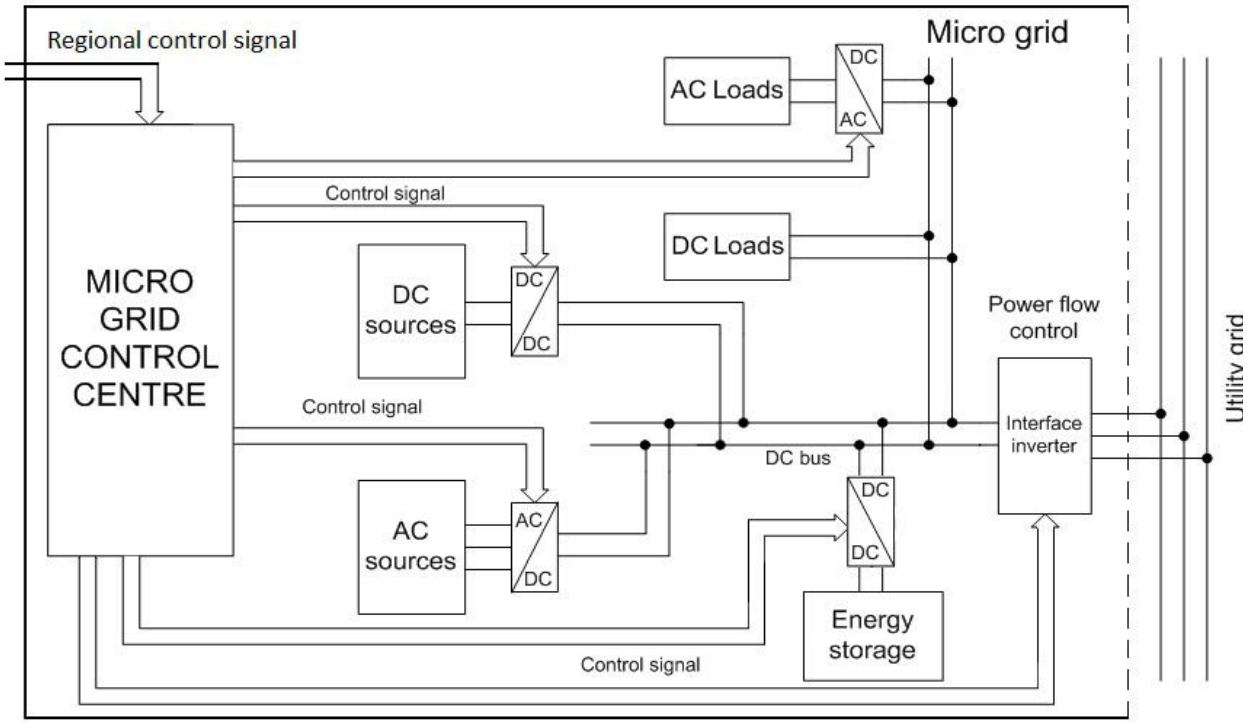

Fig.5.1. Structure of the proposed DC microgrid

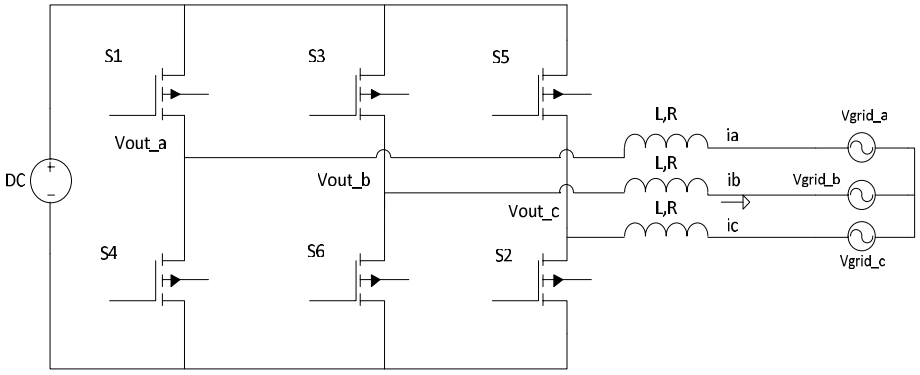

Fig.5.2. Simplified L-type filter grid-connected inverter

In this structure, the microgrid control centre is the most important part of the microgrid, as it controls the microgrid according to its status and instructions from the regional control centre. Based on all the data collected and the instructions reveived, the microgrid control centre will determine the operation of each power converter within the microgrid as well as the power and reactive power transfer with the utility grid through the grid-interfacing inverter to meet the load demands or satisfy the needs from the main grid.

According to Fig.5.2, the mathematical model in the stationary ABC frame of the three-phase grid-connected inverter is described as

$$\begin{cases} V_{out_a}(t) = V_{grid_a}(t) + Ri_a(t) + L\dfrac{d}{dt}i_a(t) \\ V_{out_b}(t) = V_{grid_b}(t) + Ri_b(t) + L\dfrac{d}{dt}i_b(t) \\ V_{out_c}(t) = V_{grid_c}(t) + Ri_c(t) + L\dfrac{d}{dt}i_c(t) \end{cases} \tag{5-1}$$

or

$$\left[V_{out_{abc}}(t)\right] = \left[V_{grid_{abc}}(t)\right] + R\left[i_{abc}(t)\right] + L\frac{\mathrm{d}}{\mathrm{dt}}\left[i_{abc}(t)\right] \tag{5-2}$$

where

$$\left[V_{out_{abc}}(t)\right]=\left[V_{out_a}(t),V_{out_b}(t),V_{out_c}(t)\right]^T$$

is the voltage vectors of three inverter legs,

$$\left[V_{grid_{abc}}(t)\right]=\left[V_{grid_a}(t),V_{grid_b}(t),V_{grid_c}(t)\right]^T$$

the grid voltage vectors, and

$$\left[i_{abc}(t)\right]=\left[i_a(t),i_b(t),i_c(t)\right]^T$$

the inverter-side inductor currents.

Any three-phase variables can be transformed from the three-phase stationary reference frame to a two-phase rotating reference frame by the constant power Park transform. The coordinate transform matrix is

$$\left[T_{ABC\to dq0}\right]=\sqrt{\frac{2}{3}}\begin{bmatrix} cos\,\theta & \cos\left(\theta-\frac{2\pi}{3}\right) & cos\left(\theta+\frac{2\pi}{3}\right) \\ -sin\theta & -sin\left(\theta-\frac{2\pi}{3}\right) & -sin\left(\theta+\frac{2\pi}{3}\right) \\ \frac{1}{\sqrt{2}} & \frac{1}{\sqrt{2}} & \frac{1}{\sqrt{2}} \end{bmatrix} \quad (5\text{-}3)$$

where $\theta=\omega t+\delta$ is the angle between the rotating and fixed coordinate system at time t, and δ the initial phase shift of the voltage. Applying this constant power Park transformation to (5-2), the mathematic model of the interfacing-inverter in the *d-q* frame can be expressed as

$$\left[V_{out_{dq}}(t)\right]=\left[V_{grid_{dq}}(t)\right]+R\left[i_{dq}(t)\right]+\omega L\begin{bmatrix}0 & -1\\ 1 & 0\end{bmatrix}.\left[i_{dq}(t)\right]+L\frac{d}{dt}\left[i_{dq}(t)\right] \quad (5\text{-}4)$$

or

$$\begin{cases} V_{out_d} = V_{grid_d} + Ri_d + L\dfrac{d}{dt}i_d - \omega L i_q \\ V_{out_q} = V_{grid_q} + Ri_q + L\dfrac{d}{dt}i_q + \omega L i_d \end{cases} \quad (5\text{-}5)$$

5.2.2. Active and reactive power control

The active and reactive power then can be controlled by controlling the current in the synchronous rotating *d-q* frame as described in Fig.5.3.

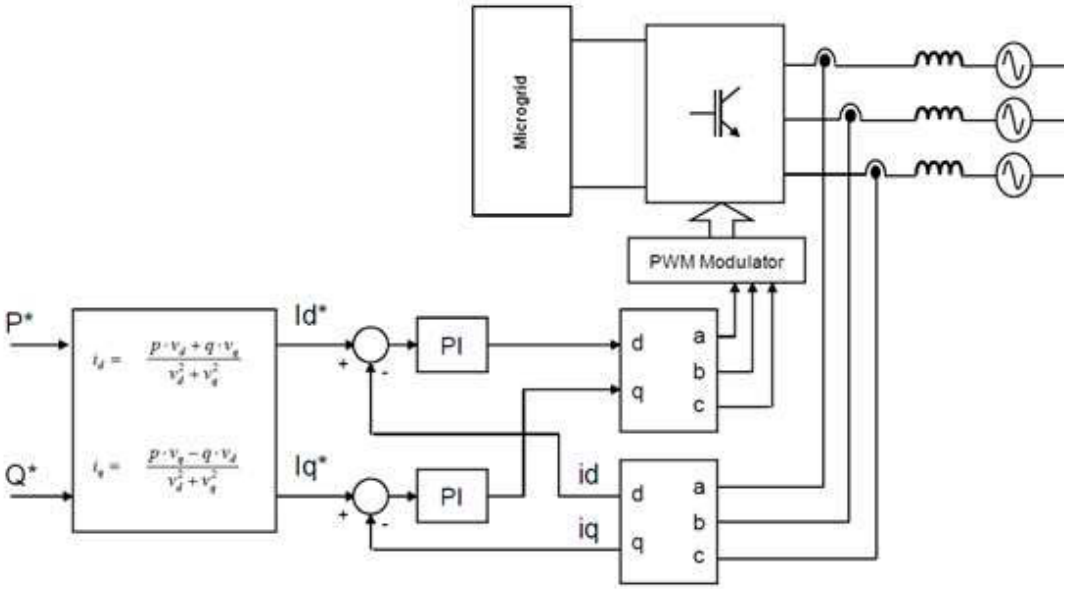

Fig.5.3. Active and reactive power control by regulating current in *d-q* frame

The synchronous *d-q* frame control has the particular advantage of controlling the active and reactive current directly. The active and reactive power for a balanced three-phase system can be written in the synchronous *d-q* frame as follows:

$$\begin{cases} P = V_d.I_d + V_q I_q \\ Q = V_d I_q - V_q I_d \end{cases} \quad (5\text{-}6)$$

Therefore, with each given P and Q, I_d and I_q can be obtained as

$$\begin{cases} I_d = \dfrac{PV_d - QV_q}{V_d^2 + V_q^2} \\ I_q = \dfrac{PV_d + QV_q}{V_d^2 + V_q^2} \end{cases} \tag{5-7}$$

Equation (5-5) indicates that the feedback of inductor currents can be used for PI control as described in Fig.5.4. With I_d and I_q control, we can control the real and reactive power transfer between the microgrid and the main grid.

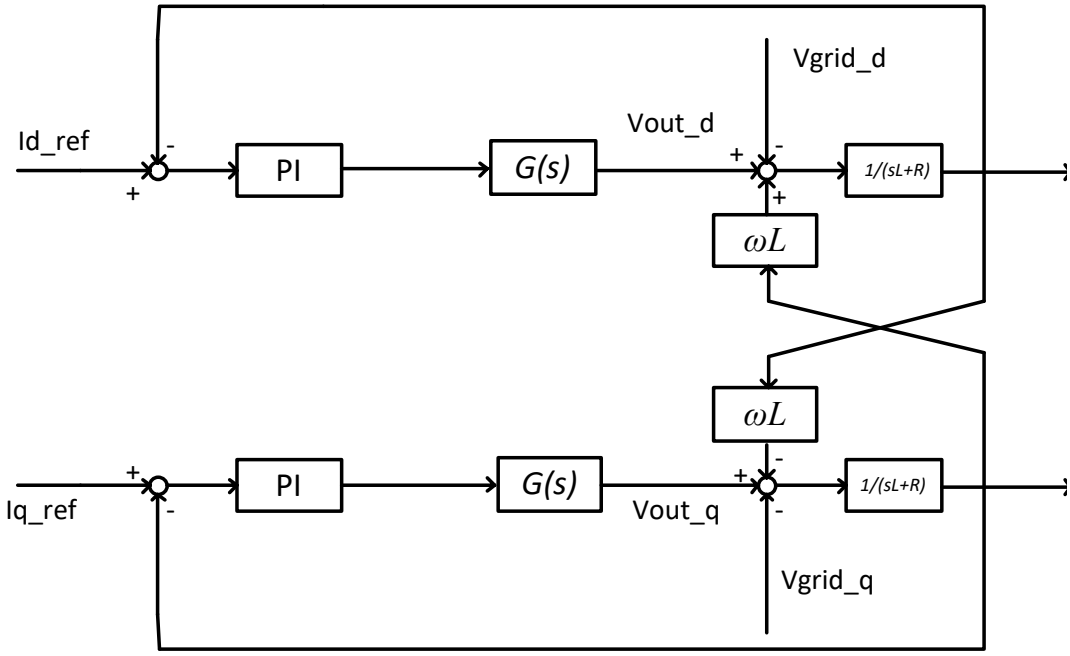

Fig.5.4. Feedforward scheme for the synchronous d-q frame

With the single-loop feedback PI control, we have a multi-variable system with double input and double outputs. The distinctive point of this multi-variable system is the interaction between the variables, which is shown by the decoupling terms of ωL in (5-5). The coupling terms will affect the stabilization, static and dynamic characteristics of the system. Therefore, this chapter will present some decoupling method to control the real and reactive power independently.

5.2.3. Simulation and result in PSIM

The system is simulated in PSIM software as shown in Fig.5.5.

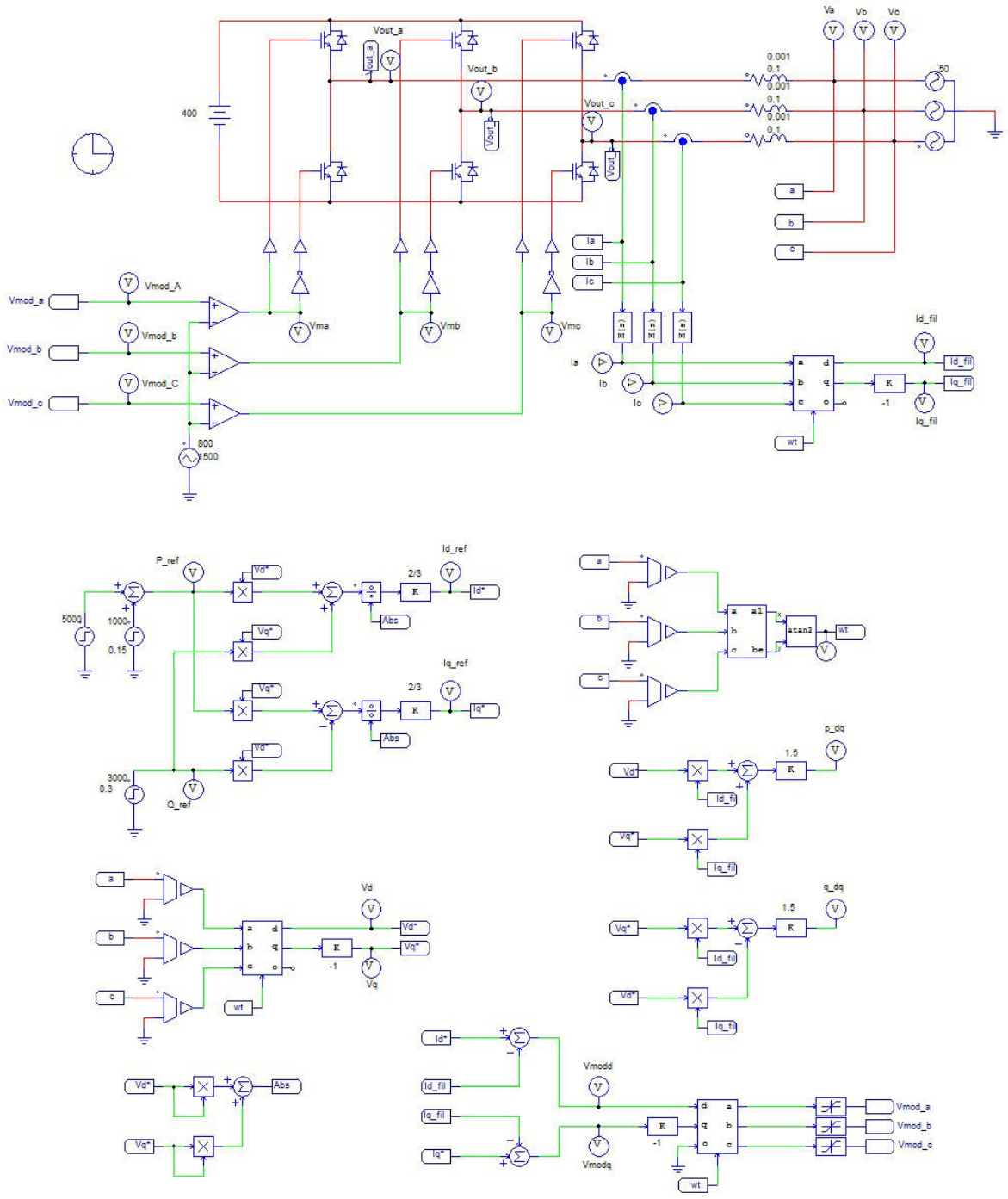

Fig.5.5. Feedback current control of I_d and I_q in PSIM

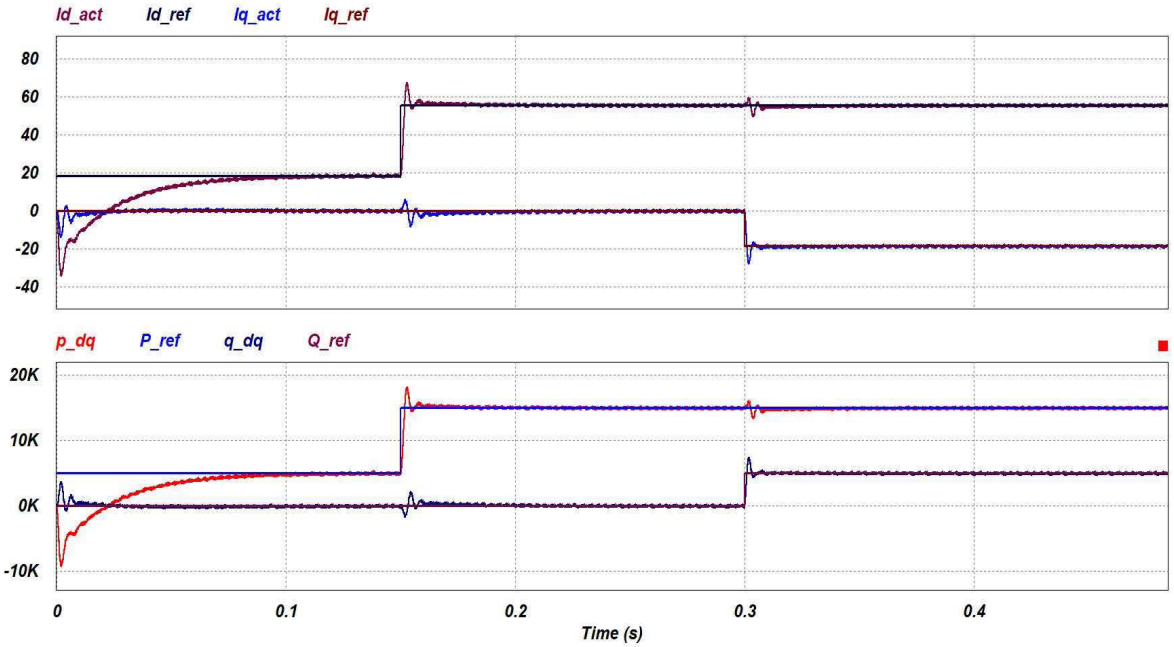

(a)

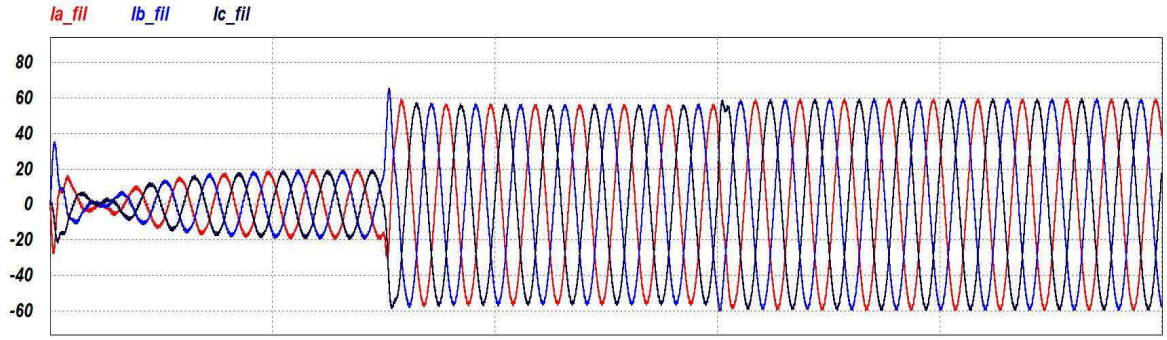

(b)

Fig.5.6. (a) Feedback current control of I_d and I_q, P and Q. THD = 4.99%

(b) Result of three-phase inverter current I_a I_b I_c

The system is simulated in the PSIM software with the following parameters: the DC bus voltage is 400V; the grid voltage is 220Vrms line-line; f = 50Hz; P= 5000W at t= [0, 0.15] s, P=15000W at t >0.165s. Q= 0VAR at t= [0, 0.3] s, and Q= 5000VAR at t > 0.3s. Fig 5.6 illustrates the simulation results.

As can be seen in Fig.5.6, the coupling effects between I_d and I_q are so obvious. When there is a step change in P or Q, it means the reference value of I_d or I_q is also changed, there is surge on the other value as well. At t = 0.15s, the set point of active power changes from 5000W to 15000W, and at t = 0.3s, the set point of reactive power change from 0VAR to 5000VAR. The peak of the fluctuations in P and Q are quite large, which are 2000VAR and 1000W in Q and P axis, respectively. In a small system, this small effect can be ignored. But in the near future, there will be a lot of microgrids that connected to the main grid, when the main grid needs the specific amount of real or reactive power, each microgrid will have to contribute to the main grid with the available amount of power. Therefore, each microgrid can cause a small surge in the real and reactive power control, and the total effect will be noticeable. In order to help the main grid avoid this disturbance, a new control scheme is proposed to reduce the coupling effect between real and reactive power control.

5.3. DIFFERENT DECOUPLING CURRENT CONTROL SCHEME FOR THE SYNCHRONOUS D-Q FRAME

5.3.1. State feedback scheme for the synchronous d-q frame

Fig.5.7 shows the additional paths, which can eliminate the effect of the grid voltages to the injected current. The cross effect between the d and q axis components will also be removed. However, in a real time circuit, there is always a difference between the dynamic responses and the regulated currents, which makes this method not ideal.

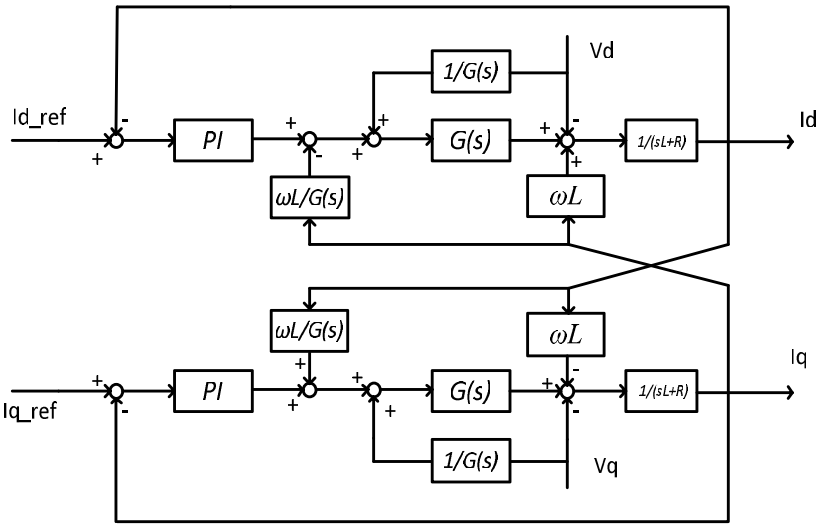

Fig.5.7. Feedforward scheme for the synchronous d-q frame

5.3.2. Series feedforward scheme for the synchronous d-q frame

Fig.5.8 describes the idea of series feedforward, which adds a series block *H(s)* behind the PI current controller to decouple completely the *d* and *q* axis components.

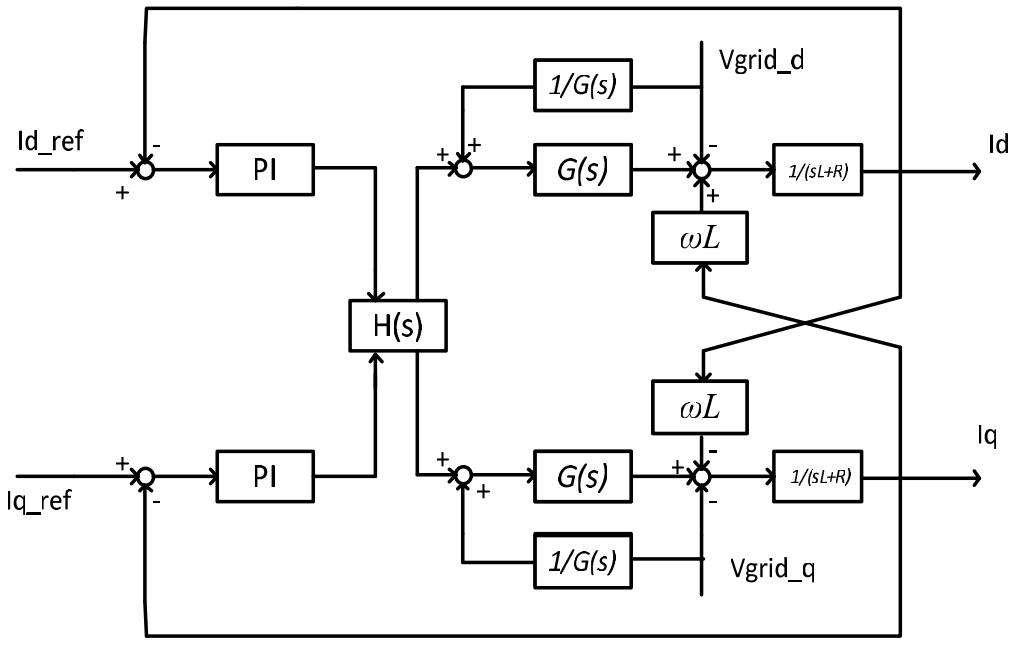

Fig.5.8. The block diagram of series feedforward in d-q frame

For this multi-variable control system, the "relative gain" concept proposed in [5.13] can be applied to scale the degree of coupling and decoupling. Suppose *y* is a row vector containing all included variables y_i and u a row vector containing all independent variables u_j, the "relative gain" between u_j and y_i can be defined as

$$\lambda_{ij} = \frac{\left.\frac{\partial y_i}{\partial u_j}\right|_u}{\left.\frac{\partial y_i}{\partial u_j}\right|_y} \tag{5-8}$$

If $\lambda_{ij} = 1$, it means that there is no interaction between the channel from u_j to y_i and the other channels. Whether the other channels are closed or not, the open-loop gain of the channel from u_j to y_i will not be affected. If $\lambda_{ij} = 0$, it means that y_i is unaffected by u_j. The greater $\lambda_{ij} \gg 1$, the stronger is the coupling between the channels. In Fig.5.8, let

$$\left[H(s)\right] = \begin{bmatrix} H_{11}(s) & H_{12}(s) \\ H_{21}(s) & H_{22}(s) \end{bmatrix} \tag{5-9}$$

From (5-5) it can be given that

$$\begin{bmatrix} R+sL & -\omega L \\ \omega L & R+sL \end{bmatrix} \begin{bmatrix} i_d \\ i_q \end{bmatrix} = \begin{bmatrix} H_{11}(s) & H_{12}(s) \\ H_{21}(s) & H_{22}(s) \end{bmatrix} \begin{bmatrix} V_{out_d} \\ V_{out_q} \end{bmatrix} \tag{5-10}$$

The relative gain between the two input variables, i_d and i_q and the two outputs, V_{out_d} and V_{out_q} is shown below

$$\lambda_{11} = \lambda_{22}$$

$$= \frac{\{(R+sL)H_{12} + \omega L H_{21}\}\{-\omega L H_{21} + (R+sL)H_{22}\}}{\{(R+sL)H_{12} + \omega L H_{21}\}\{-\omega L H_{21} + (R+sL)H_{22}\} + \{(R+sL)H_{12} + \omega L H_{22}\}\{-\omega L H_{11} + (R+sL)H_{21}\}} \tag{5-11}$$

When $\lambda_{11} = \lambda_{22} = 1$, one obtains

$$\left\{(R+sL)H_{12} + \omega L H_{22}\right\}\left\{-\omega L H_{11} + (R+sL)H_{21}\right\} = 0$$

Therefore, the interaction between the *d* and *q* axes can be decoupled completely, if one chooses

$$\begin{cases} H_{11}(s) = H_{22}(s) = 1 \\ H_{12}(s) = \dfrac{-\omega L}{sL + R} \\ H_{21}(s) = \dfrac{\omega L}{sL + R} \end{cases} \tag{5-12}$$

5.3.3. Simulation and experimental results

The system is simulated in the PSIM software with the following settings: the DC bus voltage is 400 V; the grid voltage is 220 Vrms line-line, f = 50 Hz; P = 5000 Watts = [0, 0.165] s, P = 15000 Watts > 0.165 s, Q = 0 VAR at t = [0, 0.3] s, and Q = 5000VAR at t > 0.3s. The parameters are tabulated in Table 5-1.

TABLE 5- I. Parameters

Resistance	R	0.51 Ω
Inductance	L	22 mH
DC-link capacitor	C	680 uF
Load resistance	R_L	50 Ω
Source voltage frequency	f	50 Hz
DC-link voltage	V_{dc}	50 V
Sampling period	T_s	50 μs

Fig 5.9 illustrates the PSIM model of the simulation.

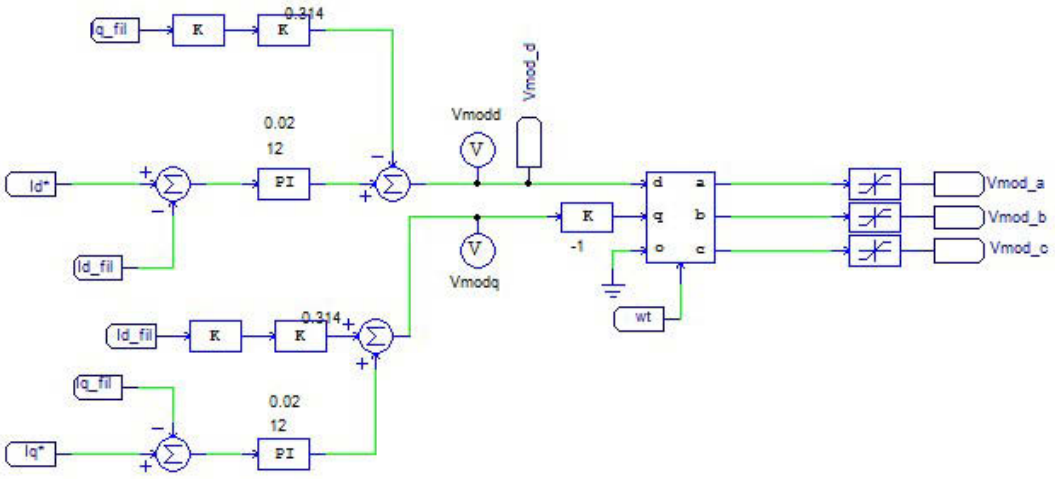

Fig.5.9. PI plus Feedforward current control simulation in PSIM

Figs.5.10 and 5.11 depict the simulation results.

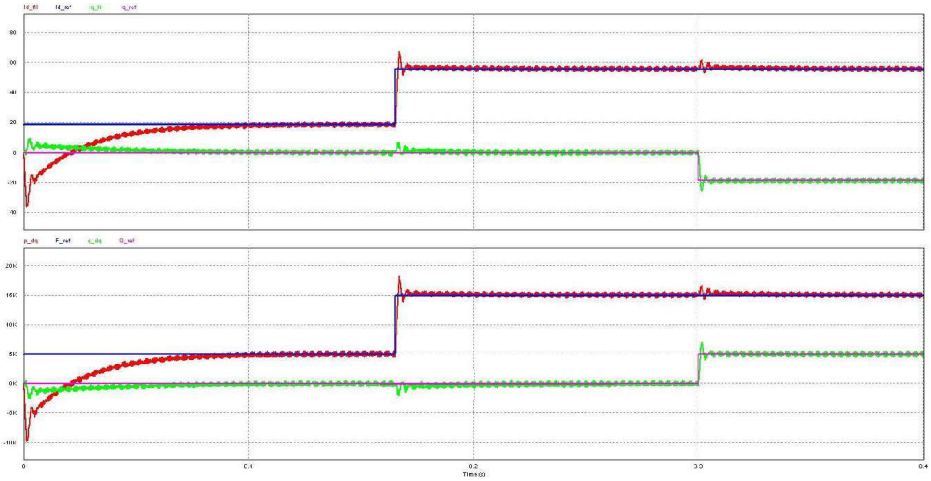

Fig.5.10. PI plus Feedforward current control result of I_d, I_q, P and Q.

THD = 3.15%

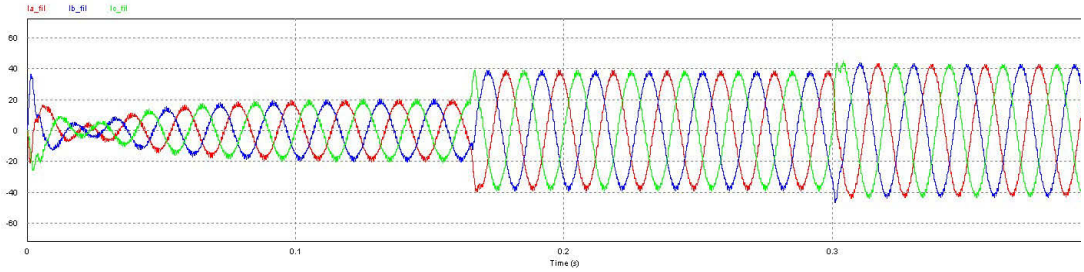

Fig.5.11. Output currents of the grid interfaced inverter

In Fig 5.10, the upper picture shows the d and q axis current components, I_d and I_q , while the lower picture describes the change in real and reactive power, P and Q respectively, when there are change in the set point of the simulation. At t = 0.165s, the set point of active power changes from 5000 W to 15000 W, and at t = 0.3s, the set point of reactive power change from 0 VAR to 5000 VAR. The surges in both current and power pictures reduce significantly in comparison with the PI current control, as the peak fluctuation in Q and P axis is only around 400 VAR and 200 W, respectively.

The theory and numerical simulation are verified by experimental tests. Fig.5.12 is a photo of the experimental setup of a grid connected inverter in the laboratory. Fig.5.13 illustrates the three phase output voltage waveforms of the grid connected inverter. As shown, they are reasonably sinusoidal as expected.

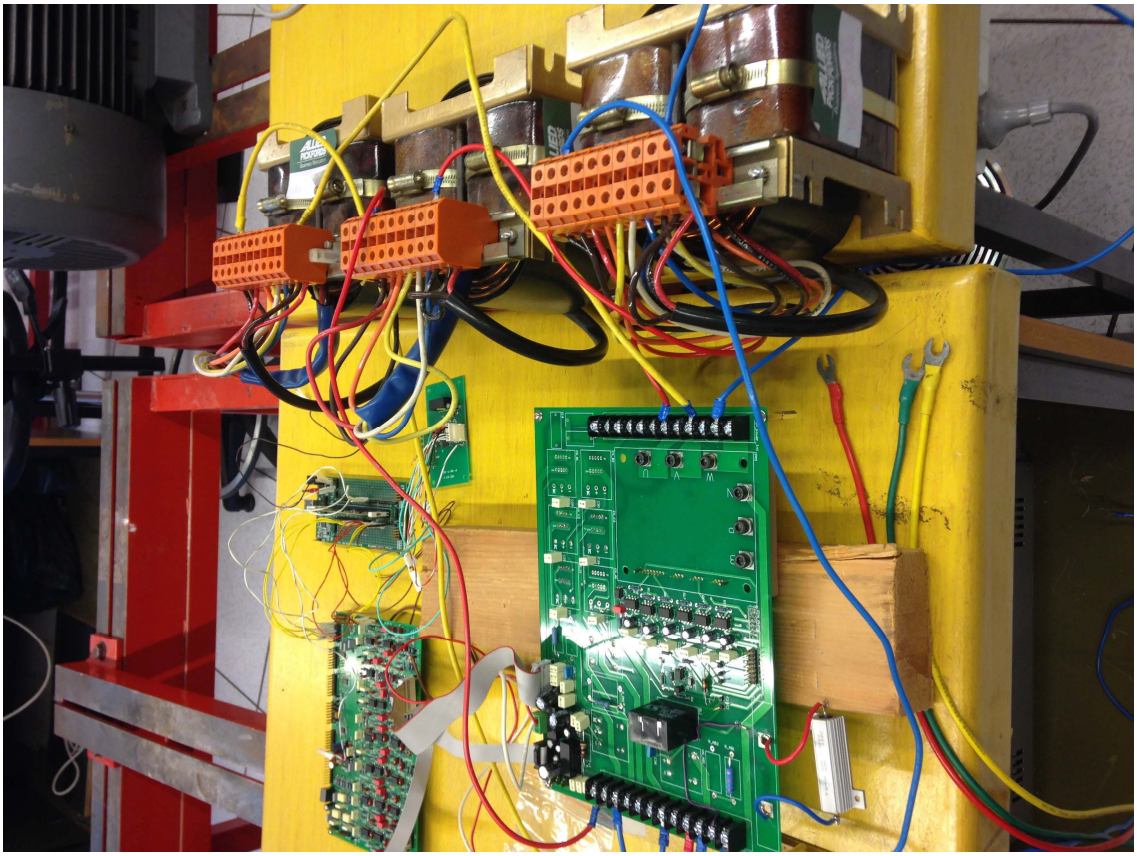

Fig.5.12. Setup in the laboratory of the grid-connected inverter

Fig.5.13.Output voltage of the grid interfaced inverter

5.4. CONCLUSION

As can be seen in Figs.5.6 and 5.10, by transforming the input variables of the system P and Q into the synchronous d-q frame, the currents can be controlled to achieve the desired active and reactive power transfer between the microgrid and utility grid by the traditional PI feedback control. Fig.5.10 shows the result of the cross-coupling feedforward. The cross effect between the d-q axes has been reduced significantly but cannot be eliminated perfectly. In Fig.5.6, when there is a step change in the active power or reactive power set point, there is also a small fluctuation in the other variable, the surge of Q is around 2000 VAR and P is around 1000 W in the figure. In Fig.5.10, the fluctuation is reduced significantly, with the value above is 400 VAR and 200 W, respectively. On the other hand, there is still some minor cross effect between them which cannot be eliminated by this method. It can be explained

that the frequency in the mathematical model of the system are assumed to be constant; three phases are balanced; and all the transformations are in the steady state. However, when there is a voltage change in the system, not all the assumptions are valid at the time of operation; also the reference and the real-time values of the system variables are not equal anymore. Therefore, the feedforward cannot achieve the perfect result. This result means that the decoupling control method using feedback with feedforward during the transient period is not an ideal solution and can be improved. The MPC, which is a new control technique that can offer a better solution than the both feedback and feedback plus feedforward especially in term of the dynamic response, will be introduced in the next chapter.

REFERENCE

[5.1] I. J. Gabe, V. F. Montagner, and H. Pinheiro, "Design and Implementation of a Robust Current Controller for VSI Connected to the Grid Through an LCL Filter," *Power Electronics, IEEE Transactions on,* vol. 24, pp. 1444-1452, 2009.

[5.2] L. Poh Chiang and D. G. Holmes, "Analysis of multiloop control strategies for LC/CL/LCL-filtered voltage-source and current-source inverters," *Industry Applications, IEEE Transactions on,* vol. 41, pp. 644-654, 2005.

[5.3] F. Blaabjerg, R. Teodorescu, M. Liserre, and A. V. Timbus, "Overview of Control and Grid Synchronization for Distributed Power Generation Systems," *Industrial Electronics, IEEE Transactions on,* vol. 53, pp. 1398-1409, 2006.

[5.4] M. Liserre, R. Teodorescu, and F. Blaabjerg, "Multiple harmonics control for three-phase grid converter systems with the use of PI-RES current controller in

a rotating frame," *Power Electronics, IEEE Transactions on,* vol. 21, pp. 836-841, 2006.

[5.5] W. Eric and P. W. Lehn, "Digital Current Control of a Voltage Source Converter With Active Damping of LCL Resonance," *Power Electronics, IEEE Transactions on,* vol. 21, pp. 1364-1373, 2006.

[5.6] M. Malinowski and S. Bernet, "A Simple Voltage Sensorless Active Damping Scheme for Three-Phase PWM Converters With an LCL Filter," *Industrial Electronics, IEEE Transactions on,* vol. 55, pp. 1876-1880, 2008.

[5.7] A. V. Timbus, M. Ciobotaru, R. Teodorescu, and F. Blaabjerg, "Adaptive resonant controller for grid-connected converters in distributed power generation systems," in *Applied Power Electronics Conference and Exposition, 2006. APEC '06. Twenty-First Annual IEEE*, 2006, p. 6 pp.

[5.8] R. Teodorescu, F. Blaabjerg, M. Liserre, and P. C. Loh, "Proportional-resonant controllers and filters for grid-connected voltage-source converters," *Electric Power Applications, IEE Proceedings -,* vol. 153, pp. 750-762, 2006.

[5.9] S. A. Azmi, G. P. Adam, K. H. Ahmed, S. J. Finney, and B. W. Williams, "Grid Interfacing of Multimegawatt Photovoltaic Inverters," *Power Electronics, IEEE Transactions on,* vol. 28, pp. 2770-2784, 2013.

[5.10] Y. Bo, L. Wuhua, Z. Yi, and H. Xiangning, "Design and Analysis of a Grid-Connected Photovoltaic Power System," *Power Electronics, IEEE Transactions on,* vol. 25, pp. 992-1000, 2010.

[5.11] R. Majumder, "Reactive Power Compensation in Single-Phase Operation of Microgrid," *Industrial Electronics, IEEE Transactions on,* vol. 60, pp. 1403-1416, 2013.

[5.12] L. Hongbo, Z. Kai, Z. Hui, F. Shengfang, and X. Jian, "Active Power Decoupling for High-Power Single-Phase PWM Rectifiers," *Power Electronics, IEEE Transactions on,* vol. 28, pp. 1308-1319, 2013.

[5.13] D. Ke, L. Ping, K. Yong, and C. Jian, "Decoupling current control for voltage source converter in synchronous roating frame," in *Power Electronics and Drive Systems, 2001. Proceedings., 2001 4th IEEE International Conference on*, 2001, pp. 39-43 vol.1.

[5.14] D. H. Pham, G. Hunter, L. Li, and Z. Jianguo, "Microgrid topology for different applications in Vietnam," in *Universities Power Engineering Conference (AUPEC), 2012 22nd Australasian*, 2012, pp. 1-6

CHAPTER 6. MODEL PREDICTIVE CONTROL OF ACTIVE AND REACTIVE POWER

6.1. INTRODUCTION

In Chapter 5, the system is modelled in the *d-q* rotating frame; therefore the active and reactive power can be controlled separately by controlling I_d and I_q. The two control methods, which are traditional PI with feedback and feedforward plus feedback, were implemented to achieving the desired active and reactive power. As we can see from the previous chapter, the decoupling effects between active and reactive power were reduced significantly, but the dynamic performance of the system and the overall result are still not quite satisfactory. In recent years, a new interesting control technique, known as direct control strategy, has been developed and applied widely. One of the most common control method, DPC uses the conventional SDPC which is derived from the original DTC for AC machine drives [6.1,6.2]. In DPC, the active and reactive power replaces the torque and flux amplitudes that are used as the controlled output in the DTC. Because of its excellent transient performance, robustness, and simplicity, this method has emerged to become one of the most popular and powerful control strategies. The switching states are determined using a switching table, which is built up from the grid voltage vector or virtual-flux vector as well as the states of the switching gates of the power converters [6.3]-[6.5]. Several system-performance-enhanced switching tables have also been proposed to improve the system behaviour [6.6]-[6.8].

The concept of predictive control emerged as an attractive alternative for the control of electrical machines and power converters more recently. Several kinds of control methods have been developed under the name of predictive control. The most important types are the deadbeat control, MPC and vector-sequence based predictive control (VPC). In the MPC, a system model is used to predict the behavior of the variables over a certain time horizon, and a cost function as the criterion to select the optimal switching states [6.9]-[6.15]. This chapter will present a new active and reactive power control method with the MPC applied to predict the current of the next sampling period. The cost function is used to minimize the differential between desired reference and actual values of active and reactive power that transfer between the main grid and microgrid through the grid-connected inverter. Other technique has also been applied to improve the performance of the MPC method [6.16-6.20].

The numerical simulation as well as a comprehensive comparison between the two control techniques in Chapter 5 and this chapter are presented also.

6.2. THE CONCEPT OF DIRECT POWER CONTROL AND MODEL PREDICTIVE CONTROL

6.2.1. Direct power control

Fig.6.1 illustrates the block diagram of the conventional DPC.

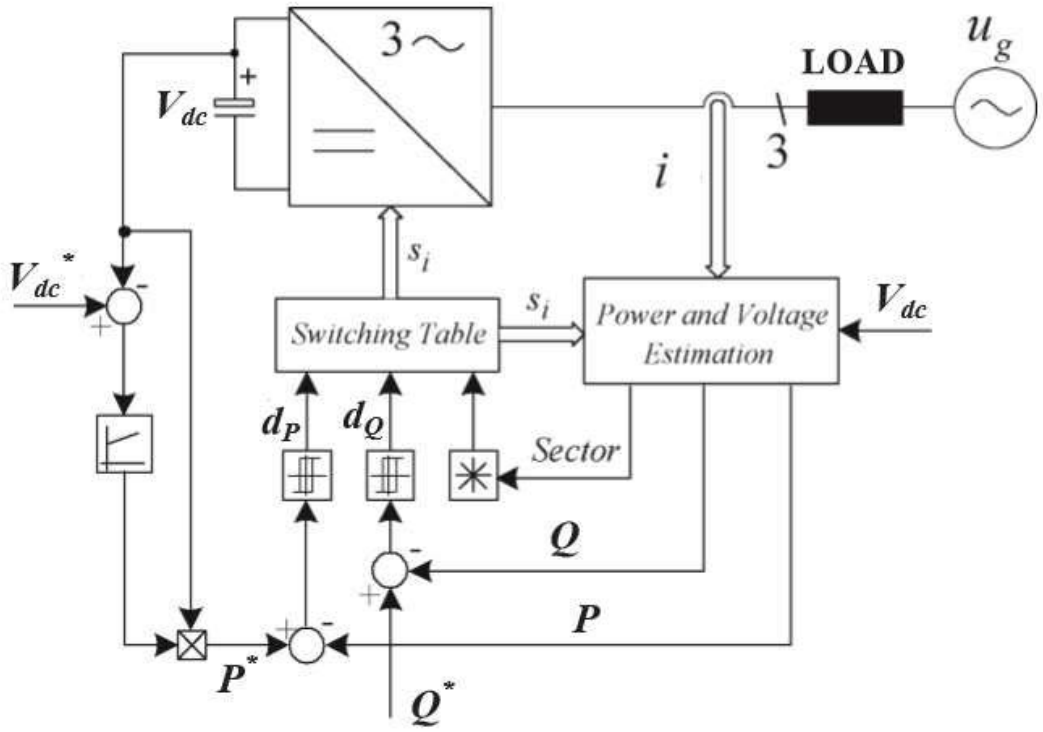

Fig.6.1. Block scheme of a conventional DPC

In order to correctly estimate the power and, at the same time, to reduce the number of implemented voltage sensors, Noguchi proposes the use of voltage vector estimation [6.21]. The implementation of such approach involves the computation of the time derivative of the measured currents. The use of a derivative can increase the noise in the control loop, thus increasing the level of distortion. The virtual-flux strategy was proposed firstly [6.5], which basically assumes that the grid voltage and the DC-sideinductors are quantities that are related to a virtual AC motor. By making an analogy with AC motors, R_g and L_g represent the stator resistance and the stator leakage inductance, respectively, and the grid voltage u_g represents the machine's electromotive force.

According to the flux definitions, the grid virtual flux can be estimated.

$$\psi_g = \int \overline{u_g . dt} \tag{6-1}$$

where

$$\overline{u_g} = \overline{u_{inv}} - R_g.\overline{i_g} - L_g.\frac{di_g}{dt} \tag{6-2}$$

By neglecting the series resistance of the grid inductor, the grid virtual flux can be calculated as

$$\psi_g = \int \overline{u_{inv}} - R_g.\overline{i_g} - L_g.\frac{di_g}{dt} \tag{6-3}$$

By using the estimated grid virtual flux and the measured currents, the active and reactive powers can be estimated as

$$p = \frac{3}{2}\omega(\psi_{g,\alpha}.i_{g,\beta} - \psi_{g,\beta}.i_{g,\alpha}) \tag{6-4}$$

$$q = \frac{3}{2}\omega(\psi_{g,\alpha}.i_{g,\alpha} - \psi_{g,\beta}.i_{g,\beta}) \tag{6-5}$$

assuming the stationary ($\alpha\beta$) transformation of

$$\begin{bmatrix} u_\alpha \\ u_\beta \end{bmatrix} = \frac{2}{3}\begin{bmatrix} 1 & -\frac{1}{2} & -\frac{1}{2} \\ 0 & \frac{\sqrt{3}}{2} & -\frac{\sqrt{3}}{2} \end{bmatrix}\begin{bmatrix} u_R \\ u_S \\ u_T \end{bmatrix} \tag{6-6}$$

Therefore, with the tracking errors between the estimated and the reference values of active and reactive power, the digitized signal, d_P and d_Q, are then generated through two fixed bandwidth hysteresis comparators. A look-up switching table according to d_P, d_Q and power source voltage is then used to select the switching states of the power converters. The major problem of the method is the high sampling frequency required and large power ripples occurred.

6.2.2. Model predictive control

More recently, to improve the performance of the system, the concept of predictive control emerged as an attractive alternative for the control of electrical machines and power converters. The principle of the vector based predictive control is to force the system variables onto the pre-calculated trajectories, where several voltage vectors are typically used within each sampling period. This section will describe the MPC method and its application in controlling the active and reactive power. Generally, the design of MPC controller can be divided into three steps: system predictive model, cost function and parameters selection. Firstly, the system model can be expressed as a discrete-time state-space model, the output of which is determined by the input, the current state of the model, and the discrete interval. In this way, the future behaviour of the system can be predicted until a certain horizon of time. Secondly, the control problem can be defined as the determination of an appropriate control action that will force a generic system variable, $x(t)$, as close as possible to a desired reference value, x^*. A cost function over a finite horizon of length N is then utilized to evaluate each switching state, and the one minimizing the error between $x(t)$ and x^* will be selected for the next sampling period. Finally, as the MPC allows the easy inclusion of system constraints and nonlinearities by revising the cost function, a trade-off between different control objectives should be taken into account in order to obtain the satisfied performance. Fig. 6.2 depicts the block diagram of MPC system, where one step prediction is employed.

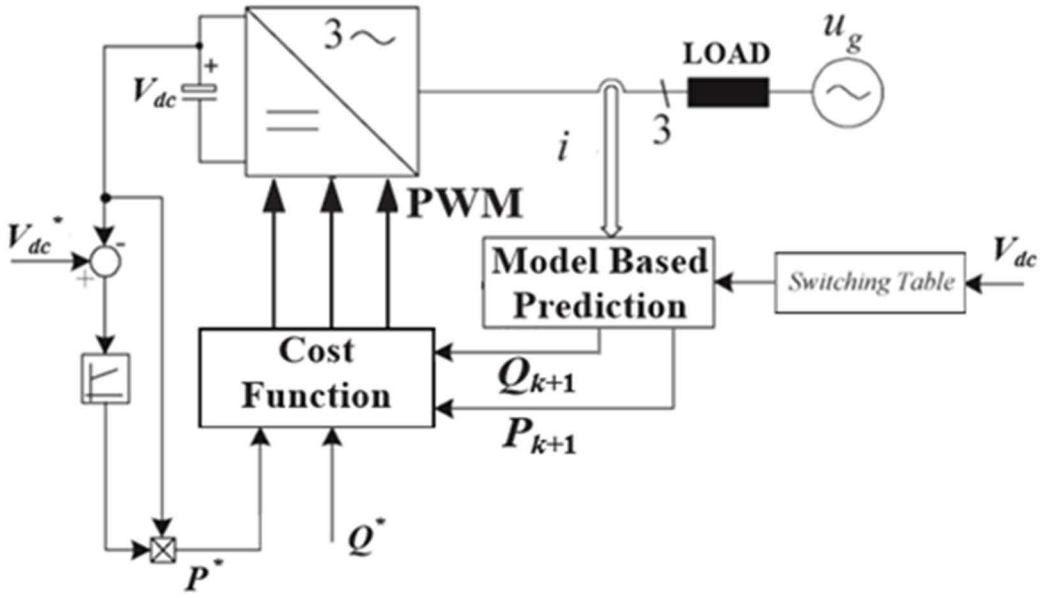

Fig.6.2. Block scheme of a conventional model predictive control

The essential concept of this predictive DPC is to predict the power of the $(k+1)^{th}$ instant for different voltage vectors. By evaluating the effects of each voltage vector on the active and reactive powers according to a specific cost function, the voltage vector that produces the least power ripple can be determined. In the rectifier control, the control objectives are chosen as the DC-link voltage and the power factor of the AC input, which can be regulated by controlling the active power, P, and reactive power, Q, respectively. Consequently, the mathematical model of the converter can be described in the stationary α-β coordinates as

$$e_{\alpha\beta} = L\frac{dI_{\alpha\beta}}{dt} + RI_{\alpha\beta} + V_{\alpha\beta} \tag{6-7}$$

$$C\frac{dV_{dc}}{dt} = \frac{3}{2}\left(I_\alpha D_\alpha + I_\beta D_\beta\right) - I_L \tag{6-8}$$

where $e_{\alpha\beta}$ is the three-phase input voltage vector, $V_{\alpha\beta}$ the converter input voltage vector, $I_{\alpha\beta}$ the line current vector, I_L the DC load current, and D_α and D_β are the switching states (0 = off, 1 = on). The active and reactive power can be calculated as

$$P = \frac{3}{2} Re\left\{eI^*\right\} = \frac{3}{2}\left(e_\alpha I_\alpha + e_\beta I_\beta\right) \tag{6-10}$$

$$Q = \frac{3}{2} Im\left\{eI^*\right\} = \frac{3}{2}\left(e_\beta I_\alpha + e_\alpha I_\beta\right) \tag{6-11}$$

The derivatives of active and reactive power can be obtained as

$$\frac{dP}{dt} = \frac{3}{2}\left(\frac{de_\alpha}{dt} I_\alpha + e_\alpha \frac{dI_\alpha}{dt} + \frac{de_\beta}{dt} I_\beta + e_\beta \frac{dI_\beta}{dt}\right) \tag{6-12}$$

$$\frac{dQ}{dt} = \frac{3}{2}\left(\frac{de_\beta}{dt} I_\alpha + e_\beta \frac{dI_\alpha}{dt} + \frac{de_\alpha}{dt} I_\beta - e_\alpha \frac{dI_\beta}{dt}\right) \tag{6-13}$$

Substituting

$$\frac{de_\alpha}{dt} = -\omega e_\beta \tag{6-14}$$

$$\frac{de_\beta}{dt} = \omega e_\alpha \tag{6-15}$$

into (6-10) and (6-11) we have

$$\frac{dP}{dt} = -\frac{R}{L} P - \omega Q + \frac{3}{2L}\left(|e|^2 - Re(eV^*)\right) \tag{6-16}$$

$$\frac{dQ}{dt} = -\frac{R}{L} Q + \omega Q - \frac{3}{2L} Im(eV^*) \tag{6-17}$$

The next time sample value of active and reactive power will be

$$P^{k+1} = T_s\left[-\frac{R}{L} P - \omega Q + \frac{3}{2L}\left(|e|^2 - Re(eV^*)\right)\right] + P^k \tag{6-18}$$

$$Q^{k+1} = T_s\left[-\frac{R}{L} Q + \omega Q - \frac{3}{2L} Im(eV^*)\right] + Q^k \tag{6-19}$$

Since the control target of this method is to control the active and reactive power the cost function can be defined as

$$F_{cost} = \sqrt{(P^{k+1} - P^{k})^2 + (Q^{k+1} - Q^{k})^2} \tag{6-20}$$

From the (6-20), with the look-up table of the switching states, it can be calculated which switching signal will give the best active and reactive power in the next sampling time period. Therefore, the exact PWM control signal can be chosen. This new control technique appears attractive has several advantages in comparison with the classical modulation methods, especially its excellent dynamic response, simple concept and easy implementation. The new control method of grid-connected inverter in this chapter is based on this MPC technique.

6.3. MODEL PREDICTIVE CONTROL OF ACTIVE AND REACTIVE POWER

In this section, the MPC is used to control the active and reactive power based on the *d-q* rotating frame. In the MPC control, a model is used to predict the future behaviour of the controlled variables. This information is then used in a cost function as the criterion to select the optimal switching state for the system. The control objectives can vary with different cost functions. For example, the control objective can be the output voltage [6.22] or current [6.23-6.25]. A few control algorithms [6.22], [6.26] have been presented as predictive control. The MPC strategy is also applied in this chapter to control the currents in *d-q* rotating frame, which can take advantage of the excellent dynamic response of the MPC method but still can get rid of the coupling effect between active and reactive power.

6.3.1. Model in the stationary frame and synchronous d-q frame

Figs.6.3 and 6.4 show the structure of the microgrid and its grid-interfaced inverter studied in this thesis, respectively.

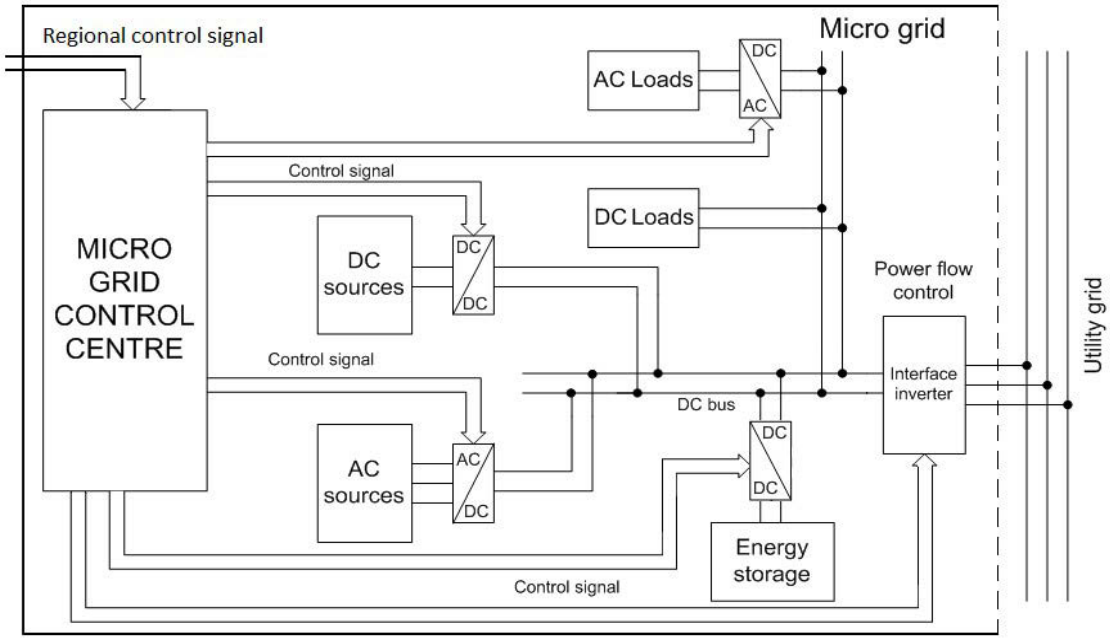

Fig.6.3. Structure of the proposed DC microgrid

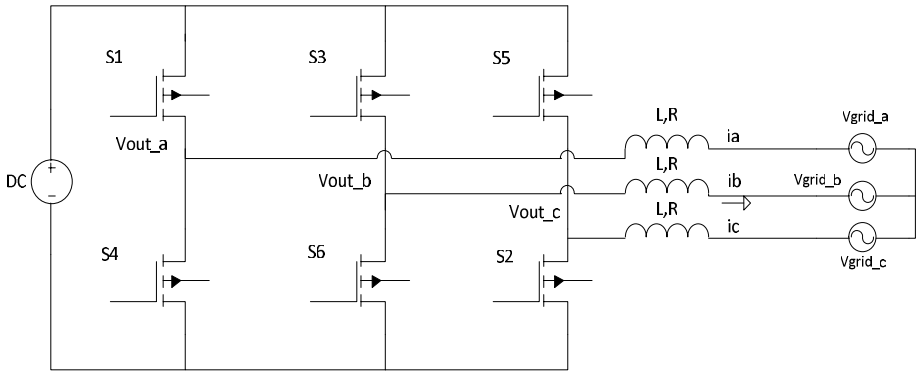

Fig.6.4. Simplified L-type filter grid-connected inverter

Assume that under the normal condition, using the droop control method within the microgrid, the DC bus voltage of the microgrid can be described as a DC

source. A standard three-phase VSI with an L filter connects the microgrid to the utility grid, where L and R are the inductor and resistor, respectively. In this structure, the microgrid control centre is the most important part of the microgrid, as it detects the condition of power sources, load and energy storage units and receives the instructions from regional control centre. When all data is collected, the microgrid control centre will determine the operation of each power converter within the microgrid as well as the power and reactive power transfer with the utility grid through the grid-interfacing inverter to meet the load demands or satisfy the needs from the main grid.

According to Fig.6.2, the mathematical model in the stationary ABC frame of the three-phase grid-connected inverter can be described as

$$\begin{cases} V_{out_a}(t) = V_{grid_a}(t) + Ri_a(t) + L\dfrac{d}{dt}i_a(t) \\ V_{out_b}(t) = V_{grid_b}(t) + Ri_b(t) + L\dfrac{d}{dt}i_b(t) \\ V_{out_c}(t) = V_{grid_c}(t) + Ri_c(t) + L\dfrac{d}{dt}i_c(t) \end{cases} \tag{6-21}$$

or

$$\left[V_{out_{abc}}(t)\right] = \left[V_{grid_{abc}}(t)\right] + R\left[i_{abc}(t)\right] + L\frac{\mathrm{d}}{\mathrm{dt}}\left[i_{abc}(t)\right] \tag{6-22}$$

where $\left[V_{out_{abc}}(t)\right] = \left[V_{out_a}(t), V_{out_b}(t), V_{out_c}(t)\right]^T$ is the voltage vectors determined by the switching status of three inverter legs,

$\left[V_{grid_{abc}}(t)\right] = \left[V_{grid_a}(t), V_{grid_b}(t), V_{grid_c}(t)\right]^T$ the grid voltage vectors,

and $\left[i_{abc}(t)\right] = \left[i_a(t), i_b(t), i_c(t)\right]^T$ the inverter-side inductor currents.

6.3.2. Model predictive control strategy for the synchronous d-q frame

The switching states of the grid-connected inverter are determined by the gating signals as the following:

$$S_a = \begin{cases} 1, & if\ S_1\ on\ and\ S_4\ off \\ 0, & if\ S_1\ off\ and\ S_4\ on \end{cases} \tag{6-23}$$

$$S_b = \begin{cases} 1, & if\ S_3\ on\ and\ S_6\ off \\ 0, & if\ S_3\ off\ and\ S_6\ on \end{cases} \tag{6-24}$$

$$S_c = \begin{cases} 1, & if\ S_5\ on\ and\ S_2\ off \\ 0, & if\ S_5\ off\ and\ S_2\ on \end{cases} \tag{6-25}$$

and can be expressed in vectorial form as

$$S = 2/3(S_a + aS_b + a^2 S_c) \tag{6-26}$$

where a =$e^{j(2\pi/3)}$. The output space vectors generated by the inverter are defined by

$$V_{out} = \frac{2}{3}(V_{out_a} + aV_{out_b} + a^2 V_{out_c}) \tag{6-27}$$

$$V_{out} = V_{dc} S \tag{6-28}$$

Here, variables $S_a, S_b\ and\ S_c$ represent the switching states of the three legs of the inverter. Considering all the possible combinations the gating signals $S_a, S_b\ and\ S_c$, eight voltage vectors are obtained, as shown in Table 6-I and Fig.6.5. The equation of the filter inductance in vectorial form is

$$v_{out} = v_{grid} + Ri_o + L\frac{di_o}{dt} \tag{6-29}$$

where

$$i_o = \frac{2}{3}(i_a + ai_b + a^2 i_c) \tag{6-30}$$

TABLE 6-I.VOLTAGE VECTORS AND SWITCHING STATES FOR THREE PHASE GRID-CONNECTED INVERTER

S_a	S_b	S_c	V_{out}
0	0	0	$v_0 = 0$
1	0	0	$v_1 = \frac{2}{3}V_{dc}$
1	1	0	$v_2 = \frac{V_{dc}}{3} + j\frac{\sqrt{3}}{3}V_{dc}$
0	1	0	$v_3 = -\frac{V_{dc}}{3} + j\frac{\sqrt{3}}{3}V_{dc}$
0	1	1	$v_4 = \frac{-2}{3}V_{dc}$
0	0	1	$v_5 = -\frac{V_{dc}}{3} - j\frac{\sqrt{3}}{3}V_{dc}$
1	0	1	$v_6 = \frac{V_{dc}}{3} - j\frac{\sqrt{3}}{3}V_{dc}$
1	1	1	$v_7 = 0$

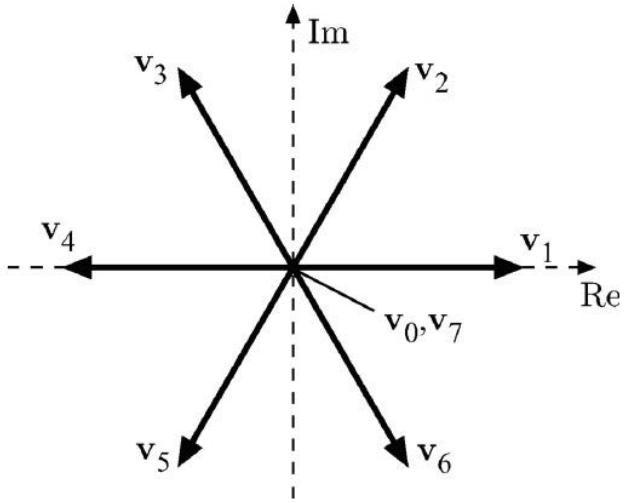

Fig.6.5. Voltage vectors generated by the inverter

This equation can be written in state-space system as

$$\frac{dx}{dt} = Ax + Bv_{out} + Cv_{grid} \tag{6-31}$$

where

$$x = i_o,\ A = -R/L\ ,\ B = -1/L,\ and\ C = 1/L$$

A discrete-time model of the filter is obtained for a sampling time T_s can be described as

$$x^{k+1} = A_q x^k + B_q v_{out}{}^k + C_q v_{grid}{}^k \tag{6-32}$$

where

$$A_q = e^{AT_s}$$

$$B_q = \int_0^{T_s} e^{At} B dt$$

$$C_q = \int_0^{T_s} e^{At} C dt$$

Based on the Park transformation (5-3) and (6-22) we can predict i_o^{k+1} as well as i_d^{k+1} and i_q^{k+1}. In order to predict the output current i_o^{k+1}, v_{out} is calculated using Table 6-I and (6-32), and v_{grid} considered as a known disturbance, along with the measured variable i_o^k. After the currents are predicted, the next step is to evaluate the effects of each vector on I_d and I_q and to select the one vector which produces the minimum mismatch between the predicted and reference variables according to the specific cost function. In this chapter, the cost function is defined as

$$F_{\cos t} = \left[I_{d\,ref} - I_d{}^{k+1} \right]^2 + \left[I_{q\,ref} - I_q{}^{k+1} \right]^2 \tag{6-33}$$

The block diagram of the grid-connected inverter controller operation is shown in Fig.6.6.

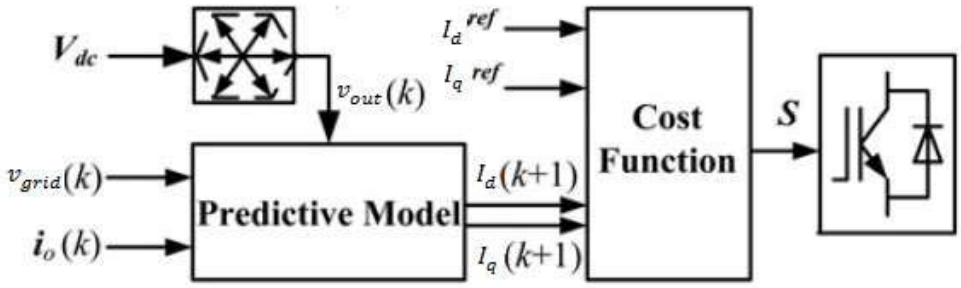

Fig.6.6. MPC block diagram of grid-connected inverter

6.3.3. Numerical simulation

The system is simulated in the PSIM software with the following parameters: the DC bus voltage is 400 V; the grid voltage is 220 Vrms line-line; f = 50 Hz; P= 5000 W at t = [0, 0.165] s, P = 15000 W at t > 0.165 s. Q = 0 VAR at t = [0, 0.3] s, and Q = 5000 VAR at t > 0.3 s.

As can be seen in Fig.6.7 (a), by transforming the input variables of the system P and Q into the synchronous d-q frame, the currents can be controlled to achieve the desired active and reactive power transfer between the microgrid and utility grid. Fig.6.7 (b) shows the result of the traditional PI feedback control and the cross-coupling feedforward. The MPC result can be seen in Fig.6.7 (c). The result of the MPC is clearly better than that of both feedback and feedback with feedforward especially in term of the dynamic response. The overshoot is smaller and the settling time is shorter.

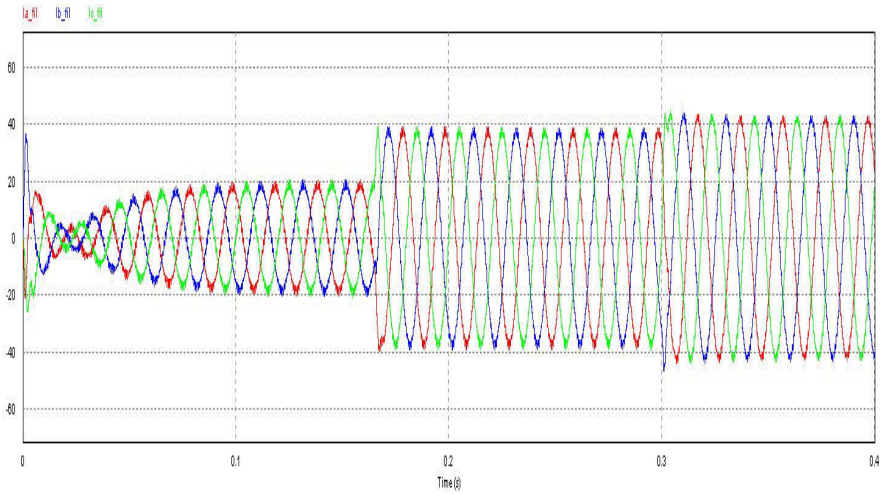

(a)

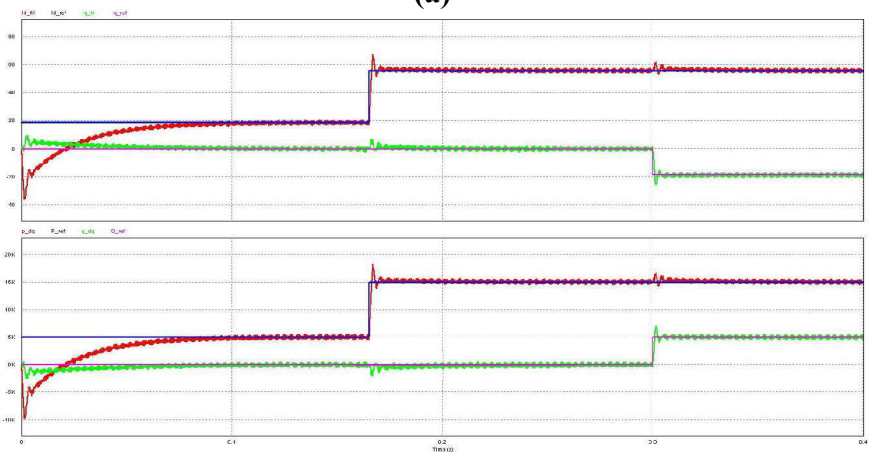

(b)

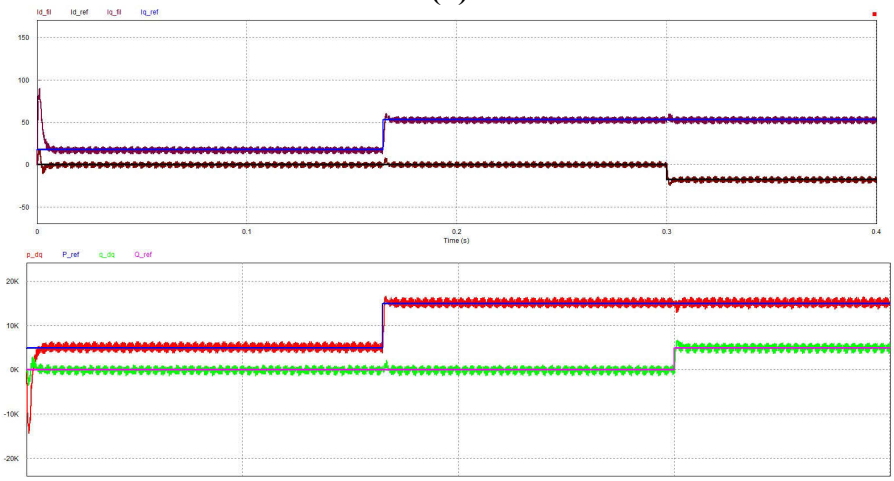

(c)

Fig.6.7. Active and reactive power control of Id and Iq (a) result of three phase current I_a I_b I_c (b) feedback control. THD = 4.99%, feedforward control. THD = 4.15% and (c) MPC current control. THD = 2.17%

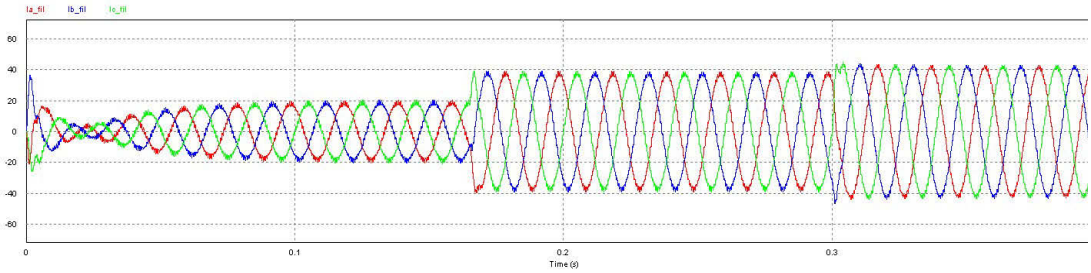

Fig.6.8.Output currents of the grid interfaced inverter by MPC

6.4. CONCLUSION

This chapter presented a power and reactive power control technique which use the MPC method to control the current in the synchronous *d-q* frames . This new control strategy has the advantages of not only the quick response and better dynamic performance from MPC method but also the decoupling technique in the previous chapter. With the reduction of power and reactive power surge during transient period, this method look very promising in the smart microgrid control scheme which will be more and more popular in the year to come.

REFERENCES

[6.1] I. J. Gabe, V. F. Montagner, and H. Pinheiro, "Design and Implementation of a Robust Current Controller for VSI Connected to the Grid Through an LCL Filter," Power Electronics, IEEE Transactions on, vol. 24, pp. 1444-1452, 2009.

[6.2] L. Poh Chiang and D. G. Holmes, "Analysis of multiloop control strategies for LC/CL/LCL-filtered voltage-source and current-source inverters," *Industry Applications, IEEE Transactions on,* vol. 41, pp. 644-654, 2005.

[6.3] F. Blaabjerg, R. Teodorescu, M. Liserre, and A. V. Timbus, "Overview of Control and Grid Synchronization for Distributed Power Generation Systems," *Industrial Electronics, IEEE Transactions on,* vol. 53, pp. 1398-1409, 2006.

[6.4] M. Liserre, R. Teodorescu, and F. Blaabjerg, "Multiple harmonics control for three-phase grid converter systems with the use of PI-RES current controller in a rotating frame," *Power Electronics, IEEE Transactions on,* vol. 21, pp. 836-841, 2006.

[6.5] W. Eric and P. W. Lehn, "Digital Current Control of a Voltage Source Converter With Active Damping of LCL Resonance," *Power Electronics, IEEE Transactions on,* vol. 21, pp. 1364-1373, 2006.

[6.6] M. Malinowski and S. Bernet, "A Simple Voltage Sensorless Active Damping Scheme for Three-Phase PWM Converters With an LCL Filter," *Industrial Electronics, IEEE Transactions on,* vol. 55, pp. 1876-1880, 2008.

[6.7] A. V. Timbus, M. Ciobotaru, R. Teodorescu, and F. Blaabjerg, "Adaptive resonant controller for grid-connected converters in distributed power generation systems," in *Applied Power Electronics Conference and Exposition, 2006. APEC '06. Twenty-First Annual IEEE*, 2006, p. 6 pp.

[6.8] R. Teodorescu, F. Blaabjerg, M. Liserre, and P. C. Loh, "Proportional-resonant controllers and filters for grid-connected voltage-source converters," *Electric Power Applications, IEE Proceedings -,* vol. 153, pp. 750-762, 2006.

[6.9] S. A. Azmi, G. P. Adam, K. H. Ahmed, S. J. Finney, and B. W. Williams, "Grid Interfacing of Multimegawatt Photovoltaic Inverters," *Power Electronics, IEEE Transactions on,* vol. 28, pp. 2770-2784, 2013.

[6.10] Y. Bo, L. Wuhua, Z. Yi, and H. Xiangning, "Design and Analysis of a Grid-Connected Photovoltaic Power System," *Power Electronics, IEEE Transactions on,* vol. 25, pp. 992-1000, 2010.

[6.11] R. Majumder, "Reactive Power Compensation in Single-Phase Operation of Microgrid," *Industrial Electronics, IEEE Transactions on,* vol. 60, pp. 1403-1416, 2013.

[6.12] L. Hongbo, Z. Kai, Z. Hui, F. Shengfang, and X. Jian, "Active Power Decoupling for High-Power Single-Phase PWM Rectifiers," *Power Electronics, IEEE Transactions on,* vol. 28, pp. 1308-1319, 2013.

[6.13] D. Ke, L. Ping, K. Yong, and C. Jian, "Decoupling current control for voltage source converter in synchronous roating frame," in *Power Electronics and Drive Systems, 2001. Proceedings., 2001 4th IEEE International Conference on*, 2001, pp. 39-43 vol.1.

[6.14] D. H. Pham, G. Hunter, L. Li, and Z. Jianguo, "Microgrid topology for different applications in Vietnam," in *Universities Power Engineering Conference (AUPEC), 2012 22nd Australasian*, 2012, pp. 1-6

[6.15] Dai N., Wong M., Han Y., “Application of a Three-level NPC Inverter as a Three-Phase Four-Wire Power Quality Compensator by Generalized 3DSVM”, *IEEE Tran. on Pow. Electronics*, vol. 21, no. 2, Mar. 2006, pp. 440-449.

[6.16] Cortés, P., Ortiz, G., Yuz, J.I., Rodríguez, J., Vazquez, S., Franquelo, L.G., "Model predictive control of an inverter with output LC filter for UPS applications", *IEEE Trans. Ind. Electron*., vol. 56, pp. 1875–1883, 2009.

[6.17] Preindl, M., Schaltz, E., Thogersen, P., "Switching frequency reduction using model predictive direct current control for high-power voltage sources inverters", *IEEE Trans. Ind. Electron*., vol. 58, pp. 2826–2835, 2011.

[6.18] Geyer, T., Papafotiou, G., Morari, M., "Model predictive direct torque control – Part I: concept, algorithm, and analysis", *IEEE Trans. Ind. Electron.*, vol. 56, pp. 1894–1905, 2009.

[6.19] Thielemans, S., Vyncke, T.J., Melkebeek, J., "Weight factor selection for model-based predictive control of a four-level flying-capacitor inverter", *IET. Power Electron*., vol. 5, pp. 323–333, 2012.

[6.20] P. Corts, M. P. Kazmierkowski, R. M. Kennel, D. E. Quevedo, and J. Rodrguez, "Predictive Control in Power Electronics and Drives," *IEEE Trans. Ind. Electron.,* vol. 55,no. 12, Dec. 2008.

[6.21] Noguchi, H. Tomiki, S. Kondo, and I. Takahashi, "Direct power control of PWM converter without power-source voltage sensors," IEEE Transactions on Industry Applications, vol. 34, pp. 473-479, 1998.

CHAPTER 7. CONCLUSIONS AND FUTURE WORKS

7.1. CONCLUSIONS

In this thesis, a smart microgrid with its application for various scenarios is proposed along with a detailed microgrid structure for rural farms in Vietnam. The active and reactive power flow control of the grid-connected inverter has been studied and developed. The general conclusions can be summarized as the following:

- A new smart microgrid structure that can apply for Vietnamese schemes, especial for rural farm case has been proposed,

- The microgrid operation has been studied in both islanded-mode and grid-connected mode for a rural farm with optimal efficiency among different structures,

- A MPC scheme with a new operation cost function has been developed for optimal smart microgrid performance and lowest cost,

- An active and reactive power control strategy in the rotating *d-q* reference frame *d-q* with feedforward plus feedback control has been developed to reduce the cross-coupling effects, and

- A MPC with a new operational cost function has been developed in rotating *d-q* reference frame to improve the performance of active and reactive power flow control.

7.2. FUTURE WORKS

Based on the progress of this thesis, the future works related to the research area can be:

- To validate the structure of the smart microgrid designed in Chapters 3 and 4 with practical implement in the Vietnamese scenario,

- To validate the MPC operation proposed in Chapter 4 with the practical results of real systems, and

- The application of the proposed MPC method in other applications with different control objectives such as the ESSs, and DC/DC converters inside the smart microgrid, etc. with smart modular designs.

APPENDIX A:
PUBLICATIONS BASED ON THE THESIS WORK

- 1. Dung H Pham; Gregory Hunter; Li Li; Jianguo Zhu, "Advanced microgrid power control through grid-connected inverters", *Power and Energy Engineering Conference (APPEEC), 2015 IEEE PES Asia-Pacific, 2015*
- **2.** Dung H Pham; Gregory Hunter; Li Li; Jianguo Zhu, "Feedforward decoupling control method in grid-interfaced inverter", *Power Engineering Conference (AUPEC), 2013 Australasian Universities, 2013*
- *3.* Dung H. Pham; Greg Hunter; Li Li; Jianguo Zhu, "Microgrid topology for different applications in Vietnam", *Universities Power Engineering Conference (AUPEC), 2012 22nd Australasian*

Papers to be submitted:

1. Dung H Pham; Gregory Hunter; Li Li; Jianguo Zhu, "Smart Microgrid Application and Optimized Operation with Model Predictive Control for Vietnam", *IEEE Transactions on Sustainable Energy*

2. Dung H Pham; Gregory Hunter; Li Li; Jianguo Zhu, "Model Predictive Control for Grid-Connected Inverter of Smart Microgrid", *IEEE Transactions on Energy Conversion*

3. Dung H Pham; Gregory Hunter; Li Li; Jianguo Zhu, "Optimized Operation of Smart Microgrids with Model Predictive Control", *The 9th Asia-Pacific Power and Energy Engineering Conference* (APPEEC 2017)